JYVÄSKYLÄ STUDIES IN COMPUTING
227

Vesa Hytönen

Enhancing the Performance of HSDPA Communication with Multipoint Transmission Techniques

JYVÄSKYLÄN YLIOPISTO

JYVÄSKYLÄ STUDIES IN COMPUTING 227

Vesa Hytönen

Enhancing the Performance of HSDPA Communication with Multipoint Transmission Techniques

Esitetään Jyväskylän yliopiston informaatioteknologian tiedekunnan suostumuksella
julkisesti tarkastettavaksi yliopiston Agora-rakennuksen Beeta-salissa
joulukuun 16. päivänä 2015 kello 12.

Academic dissertation to be publicly discussed, by permission of
the Faculty of Information Technology of the University of Jyväskylä,
in building Agora, Beeta hall, on December 16, 2015 at 12 o'clock noon.

UNIVERSITY OF JYVÄSKYLÄ

JYVÄSKYLÄ 2015

Enhancing the Performance of HSDPA Communication with Multipoint Transmission Techniques

JYVÄSKYLÄ STUDIES IN COMPUTING 227

Vesa Hytönen

Enhancing the Performance of HSDPA Communication with Multipoint Transmission Techniques

UNIVERSITY OF JYVÄSKYLÄ

JYVÄSKYLÄ 2015

Editors
Timo Männikkö
Department of Mathematical Information Technology, University of Jyväskylä
Pekka Olsbo, Ville Korkiakangas
Publishing Unit, University Library of Jyväskylä

URN:ISBN:978-951-39-6434-4
ISBN 978-951-39-6434-4 (PDF)

ISBN 978-951-39-6433-7 (nid.)
ISSN 1456-5390

Jyväskylä University Printing House, Jyväskylä 2015

ABSTRACT

Hytönen, Vesa
Enhancing the Performance of HSDPA Communication with Multipoint Transmission Techniques
Jyväskylä: University of Jyväskylä, 2015, 76 p.(+included articles)
(Jyväskylä Studies in Computing
ISSN 1456-5390; 227)
ISBN 978-951-39-6433-7 (nid.)
ISBN 978-951-39-6434-4 (PDF)
Finnish summary
Diss.

The evolution of mobile phones, tablets and other mobile communication devices has led to a significant increase in the amount of data delivered over mobile networks. In order to satisfy the climbing data rate demands of customers, existing mobile broadband networks are being expanded with new features that allow ubiquitous and consistent networking experience. This research presents three multipoint transmission techniques for Wideband Code Division Multiple Access (WCDMA) based High-Speed Downlink Packet Access (HSDPA) communication protocol. Multiflow, High-Speed Single-Frequency Network (HS-SFN) and Multipoint-to-Point Single-Frequency Network (M2P-SFN) enable transmission of user-dedicated data from several cells, with the objective to improve performance, especially in cell edges where the signal quality is usually weak. The main difference between the concepts is the way cell-specific scrambling codes are configured in the network, which eventually determines how flow control, physical layer resource allocation and signal formation and reception will be conducted. The performance of each technique is separately evaluated with system-level simulations. In addition, the dissertation discusses issues with regard to interference conditions and mobility control that may originate from multipoint transmissions.

Keywords: 3G, HSDPA, HSPA, WCDMA, Multiflow, HS-SFN, HS-DDTx, M2P-SFN, multipoint transmission, single-frequency network, scheduling, simulation

Author

Vesa Hytönen
Department of Mathematical Information Technology
University of Jyväskylä
Finland

Supervisors

Professor Timo Hämäläinen
Department of Mathematical Information Technology
University of Jyväskylä
Finland

Dr. Alexander Sayenko
Technology & Innovation, 3GPP standardization
Nokia Networks
Finland

Reviewers

Professor Peter Chong
School of Electrical and Electronic Engineering
Nanyang Technological University
Singapore

Professor János Sztrik
Department of Informatics Systems and Networks
Faculty of Informatics, University of Debrecen
Hungary

Opponent

Professor Mohammed Elmusrati
Department of Computer Science
Faculty of Technology, University of Vaasa
Finland

ACKNOWLEDGEMENTS

I would like to express my deepest gratitude to my supervisor Professor Timo Hämäläinen, for his valuable support and encouragement throughout my study. I would also like to sincerely thank my second supervisor Dr. Alexander Sayenko, for his technical advice and feedback. It would be hard to imagine completing this work without their patient guidance.

I would like to thank Nokia Networks and the Department of Mathematical Information Technology for the financial support and giving me the opportunity to work in inspiring projects and to learn from professionals. That said, I wish to thank all my colleagues and co-authors who participated in this research.

I would like to thank the reviewers of my thesis, Professor Peter Chong and Professor János Sztrik, and Professor Mohammed Elmusrati for being my opponent.

I am grateful to all my friends who have kept my mind fresh after work, especially to those I have played with during my floorball career. The sport is enjoyable now and then, but good friends are the reason to continue playing year after year.

Finally, I would like to express my warmest gratitude to my parents Onni and Elna, my brother Aki and my girlfriend Liinu, for their love, encouragement and advice. This achievement would not have been possible without their support.

Jyväskylä, November 2015
Vesa Hytönen

GLOSSARY

3G	Third Generation
3GPP	Third Generation Partnership Project
4G	Fourth Generation
5G	Fifth Generation
AMC	Adaptive Modulation and Coding
AVI	Actual Value Interface
BLER	Block Error Rate
CIR	Carrier-to-Interference Ratio
CoMP	Coordinated Multipoint
CPICH	Common Pilot Channel
CQI	Channel Quality Indication
CS/CB	Coordinated Scheduling / Coordinated Beamforming
CSoHS	Circuit Switched Voice over HSPA
DCH	Dedicated Channel
DF4C	Dual-Frequency Four-Cell
DFDC	Dual-Frequency Dual-Cell
DL	Downlink
DRX	Discontinuous Reception
DTX	Discontinuous Transmission
D-TxAA	Dual Stream Transmit Antenna Array
DVB-T	Digital Video Broadcasting - Terrestrial
EWMA	Exponential Weighted Moving Average
FCSS	Fast Cell Site Selection
FTP	File Transfer Protocol
G-factor	Geometry Factor
HARQ	Hybrid Automatic Repeat Request
HO	Handover
HS-DDTx	High-Speed Data-Discontinuous Transmission
HS-DPCCH	High-Speed Dedicated Physical Control Channel
HS-PDSCH	High-Speed Physical Downlink Shared Channel
HS-SCCH	High-Speed Shared Control Channel
HS-SFN	High-Speed Single-Frequency Network
HSDPA	High-Speed Downlink Packet Access
HSPA	High-Speed Packet Access
IEEE	Institute of Electrical and Electronics Engineers
IR	Impulse Response
JP	Joint Processing
LMMSE	Linear Minimum Mean Square Error
LPN	Low Power Node
LTE	Long Term Evolution

LTE-A	Long Term Evolution - Advanced
M2P-SFN	Multipoint-to-Point Single-Frequency Network
MAC	Medium Access Control Layer
MAI	Multiple Access Interference
MBMS	Multimedia Broadcast Multicast Service
MBSFN	MBMS over Single-Frequency Network
MCS	Modulation and Coding Scheme
MIMO	Multiple-Input Multiple-Output
MMSE	Minimum Mean Square Error
MPTx	Multipoint Transmission
OVSF	Orthogonal Variable Spreading Factor
PCI	Precoding Control Indication
PDU	Protocol Data Unit
PHY	Physical Layer
QoS	Quality of Service
RLC	Radio Link Control Layer
RNC	Radio Network Controller
RRH	Remote Radio Head
RRM	Radio Resource Management
SFDC	Single-Frequency Dual-Cell
SFN	Single-Frequency Network
SI	Study Item
SINR	Signal-to-Noise-plus-Interference Ratio
SN	Sequence Number
TB	Target Buffer
TBD	Target Buffer Delay
TDM	Time Division Multiplexing
TFRC	Transport Format and Resource Combination
TSG	Technical Specification Group
TTI	Transmission Time Interval
TTT	Time-to-Trigger
TxAA	Transmit Antenna Array
UE	User Equipment
UL	Uplink
UMTS	Universal Mobile Telecommunication System
UTRA	Universal Terrestrial Radio Access
UTRAN	Universal Terrestrial Radio Access Network
VoHS	Voice over HSPA
VoIP	Voice over Internet Protocol
WCDMA	Wideband Code Division Multiplexing
WG	Work Group

LIST OF FIGURES

LIST OF TABLES

CONTENTS

LIST OF INCLUDED ARTICLES

PI Vesa Hytönen, Oleksandr Puchko, Thomas Höhne and Thomas Chapman. Introduction of Multiflow for HSDPA. *Proceedings of the 5th IFIP International Conference on New Technologies, Mobility and Security (NTMS)*, 2012.

PII Ali Yaver, Thomas Höhne, Jani Moilanen and Vesa Hytönen. Flow Control for Multiflow in HSPA+. *Proceedings of the 77th IEEE Vehicular Technology Conference (VTC2013-Spring)*, 2013.

PIII Vesa Hytönen, Pavel Gonchukov, Alexander Sayenko and Subramanya Chandrashekar. Downlink Bicasting with Multiflow for Voice Services in HSPA networks. *Proceedings of the 6th IEEE International Workshop on Selected Topics in Wireless and Mobile computing (STWiMob)*, 2013.

PIV Vesa Hytönen. Voice Traffic Bicasting Enhancements in Mobile HSPA Network. *Proceedings of the 11th IEEE International Symposium on Wireless Communication Systems (ISWCS)*, 2014.

PV Vesa Hytönen, Oleksandr Puchko, Thomas Höhne and Thomas Chapman. High-Speed Single-Frequency Network for HSDPA. *Proceedings of the IEEE Swedish Communication Technologies Workshop (Swe-CTW)*, 2011.

PVI Oleksandr Puchko, Mikhail Zolotukhin, Vesa Hytönen, Thomas Höhne and Thomas Chapman. Enhanced LMMSE Equalizer for High-Speed Single Frequency Network in HSDPA. *Proceedings of the IEEE Swedish Communication Technologies Workshop (Swe-CTW)*, 2011.

PVII Oleksandr Puchko, Mikhail Zolotukhin, Vesa Hytönen, Thomas Höhne and Thomas Chapman. Phase adjustment in HS-SFN for HSDPA. *Proceedings of the 5th IFIP International Conference on New Technologies, Mobility and Security (NTMS)*, 2012.

PVIII Fabian Montealegre Alfaro, Vesa Hytönen, Oleksandr Puchko and Timo Hämäläinen. Scheduling Multipoint-to-Point Transmissions over HSDPA Based Single Frequency Network. *Proceedings of the 3rd IEEE International Conference on Information Science and Technology (ICIST)*, 2013.

1 INTRODUCTION

According to several mobile telecommunication forecasts, including [1] and [2], Wideband Code Division Multiple Access (WCDMA) based High-Speed Packet Access (HSPA) will retain its place in coming years as the dominant mobile broadband technology in many parts of the world in terms of number of subscriptions and the amount of data carried over the network, as illustrated in Figure 1. Although the popularity of Long Term Evolution (LTE) is increasing its foothold

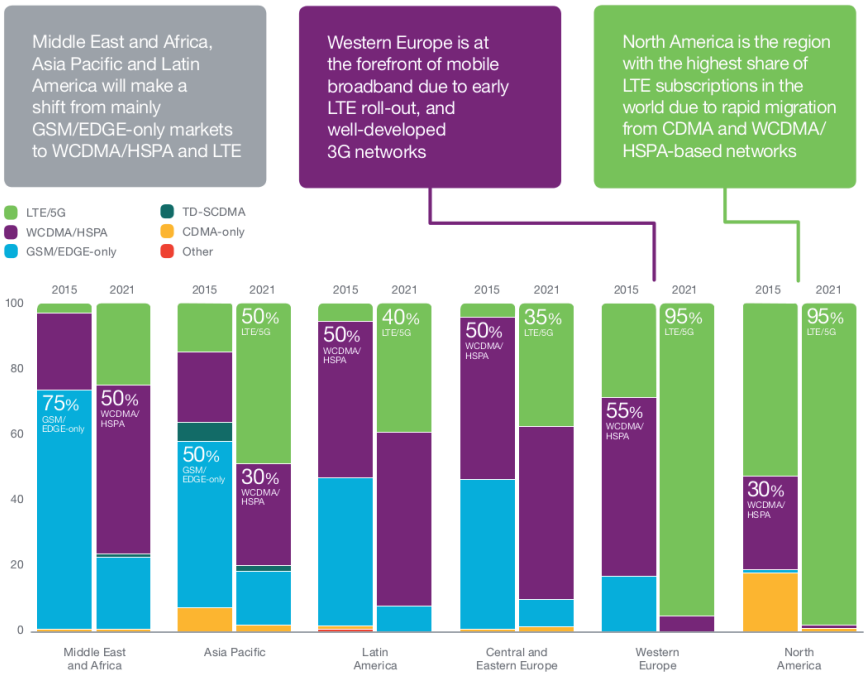

FIGURE 1 Forecast of the mobile subscriptions by region and technology [1]

in the market shares and the research on the Fourth (4G) and Fifth (5G) Generation mobile networks is thriving among the academia, compelled by the planned

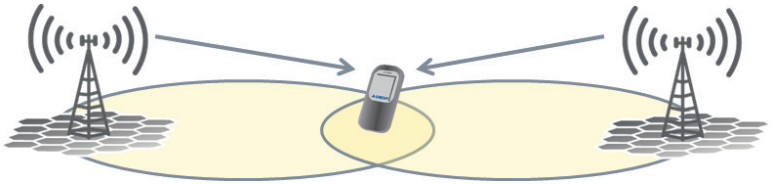

FIGURE 2 Concurrent downlink multipoint transmission from two cells

initial 5G network deployment in 2020 ([3]), the main part of the revenue for the network operators originate from the widespread Third Generation (3G) mobile network infrastructure and growing usage of the technology.

Along with the number of subscribers, the volume of data that is delivered over the HSPA network is experiencing a vast increase. Consequent to the mobile revolution, [1] characteristic network usage has evolved from audio calls, e-mail traffic and web browsing to always-on social networking and video content viewing. Confined to work with a limited spectrum, network operators are pushed to seek new ways to improve the spectral efficiency of the existing cellular networks in order to maintain customer satisfaction and to provide consistent communication experience throughout the network. The primary issue in terms of consistency are the users residing at the cell edges. They often sustain a high signal propagation loss as a result from having a long distance to their serving cell. Furthermore, a neighboring cell often creates high interference towards the user since the path loss imbalance between the serving cell and the interfering cell is small. One option to alleviate the cell-edge issue is to turn the strong interferer into a contributing transmitter, allowing the terminal to be served from the neighboring cell together with its primary serving cell. Since the transmissions originate from different service points, the method is called multipoint transmission.

The basic idea of multipoint transmission is that data is transmitted within a certain time window from multiple physical locations, as depicted in Figure 2. Depending on the implementation, each transmitter may emit the same or a different bit-stream and the transmissions may or may not be synchronized. Furthermore, the physical separation of the transmitters can vary significantly. The antennas may reside side-by-side with inter-antenna distance clearly less than the wavelength, like in conventional Multiple-Input Multiple-Output (MIMO) systems, or the transmitters may be distributed in the range of several hundreds of meters to enable macro-diversity.

Development of the HSPA standard (as well as the LTE standard) is led by the 3rd Generation Partnership Project (3GPP), a world-wide consortium of operators, vendors and hardware manufacturers [5]. In the recent development milestone of the HSPA specification, *Release 11*, a multipoint transmission concept

[1] The growth in the number of smart phones, tablets, USB dongles and other mobile broadband devices has been immense in the recent years, entailing a proliferation of the traffic created in the networks. In 2000, one exabyte of traffic was delivered in the entire global Internet, while in 2013, almost 18 exabytes was carried over the mobile networks [4].

called Multiflow was introduced among various other amendments [6]. It is one of the ways the capacity of the network is designed to be improved, especially in the cell edges, by utilization of multiple cells that concurrently transmit data to same user terminal in downlink (DL) direction. Multiflow plays the main role among the discussed concepts in this thesis, yet a few other techniques for DL multipoint transmission are also presented. Namely, the following concepts related to downlink HSPA, or High-Speed Downlink Packet Access (HSDPA), are covered in detail in this dissertation:

- Multiflow
- High-Speed Single-Frequency Network (HS-SFN)
- High-Speed Data-Discontinuous Transmission (HS-DDTx)
- Multipoint-to-Point Single-Frequency Network (M2P-SFN)

The listed techniques fall into the macro-diversity category, where the multipoint service is provided from cells controlled by one or many NodeBs. Well-known parallel transmission schemes, such as MIMO or multi-carrier operations, can in theory be applied on top of these techniques. Several geographically separated cells can also be controlled by a single network device in a centralized manner. In fact, in a dense urban environment a large number of femto- and pico-cells are usually steered by the same baseband unit and the remote radios just provides network coverage in the area. Similar flexibility in network deployment is also utilized in certain parts in this study.

It is shown that regardless of the technique, the cell-edge performance can be improved. It becomes evident that multipoint operation is a key element in increasing the stability and consistency of the communication, given that the operation is carefully designed to maximize the benefit and to avoid issues that modifications to the legacy system might create.

1.1 Review of Multipoint Transmission Schemes in Wireless Communication Systems

The wide category of Multipoint Transmission (MPTx) concepts is not limited to the main topics of the thesis. This section presents several concepts that can be compartmentalized into the same category.

The first standard for Wideband Code Division Multiple Access (WCDMA) based Universal Mobile Telecommunication System (UMTS), commonly known as 3G, that was completed in 1999 and named *Release 99* by the 3GPP community, defined Dedicated Channel (DCH) for user plane data which allowed the cells in user's Active Set to concurrently transmit data to User Equipment (UE) in downlink direction [5, 7]. Multipoint transmission from the Active Set cells is not supported in HSDPA, for which the first standard was finalized in *Release 5*.

Multimedia Broadcast Multicast Service (MBMS), introduced in *Release 6*, is a service for transmitting broadcast or multicast data over common physi-

cal channels to multiple users within a cell [8]. Although *Release 6* already included HSDPA, MBMS is available only to the DCH (*Release 99*) channel. MBMS over Single-Frequency Network (MBSFN), introduced in *Release 7* is a physical layer extension to MBMS to enhance the spectral efficiency of the scheme [9]. In MBSFN, a uniform cluster of cells is constructed. The cell cluster transmits an identical waveform in synchrony, thereby ideally enhancing the received signal strength and reducing inter-cell interference [10, 11]. In the WCDMA system, this is achieved by applying a common scrambling code in each MBSFN cell. SFN-based broadcasting is known especially from Digital Video Broadcasting - Terrestrial (DVB-T) systems, which is studied in [12, 13].

One of the latest studies related to HSPA MPTx was opened by 3GPP for a concept called Combined cells in the preparation of *Release 12* [14]. The concept relies on deployment of heterogeneous networks and usage of a common primary scrambling code in the central node, NodeB for example, and in Low Power Nodes (LPNs) that are controlled by the central node [15]. This allows unified cell identity in multiple geographically-separated cells, which improves signal quality, alleviates network coverage issues and extends seamless mobility over a large area, at the same time, however, posing additional complexity with DL/UL imbalance, interference avoidance and network management. It also requires temporal synchronization between LPN's and master node's transmissions which is achieved by using a direct interface between the LPNs and the master node. Although the Combined cell concept was made a Study Item in 3GPP, the research on the scheme was not continued in the Work Item phase.

Coordinated Multipoint (CoMP) is a downlink multipoint transmission technique in LTE-Advanced (LTE-A) and it can be divided into two subcategories: Joint Processing (JP) and Coordinated Scheduling / Coordinated beamforming (CS / CB) [16]. Furthermore, two approaches are defined for Joint Processing: Dynamic Cell Selection, where data is transmitted from one eNodeB at a time, and Joint Transmission, where multiple eNodeBs transmit to the same UE simultaneously [17, 18]. An overview of CoMP with performance demonstration based on field trials can be found in [19] CoMP is currently a very widely studied topic, and although the technology behind it is different from the technologies of the topics in this study, there are various similarities between the schemes, regardless of the technology. The research on the discussed multipoint concepts can thus offer valuable input for the 4G development.

Part of the LTE *Release 12* Small Cell Enhancements item is a concept called Dual Connectivity, which is also known as Inter-site carrier aggregation [20]. It can improve user plane throughput by allowing user to communicate concurrently with master eNodeB (i.e. macro cell) and at least one secondary eNodeB (i.e. low power node) [21]. Deployment and joint usage of small cells enhances network capacity, but may create issues with mobility with regard to increased number of handovers. Still, Dual Connectivity is considered one of the main designs for future advanced heterogeneous networking.

In addition to the above concepts, a few other schemes exist that can be included in the category of multipoint transmission but may not be as compatible

with this research as those mentioned in this chapter. These include, for instance, Fast Cell Site Selection (FCSS, deprecated at an early stage of the HSDPA standardization, [22]), MIMO ([23]) and multi-carrier HSPA ([24]).

1.2 3GPP Standardization

Some of the work included in the dissertation was initially used for promoting the multipoint services in the 3GPP standardization workflow. It is therefore recommended that to understand the nature of the thesis and the work behind it one should have knowledge of the workflow process.

The standardization organization comprises four Technical Specification Groups (TSGs). Each TSG is divided into multiple Work Groups (WGs) responsible for a small part of the 3GPP standards. The structure of the organization is depicted in Figure 3 [5]. Technical contributions for Multiflow, HS-SFN and HS-DDTx were prepared for the 3GPP RAN WG1 (Radio layer 1) specification group by the author and other members of the projects.

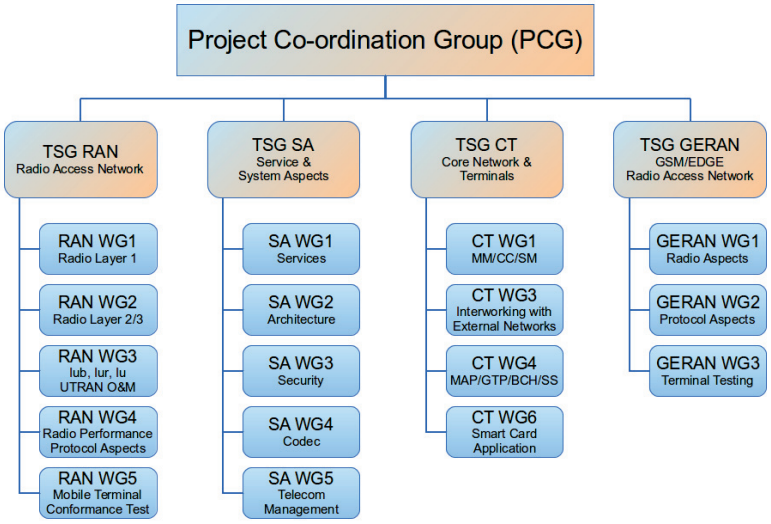

FIGURE 3 3GPP Specification Group Structure [5]

The 3GPP standardization process is presented in Figure 4 [7]. Each aforementioned contribution was submitted during the Study Item (SI) phase, in which the feasibility of the feature is evaluated among the 3GPP members. The feasibility assessment is strongly based on the ratio of gain achieved with the new item and on the estimated impact on the equipment and existing features [7]. As mentioned earlier, Multiflow was accepted to the Work Item phase and thereafter found its way to the specification in *Release 11*. HS-SFN and HS-DDTx were left out after the feasibility study; too little benefit was seen in them by different companies, and additional complexity would have been required for the

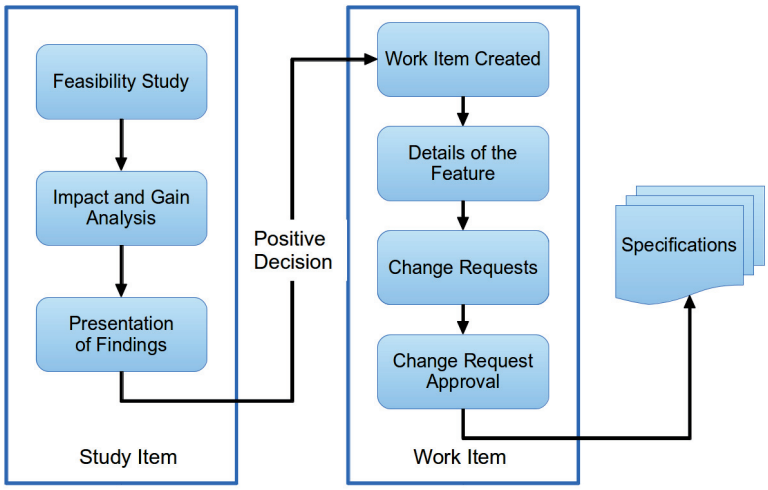

FIGURE 4 3GPP Standardization Workflow [7]

user terminal to support the schemes.

1.3 Research Objective

The reliability and speed of wireless communication usually decreases when user moves from one cell to another. In the worst case, a reception outage is encountered, and the terminal disconnects from the network. One of the primary objectives of the study is to improve cell border communication by different multipoint techniques. Several algorithms are proposed for efficient handling of user and control plane traffic, with the majority of them concerning resource allocation over the Physical (PHY) layer.

System level simulations are used for obtaining performance results. The simulator is implemented in C++ and the raw results are post-processed with MATLAB®. The main target is to assess the general performance of each concept, and also the performance of certain sub-processes, such as scheduling algorithms. Common for each research article is that the studies were performed in downlink direction in a HSPA network. Furthermore, each paper discusses and evaluates mainly PHY, Medium Access Control (MAC) and Radio Link Control (RLC) layer operations between the entities within Universal Terrestrial Radio Access (UTRA) and its access network called Universal Terrestrial Radio Access Network (UTRAN).

The integral parts of the implementation regarding simulation of each MPTx concept are described in order to give a view of what is required for achieving reliable communication models. Several deductions are drawn from the results of simulations. The correctness of the simulator and the results have been validated against the results and feedback obtained from other 3GPP companies.

The research is industry-driven in the sense that the described limitations and possibilities are often strictly determined by the existing standards. Also, one of the main during the research was to provide support and material for the 3GPP standardization which makes the work highly practically-oriented. When proposing new algorithms or features, hardware and software modifications that would be required in the user terminal equipment are kept to a minimum, as proposals for them would likely increase the objections from chipset and device manufacturers due to implementation and deployment costs, and hence restrict the potential of the concept for wider use. Network-side software changes without any requirement for additional infrastructure deployment, however, are more likely to be approved since reprogramming the devices is much more straightforward, cheaper and can be done by the network operator. Nevertheless, functionality of some concepts depend on new and unspecified signaling between the network elements, so occasionally the modifications cannot be constrained to the network domain.

The dissertation gives a broad description of each of the individual topics studied during the research. In the end, the reader should have a clear image of how each MPTx scheme works, the purpose they are used for and the phenomena and features that affect the performance of the schemes in both real world deployment and in simulations.

1.4 Structure of the Thesis

The rest of the thesis is organized as follows. Chapter 2 is a preface that introduces the reader to the studied MPTx schemes. The discussion includes a theoretical basis on how the concepts should operate from the standard viewpoint. This part is mainly concentrating on the PHY, MAC and RLC layers of the protocol stack. The demand for certain sub-processes and algorithms related to MPTx are given in this chapter.

Solutions for the discussed MPTx issues are presented in Chapter 3, accompanied with the related simulation results. An introduction of the simulation model that is used for the studies is also included. The emphasis in the modeling part is on the scheduling, signal and receiver models since each of the MPTx modes rely strongly on efficient resource allocation, and especially with SFN-based schemes the signal formation and reception play an essential role.

Finally, Chapter 4 concludes the dissertation.

1.5 Author's Contribution

The author has participated in the preparation of several peer-reviewed publications during the work on the dissertation. In this chapter, the responsibilities and

contribution of the author to the research and the included articles are explained.

PI extensively describes how Multiflow operates on RLC, MAC and PHY layers. The article presents a slightly modified subset of results that were earlier collected by the author and provided to the 3GPP Technical Specification Group-Radio Access Network Work Group 1 (TSG-RAN WG1) specification group during the Study Item phase of the concepts [25]. In addition to extensive simulations and acquisition and analysis of the results, the author's contribution prior to the preparation of the article focused on further verification of the simulator reliability and especially on the extension of the scheduling algorithms related to multi-cell transmission. The author was the main party responsible for writing this article.

PII concentrates on the impact of RLC flow control on PHY layer performance with Multiflow. As in the previous article, the author was responsible for the verification of the flow control as well as most of the simulations from which the results were obtained for the contribution. Regarding specific parts of the implementation, the author implemented a large part of the RLC flow control on the network side, a so-called de-jitter buffer state machine on the UE side and a support for the RLC layer retransmissions of Protocol Data Units (PDUs).

PIII and **PIV** address the question of how Multiflow could be utilized for delivering QoS-dependent voice traffic. The former article describes the foundation that allows the use of Multiflow for serving real-time data in addition to a downlink power control mechanism that ensures a reliable communication without extensive usage of the cells' transmission power capacity. Power control, in line with the input received from and industrial collaboration partner, was implemented by the author. The latter article extends the topic by introducing an efficient flow control and scheduling approaches for real-time voice-traffic delivery. The algorithms, results and deductions presented in the paper were provided solely by the author.

PV introduces HS-SFN and HS-DDTx on elementary level together with system simulation results. As was the case with the first Multiflow related article, some of the results given in the paper were first submitted to the 3GPP specification group in the Study Item phase [26]. From the implementation viewpoint, the author was partially responsible for a so-called coordinated scheduler, which processes each cell and their UEs as a single entity, trying to optimize the site-specific performance metric on the TTI-to-TTI (Transmission Time Interval) basis. The coordinated scheduler took both HS-SFN and HS-DDTx into account in its evaluation. During the preparation of the article, a patent application, with which the author was also involved, was submitted and later accepted regarding the PHY layer Channel Quality Indication (CQI) signaling aspects with HS-SFN and HS-DDTx (patent publication number WO 2012136450 A1).

PVI and **PVII** deepen the research on HS-SFN. The first paper discusses an improved receiver architecture for efficient combining of the PHY layer signals. The second paper, by applying a precoding-like phase adjustment, aims to improve the coherence of the signals originating from different cells. For these articles, the author had a supporting role in the implementation and verification

of the simulator and during the writing process.

PVIII presents the Multipoint-to-Point Single-Frequency Network (M2P-SFN) concept, where multiple HSPA cells serve the same user simultaneously in order to improve the received chip energy and thereby the Signal-to-Noise-plus-Interference Ratio (SINR). The working title of the topic was simply *Single-Frequency Network*. However, due to the possibility of confusion with HS-SFN, henceforth in this thesis a term M2P-SFN will be used. A simplified system simulator was used to evaluate the performance of M2P-SFN with limited physical layer modeling. The results presented in the article provide high-level information on how clustering of cells into SFN groups and scheduling affect user-specific SINR and throughput. The author designed and implemented a bursty traffic model for the simulator and finally gathered the results for the paper. Most of the text in the article was written by the author.

The research on M2P-SFN was continued after **PVIII**, and the concept was implemented in higher detail in the system level simulator used with the other topics. A follow-up study concentrates on practical issues that arise if the technique is applied on HSPA network. The modeling approaches and performance evaluation are presented in this dissertation.

The aforementioned articles are the main contribution for this thesis. Moreover, the author has participated in other academic research during the progress of his Ph.D. studies, mostly covering features of IEEE 802.16 WiMax technology. The following lists the related contributions not directly applicable to the current work:

- V. Hytönen, A. Sayenko, H. Martikainen and O. Alanen. Handover Performance in the IEEE 802.16 Mobile Networks. *Proceedings of the 3rd ACM International Conference on Simulation Tools and Techniques (SIMUTools)*, March 2010.
- A. Sayenko, O. Alanen, H. Martikainen, V. Tykhomyrov, O. Puchko, V. Hytönen and T. Hämäläinen. WINSE: WiMAX NS-2 Extension. *SAGE. Simulation. Transactions of the Society for Modeling and Simulation International*, Volume 87, Issue 1-2, pp. 24-44, 2011.
- M. Zolotukhin, V. Hytönen, T. Hämäläinen and A. Garnaev. Optimal Relays Deployment for 802.16j Networks. *Springer. Mobile Networks and Management. Lecture Notes of the Institute for Computer Science, Social Informatics and Telecommunications Engineering*, Volume 97, pp. 31-45, 2012.

In addition to the preparation of the above papers, the author has been invited to peer-review multiple contribution papers for the Springer journal *Wireless Networks* as well as one submission for the *IEEE Communications Magazine*.

2 DESCRIPTION OF THE CONCEPTS

This chapter outlines the research subjects with regard to the topics of the included publications. The focus is on the downlink, PHY, MAC and RLC layers, while the access network is considered from the system architecture viewpoint only.

The use of single-carrier WCDMA is assumed throughout the dissertation, where all users are transmitting on the same frequency band. In order to allow parallel transmissions, interference between signals has to be controlled and signals from different sources have to be separated. This is done with the help of channelization (spreading) codes and complex-valued scrambling codes. Within a cell, Orthogonal Variable Spreading Factor (OVSF) channelization codes are used for separating DL transmissions to different UEs (code domain multiplexing) from each other. For DL, WCDMA scrambling codes differentiate the cells that operate on the same carrier frequency.

One of the main differences between the multipoint transmission schemes is the configuration of the scrambling codes in the cells serving the same UE. The scrambling setup determines how the signals from different origins interfere with each other, fundamentally impacting the receiver architecture at the user terminal as well as mobility control on the network side. The configuration may change from one cell to another, but even a single cell may transmit superimposed signals with different scrambling. This is actually the main characteristic of HS-SFN, where different scrambling may be applied to data and control channels. Table 1 lists, among a few other important features, the scrambling code configuration with different schemes, assuming two cells serve the same UE simultaneously. The scrambling code configurations are relevant especially for SFN based concepts. The configurations are explained in detail in the corresponding sections. Transmit synchronization refers to chip-level synchronization, which allows reception of aligned signal components. Synchronization is relevant for HS-SFN/DDTx and M2P-SFN, which are sensitive to misalignment of the components. Type 3i receiver is required for efficient utilization of Multiflow, as it allows interference cancellation between the traffic flows. Serving one UE from physically separated cell sites is possible with each of the concepts. However,

TABLE 1 Features of the MPTx techniques

	MPTx scheme			
	Multiflow	**HS-SFN**	**HS-DDTx**	**M2P-SFN**
Specification release	Release 11	-	-	-
Primary serving cell scrambling codes				
HS-PDSCH	A	A	A	A
HS-SCCH	A	A	A	A
Common control channels	A	A	A	A
Assisting serving cell scrambling codes				
HS-PDSCH	B	A	-	A
HS-SCCH	B	-	-	A
Common control channels	B	B	B	A
Requires Tx synchronization	-	X	X	X
Requires Type 3i receiver	X	-	-	-
Supports inter-NodeB transmission	X	With RRH	With RRH	With RRH
Affected protocol stack layers	RLC, MAC/PHY	MAC/PHY	MAC/PHY	-

in a conventional system where a cell site is controlled by a dedicated NodeB, inter-NodeB transmission is natively supported only by Multiflow. Other concepts require centralized control and use of remote radio heads (RRH) to allow concurrent transmission from different locations. Finally, Multiflow will affect the RLC layer due to the need for PDU re-ordering and MAC/PHY layer due to the need for modifications in the HS-DPCCH processing logic. HS-SFN does not affect RLC, but the custom dual-CQI reporting affects the MAC layer. M2P-SFN is founded completely on network-side procedures and thus will not impact the protocol stack.

According to the table and recalling that signals received on the same frequency and coded with different scrambling create interference with each other, it is obvious that interference avoidance or cancellation is the key element that determines the feasibility and performance of each concept. On the other hand, setting up an identical scrambling for different transmitters may create issues related to large-scale interference conditions, implicitly impeding the mobility control in the system. This affects especially SFN-based techniques as explained in higher detail in Chapter 2.3. The main mechanisms for interference control with MPTx schemes are mainly affected via scheduling and modifications to transmitter and receiver functionality.

2.1 Multiflow

Multiflow is the only from the studied concepts that has found its way to the 3GPP HSPA+ [1] standard in *Release 11*. It allows the interferer to be converted to another serving cell, thus explicitly improving the received data rates at the cell borders. In the basic Multiflow operation, the user is served from two cells which transmit different data blocks to user [28, 29].

Multiflow is a common nominator for a few specific sub-types of the tech-

[1] HSPA+ is the evolution of the HSPA standard that started from *Release 7* in 2007 [7, 27].

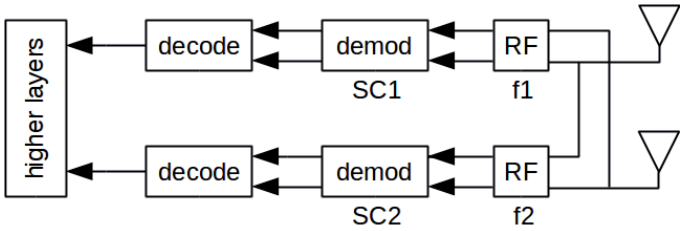

FIGURE 5 Typical SF-DC Multiflow UE receiver architecture supporting dual-carrier HSDPA [34]

nology. The basic Multiflow configuration is called Single-Frequency Dual-Cell (SF-DC) Aggregation, where the terminal is served by two cells on the same carrier frequency [30]. SF-DC Aggregation operation, including a performance evaluation obtained with system simulations, was discussed in **PI**. SF-DC was standardized in *Release 11* together with DF-3C and DF-4C Multiflow. Dual-Frequency Dual-Cell (DF-DC) Aggregation was proposed to standard in *Release 12* but eventually was not adopted. The latest variant is 3F-4C Multiflow, that is standardized in *Release 13* [31, 32].

The performance gain with Multiflow is achieved with a combination of traffic control at the network side and efficient signal processing at the receiver. In order to avoid inflicting negative effects to the primary users of the cell (users who are camped in that cell), an efficient way of resource allocation mandates that the cell is confined to serve the Multiflow user located in another cell only when there are no active primary users in its vicinity. Using the free resources in the neighbor cell enables short-term load-balancing between the cells. From the user perspective, receiving different transmissions on a common frequency implicates a requirement for an interference mitigating (Type 3i) receiver with antenna diversity [33]. Such receiver architecture enables chip-level equalization, allowing maximization of the SINR on both links. A typical receiver architecture for SF-DC Multiflow is given in Figure 5. It should be noted that the receiver supporting SF-DC Multiflow can also be used with dual-carrier HSDPA.

In general, the gain is created not only by the usage of an additional data flow. Multiflow's load balancing capability implicitly improves the network performance, since the activity time of a Multiflow user can be reduced, thus leading to fewer users sharing the cell's resources in coming TTIs.

It is likely that the PDUs will not arrive to the UE in a correct order when they are sent from two independent transmitters as is the case with Multiflow. This leads to skew, which is the difference of the arrival times of two PDUs with subsequent sequence numbers (SN) as

$$Skew_{PDU_{SN}} = t_{arrival}(PDU_{SN}) - t_{arrival}(PDU_{SN-1}). \quad (1)$$

Positive skew arises from reception of correctly ordered subsequent PDUs at different times, while *negative* skew in a legacy network happens due to (H)ARQ retransmissions; PDU_{SN-1} may be received before PDU_{SN} in case PDU_{SN} needs

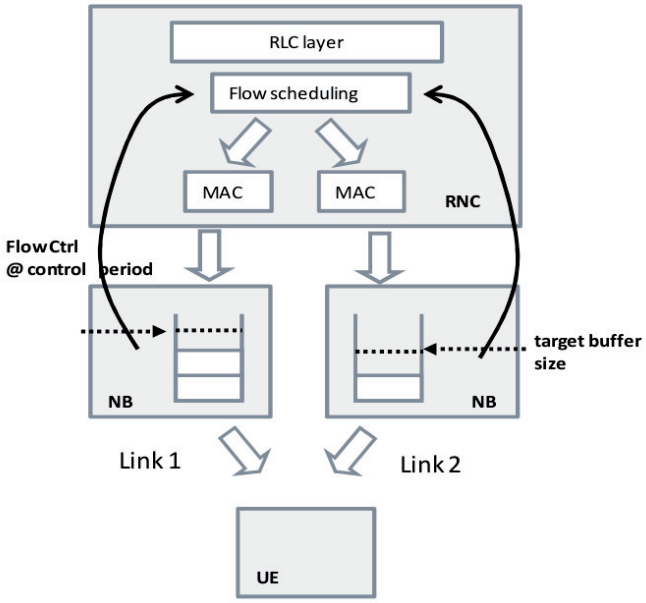

FIGURE 6 Flow control block diagram

to be retransmitted. The probability of *negative* skew increases after enabling Multiflow, which may lead to unnecessary RLC layer PDU retransmissions and thus creates a need for counter measures against the skew. Elimination of skew is one responsibility of the flow and split control operations that are explained in the following sections.

2.1.1 Flow Control

In contrast to LTE-A, a direct interface between two NodeBs does not exist for HSPA+. The networking unit that connects two NodeBs is the Radio Network Controller (RNC). The conventional way in which Multiflow works is that serving cells transmit different data blocks to the user. Data split for the cells is done at the RLC protocol layer in RNC which is depicted in Figure 6 [35]. In order to be able to utilize multiple data streams that carry different content, the UE needs to merge and re-order the received data. This takes place at the RLC layer for which the data is delivered from separate receive chains and corresponding MAC layers.

Usually the UE cannot be served from the Multiflow cells at equal speed, due to different channel characteristics and uneven load levels of the cells. The amount of data delivered from the RNC to the serving and assisting NodeB should thus adapt to the capability of the cell, which is one of the main parts of flow control with Multiflow. This type of realistic RLC layer flow control was studied in **PII**. The paper describes one of the flow control design issues that relates to sub-optimal filling of NodeBs' transmission buffer. Mandated by feedback signaling from NodeB to RNC, transmission buffer at NodeB is periodically

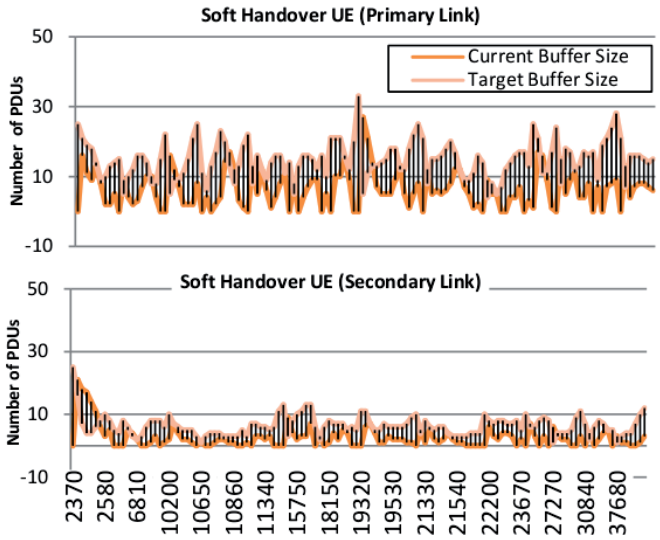

FIGURE 7 Dynamic buffer state over several time slots (1 X-axis time slot = 0.667 ms)

filled by RNC in predefined flow control intervals as shown in Figure 6. However, in case too many PDUs are delivered to NodeB, with respect to how fast they can be transmitted over the physical channel, the PDUs pile up and the user-specific throughput decreases. In an opposite case, the NodeB does not have anything to transmit even though it could serve the UE. Flow control at the RNC relies on the requests from the NodeB, which indicates the estimated packet transmission capability. Based on the request, the RNC sends a certain number of new PDUs to the NodeB. An example of the buffer size progression over time is given in Figure 7. In the example, it is shown how the user can be served with a lower rate over the assisting Multiflow link, thus the transmission buffer size remains also smaller than that of the primary link. When the 'Current Buffer Size' stays at zero level, an undesired under-run is detected. In the optimal case, the buffer reaches zero exactly at the end of the flow control period, after which new data is obtained from the RNC. In reality it is hard to estimate the exact PDU count, and in general it is better to slightly over-estimate the cell's capability upon requesting new data so as to avoid under-runs. A proposal for the flow control algorithm that performs the capacity estimation and related results are presented later in Chapter 3.2.1.

2.1.2 Split Control

In addition to calculating the number of PDUs that are pushed to the serving and assisting cell, another part of the Multiflow flow control is the PDU split logic that determines in which order the PDU are sent to primary and assisting serving cells from the RNC. The split control is conducted specifically to minimize the skew effect.

The UE can eliminate certain amount of skew with its re-ordering buffer which stores and rearranges the received PDUs according to their SN before delivering the data to the upper layer [36]. However, the reordering timer, which triggers an RLC layer retransmission for missing PDUs upon expiration, limits the capability to eliminate all skewness. In a traditional network, RLC layer retransmission is executed if a HARQ process fails and the reordering timer therefore expires. With Multiflow, the timer might expire also if UE is expecting a PDU that for some reason stays in other cell's buffer for too long. The problem can be alleviated by the split control design that tries to minimize the extensive skewness that might trigger the retransmission. Chapter 3.2.2 presents three split control algorithms that allocate PDUs to serving cells in different order.

2.1.3 RLC Layer Bicasting

Multiflow was designed to enhance the downlink data rates for delay-tolerant traffic, such as best effort FTP. Another possible use case for Multiflow is in improvement of QoS-dependent traffic performance. In contrast to conventional Multiflow that aims for higher throughputs, the objective with bicasting is to increase PDU reception probability and thus reduce network outages in the cell edges.

It was discussed in the previous chapter that the flow control splits RLC layer data to serving cells. In order to use Multiflow for delivering, for example, voice data, splitting the data to different cells would likely reduce the quality of service due to extended end-to-end delays and the skew effect that was determined by the order and timing of received PDUs. Instead, RLC PDUs can be duplicated to both cells when the objective is to improve QoS.

First experiments to adapt Multiflow for use with Circuit Switched Voice over HSPA (CSoHS) or Voice over HSPA (VoHS) services were done in **PIII**. The RNC's operation was changed to make it duplicate each PDU to both serving cells instead of splitting the data. NodeB was assumed simple in the study in the sense that it omits all further flow control, such as avoiding unnecessary duplicate PHY layer transmission of PDUs. As a result, both serving cells transmit each PDU they receive from the RNC. The PDU re-ordering buffer, which resides in the terminal receiver, then discards duplicate packets in order to avoid issues in upper layers. The operation in depicted in Figure 8. From the architectural viewpoint, this does not increase the user terminal complexity since bicasting of PDUs is purely a network-side operation and the re-ordering buffer is already present in *Release 7/8* terminals that support VoIP and CSoHS [34, 37, 38].

It was observed that the selected approach clearly lacked some flow control at the NodeB and that another bicasting method should be implemented in the RNC. Duplicating each packet's transmission over the PHY layer led to the elimination of outage, but with the cost of extensive loss of air interface resources. The reduction in residual cell capacity after scheduling users with voice traffic dropped unacceptably, which left space for further optimizations.

In order to reduce residual capacity loss, a clear requirement is that a packet

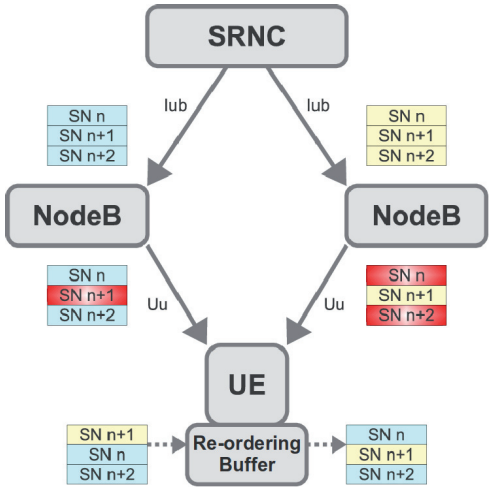

FIGURE 8 PDU Bicasting with Multiflow

should be transmitted only from one cell. Moreover, of the two serving cells only the one with better channel conditions should transmit if possible. The main reasons for selecting the better cell for transmission are better reception probability and the reduction of transmission power which creates less interference in the system. In normal HSPA operation with best effort traffic for which a higher data rate is desirable, link adaptation is performed by changing the Modulation and Coding Scheme (MCS) according to the channel quality. This allows a varying data rate to be used in different channel conditions. With constant low data rate communication, however, Adaptive Modulation and Coding (AMC) is of little use since a robust MCS is already capable of carrying all data. Therefore, AMC can be partially replaced or complemented by power control that is based on per-OVSF-code power requirement and code allocation. Chapter 3.2.3 presents an improved algorithm that utilizes power control and composite HS-DPCCH report to allow NodeBs to make the decision on whether they should transmit the PDU over the air interface.

2.2 HS-SFN

3GPP published an official Study Item (SI) on HSPA multipoint transmission schemes in January 2011 [39]. In that SI, a compound feature of High-Speed Single-Frequency Network (HS-SFN) and High-Speed Data-Discontinuous Transmission (HS-DDTx) were accompanied by Multiflow. The SI promotion was an initiative for the HS-SFN study now included in this thesis.

Most of the research done during the project on HS-SFN and HS-DDTx has already been compiled and published in a Ph.D. thesis [40], thus the discussion on HS-SFN in this chapter and later the presentation of the results merely focus on

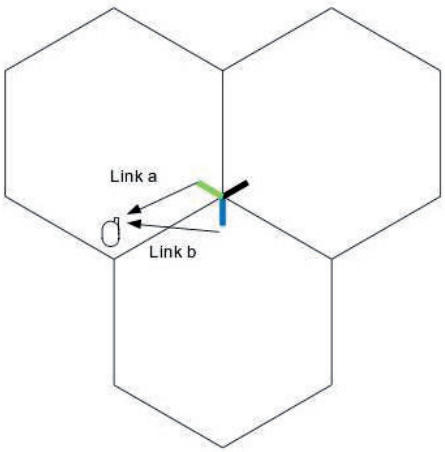

FIGURE 9 Intra-site HS-SFN transmission

explaining issues and their solutions, with a lesser emphasis on the presentation of detailed results.

In the SI mentioned above, HS-DDTx was merged with HS-SFN. The only difference from the operational viewpoint is that in HS-DDTx the neighbor cell omits the transmission on HS-PDSCH, thus reducing Multiple Access Interference (MAI) and interference towards other users. Due to the coupling of the schemes, henceforth the term HS-SFN can be assumed to cover also HS-DDTx.

A distinctive feature of HS-SFN is the configuration of the same scrambling code for DL HS-PDSCH in the two cells controlled by the same NodeB, as shown in Figure 9. Pilot and other common control channels continue using cell's native scrambling, thus leading to transmission of parallel, superimposed signals. Not shown in the figure is the HS-SCCH, which is not transmitted from the assisting cell when HS-SFN is activated. As depicted in Figure 10, ideally the two identical, TTI-aligned transmissions from the neighboring cells allow a perception of elevated chip energy at the receiver, thus improving the instantaneous data channel Carrier-to-Interference Ratio (CIR). The figure reflects how the received signal is affected by the characteristics of both links which are indicated by different channel impulse response (IR) patterns. CIR can be expressed in a simplistic format by using the received signal powers as

$$CIR = \frac{P_{0,HS-PDSCH} + P_{1,HS-PDSCH}}{\sum_{i=1}^{N_{cells}} P_{i,tot} - P_{1,HS-PDSCH}}, \tag{2}$$

where the data channel power from the assisting cell is aggregated to the contributing signal. In practice, signal quality and overall performance are affected by a number of factors, both explicitly and implicitly.

The receiver architecture is shown in Figure 11. In order to efficiently measure the quality of the second serving cell, separate channel estimators need to be deployed. This requirement increases the complexity of the terminal compared to legacy device which is one of the disadvantages of HS-SFN.

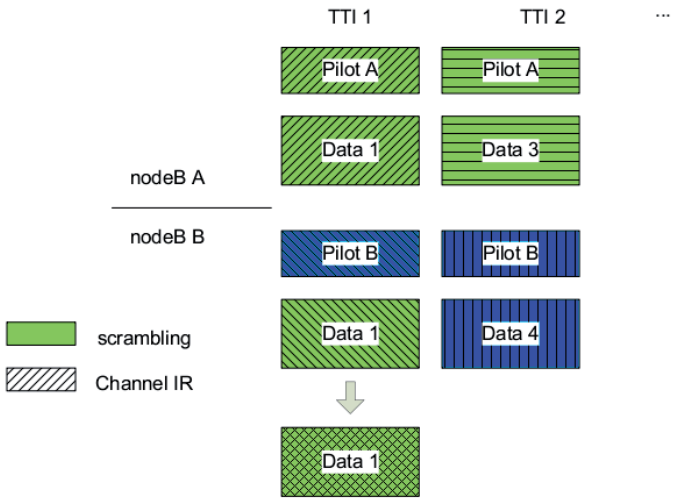

FIGURE 10 Data (HS-PDSCH) and control channel scrambling configuration during a HS-SFN transmission

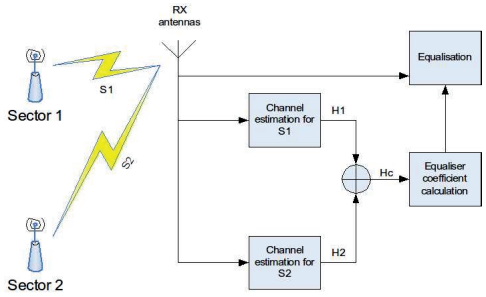

FIGURE 11 HS-SFN receiver architecture

Three main issues in terms of improvement of HS-SFN performance are discussed. The first recognized and tackled challenge with HS-SFN is the maximization of data rate via scheduling, which is discussed in Chapter 2.2.1 and **PV**. The second challenge arises from the estimation of the channels with two serving cells done by the receiver terminal. Receiver enhancement for achieving a more accurate channel estimation is presented in Chapter 2.2.2 based on **PVI**. The third challenge is the mis-alignment of the signal phases at the receiver that can be partially eliminated by precoding at the transmitter. The phase adjustment technique is discussed in Chapter 2.2.3 and published in **PVII**.

In addition to the mentioned subtopics, the following details of the technique are discussed in the contribution papers. First, HS-SFN is limited to the co-operation of cells served by the same NodeB. Compared to inter-site operation, the limitation may actually lead to a suitable power delay profile at the HS-SFN receiver since the distance to both cells remains rather similar, which in turn alleviates the equalizer complexity requirement. Second, the change of

the HS-PDSCH scrambling code imposes a strong interfering power to the assisting cell area, due to superimposed scrambling codes used for data and control channels. This leads to legacy communication as well as channel estimation from CPICH becoming difficult for the users in the assisting cell. HS-SCCH is also affected, and for a successful reception, which is mandatory for HSDPA communication, the power of HS-SCCH needs to be increased to maintain sustainable connections, as described in **PV**.

The UE needs to estimate the channel quality from both cells, then transmit a HS-SFN specific compound CQI, containing information from both cells, to NodeB. The compound CQI reporting is not standardized. However, more information on the report is included in the patent published during the research on CQI signaling with HS-SFN (patent publication number WO 2012136450 A1).

2.2.1 Coordinated Scheduling

HS-SFN transmission occupies two cells simultaneously which directly affects, for instance, interference conditions. The scheduling algorithm is responsible for minimizing any detrimental influence on network's performance by deciding on when the assisting transmission should be scheduled. As the assisting serving cell transmits superimposed signals when used in HS-SFN mode, it will have an elevated impact on the cell measurements performed by its own camped UEs. Therefore the algorithm should consider how much gain HS-SFN transmission can produce compared to inflicted negative influence due to changed interference conditions. Assuming each NodeB in the network controls only a few cells in the same site [2], the algorithm is run by the NodeB and it is capable to assess only the load and user distribution in its own cells.

A scheduling algorithm that covers each cell in the site controlled by the same NodeB is presented in Chapter 3.3. The algorithm maximizes the site-specific performance metric which the NodeB uses to determine the served UEs and the transmission modes of the cells on TTI-to-TTI basis. Each cell will either serve its own UEs in conventional way, assist another cell by transmitting to a UE that is scheduled in the neighbor cell or silence HS-PSCH by HS-DDTx selection. The algorithm uses a combinatorial approach to estimate the performance of each transmission mode and selecting the most efficient one for the TTI.

2.2.2 LMMSE Equalizer Enhancement

Two signal processing methods improving the HS-SFN performance are discussed. The first method, applied in the receiver side, affects the LMMSE equalization, which is used in user terminals later in the simulation part.

A conventional LMMSE estimation of HS-SFN signals may involve elevated inaccuracy, due to the mixture of scrambling codes. An improvement to the equalization algorithm discussed in **PVI** alleviates the issue by taking into ac-

[2] In contrast to remote radios where single baseband unit can control multiple transmitters in different locations.

count the control channel information when minimizing the LMMSE quadrature cost function for data channel reception.

The proposed equalizer algorithm exploits the interfering non-superimposed and thus separable pilot and control channel signals from both serving cells to formulate an estimation of the channel quality. Previous studies on LMMSE equalization with high similarity with the proposed idea, for example in [41], show that the awareness of out-of-cell interference can dramatically improve equalization performance.

2.2.3 Phase Adjustment

The second signal processing method has a resemblance to MIMO precoding with phase modification and related uplink signaling. The HS-SFN phase adjustment scheme performs, according to its name, phase shifting of the transmissions in order to provide coherent, in-phase signal components at the receiver. The scheme can be compared to single-stream MIMO, i.e. Transmit Antenna Array (TxAA), or Dual Stream Transmit Antenna Array (D-TxAA) that 3GPP standardized in *Release 7* as the 2×2 MIMO scheme [42]. HS-SFN phase adjustment, as well as D-TxAA, depends on the precoding weight vector that the UE reports to NodeB in a Precoding Control Indication (PCI) message [43]. In HS-SFN, the vector is taken from a fixed codebook, which is similar to the codebook in closed-loop transmit diversity mode 1 and consists of the following weights that shift the phase by a factor of $\frac{\pi}{2}$ [44]:

$$w \in \left\{ \frac{1+j}{2}, \frac{1-j}{2}, \frac{-1+j}{2}, \frac{-1-j}{2} \right\}. \tag{3}$$

One of the above weights is reported to the assisting cell and applied to HS-PDSCH. Only the data channel is modified by the weight. Furthermore, the primary serving cell's HS-PDSCH remains unaltered.

2.3 Multipoint-to-Point SFN

A Single-Frequency Network refers to wireless communication with a group of sources jointly transmitting the same signal [11]. It was mentioned earlier that in WCDMA systems this is achieved by applying the same scrambling code in each transmitter. In case of HS-SFN, for example, this applies for HS-PDSCH channel.

M2P-SFN, as the name suggests, aims to utilize joint downlink transmissions for delivering user-dedicated data instead of multicasting or broadcasting to multiple receivers. In contrast to HS-SFN, M2P-SFN cells use the same scrambling code also for control and common channels, which ideally dissipates the cell borders. A major advantage of M2P-SFN is that it does not require any modifications to the user terminal nor new Uu interface signaling, but the efficiency of receiving SFN transmission might depend on the receiver and equalizer type. For instance, an extended equalizer filter length allows capturing the channel better

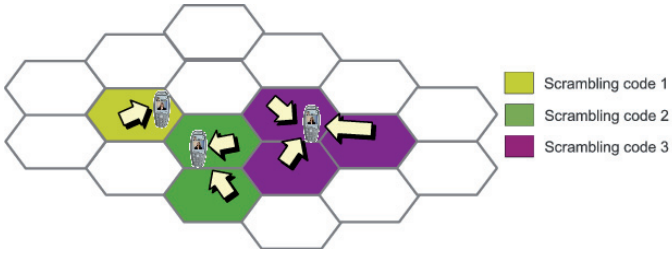

FIGURE 12 Cells dynamically configured in three SFN clusters

than with a short filter length as the delay spread is likely to be longer with a MP2-SFN transmission than with a normal transmission.

The basics of the technique were presented in **PVIII**, together with performance results from a simplified system model. The results presented in that publication were obtained with a stripped simulator that did not cover all the important characteristics of M2P-SFN. In order to evaluate the concept in higher detail, the M2P-SFN study is extended in this dissertation by discussing the issues arising from actual deployment and usage of the scheme.

2.3.1 Clustering of cells

The term *cluster* refers to a group of cells that share the same networking parameters, such as scrambling code and cell ID. Sharing the same parameters allows the cells to transmit the same waveform synchronously. In theory, a cluster can be formed from all cells that are controlled by the central node but in practice the size of the cluster is limited to a few cells. An example of clustering is given in Figure 12, where the clusters are dynamically formed around three UEs.

In an ideal SFN, chip energy from each signal originating from different transmitters in the cluster accumulates at the receiver which increases the SINR. At the same time, the cells that previously interfered with the receiver now turn into contributing transmitters. Assuming all the signals arrive in-phase, the chips will have maximum additive influence. This is illustrated in Figure 13, where SINR is presented in different parts of a hexagonal network with 0, 3, 21 and 57 sectorized cells configured in the same M2P-SFN cluster. The inter-site distance in the figure is 2000 meters.

Two major issues related to efficient M2P-SFN communication are identified which are both related to cluster configuration. First, like with HS-SFN, phase disparity of the received signal components becomes an issue especially now that the clustered cells may reside in different cell sites and at different distances from the receiver. Second, an SFN cluster is formed transparently to the user, meaning that the UEs see only one large serving cell within the cluster area. Each cell in the cluster serves the same UE in one TTI, which means that Time Division Multiplexing (TDM) has to be applied for the whole UE pool within the cluster area. The M2P-SFN gain is therefore fundamentally determined by a trade-off between an improved signal quality and fewer scheduling opportunities per UE.

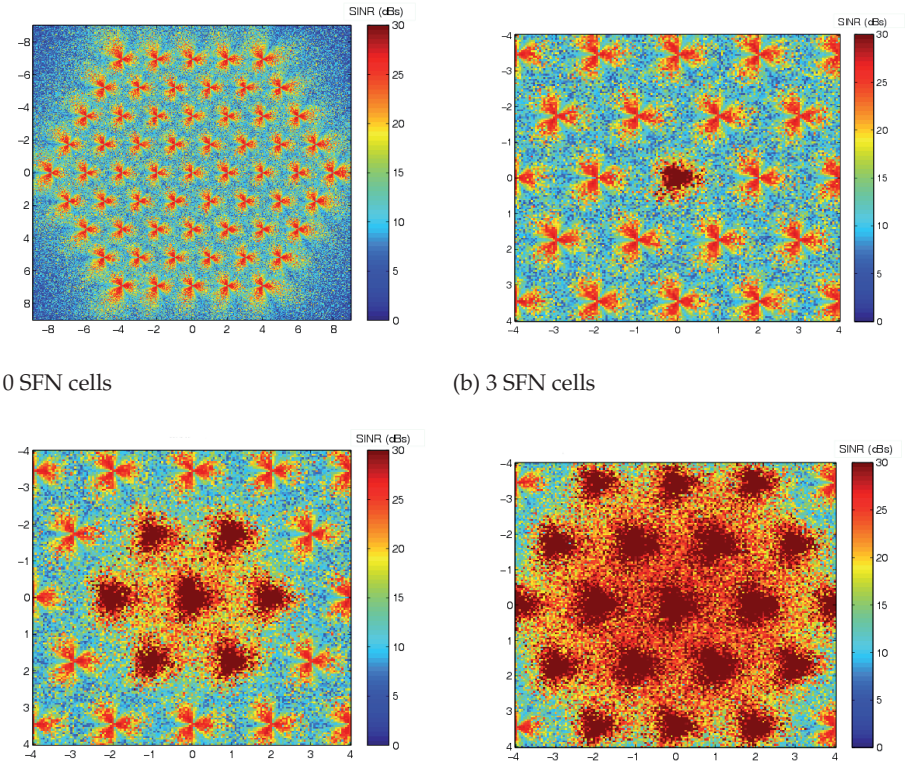

(a) 0 SFN cells

(b) 3 SFN cells

(c) 21 SFN cells

(d) 57 SFN cells

FIGURE 13 Idealistic SINR map with different SFN cluster sizes

Both are affected by the size of the SFN cluster, which is why it is imperative to form the cluster dynamically according to localized traffic demands while taking into account the large-scale effects of cell identity changes. In addition to the accuracy aspect, the cluster update interval should be as short as possible in order to avoid having outdated clusters while UEs move or end or start a call.

The efficiency of M2P-SFN depends on how the clustering is done, and a few practicalities need to be considered when configuring the clusters. The following sections discuss practical issues with regard to deployment of M2P-SFN, including their impact on the clustering. The clustering algorithm that is implemented for the simulations is presented in Chapter 3.4.

2.3.2 Practical Impairments

Although the cluster configuration sounds straightforward, multiple impairments caused by real-life phenomena impact the accuracy and thereby the performance. The fact that the SFN transmitters may reside in different sites means that the signals from those cells may be received at very different times due to propagation delay, as shown in Figure 14. The delay spread affects the perfor-

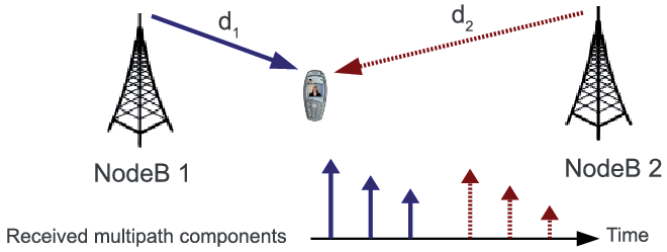

FIGURE 14 Extended delay spread due to propagation distance variation

mance of SFN when a chip-level equalizer is used in the user terminal. Different distances the signals have to travel result also in altered phases of the radio wave as they reach the receiver. Furthermore, a limited receiver equalizer filter length specifies a time window when radio wave can be captured. A large variety in the propagation distances lengthen the impulse response, and, in the worst case, the last signal components expand over the filter length, automatically increasing the interference in the system instead of contributing to the beneficial signal.

Besides their unusual length, the compound channels spanned between the NodeBs with SFN may also consist of an unusual number of weak but still not negligible channel taps. This creates inaccuracy in the DL channel estimation performed by the user terminal and becomes an issue especially with pre-*Release 7* legacy terminals which do not include an advanced channel estimator, for example MMSE.

The clustering is done by the network element that controls each cell in the SFN. In order to conduct an accurate clustering, that network element needs information on the channel qualities between the cells and their terminals. One option to obtain the information is to use periodical cell measurement reports the terminal transmits to RNC, but, since the cells in one SFN cluster are transparent to terminal due to scrambling code reconfiguration, the measurement report would not contain valid information. The granularity of the report might also be insufficient to achieve timely data. A better option, used also in the simulations, is to perform UL measurements by NodeBs, since terminal sends UL DPCCH constantly in every TTI, unless Discontinuous Transmission/Reception (DTX/DRX) is configured. The main problem with the measurements on DPCCH is that the UL channel might not perfectly correlate with the DL channel, thus creating inaccuracy in clustering. In some studies however, [45] for example, the correlation of shadow fading is found to be as high as 0.9. Since path loss usually have a high correlation regardless the direction and since fast fading can be ignored in the long term ([46]), UL-to-DL matching can be assumed to be sufficiently accurate for the SFN clustering.

2.3.3 Effects of Changing Cell Identities

Introducing dynamic SFNs in WCDMA networks, where the cell configuration is changed periodically, may lead to a number of severe issues. All cells par-

ticipating in the SFN scheme transmit exactly the same signals and also apply the same scrambling code. This leads to the fact that UEs are not able to identify separate cells within an SFN cluster anymore, and the changes of scrambling codes in the context of SFN reconfiguration may trigger handovers and cell re-selection procedures when cells where UEs are camped suddenly disappear. The UEs that are forced to make a cell re-selection may also need to perform registration area updates for paging [47]. If SFN reconfiguration is performed often, these issues result in increased signaling as well as augmented battery consumption at the user terminal. This is a problem especially with UEs in the CELL_PCH and CELL_FACH states, since the location update of these UEs is triggered after each cell change. After several cell updates, CELL_PCH may be changed to URA_PCH to reduce the required signaling from the perspective of UE, but it increases network load by additional paging messages. The mobility state changes for idle mode UEs, due to several cell re-selections, may also cause false behavior of mobility management and additional confusion regarding handover triggering threshold tuning on the network side.

Another possibility, which is also used in the corresponding simulations for M2P-SFN, is to reconfigure SFNs at a slow pace in a way that the above issues are alleviated. A slow configuration cycle of course reduces the capability of the system to adapt to changes in user distribution and traffic demands. Depending on the user location and traffic demand fluctuation, the created SFN may become suboptimal for some users until the next reconfiguration cycle takes place. A slowly changing SFN configuration, however, may be a valid choice in rural or sub-urban areas, where the network and traffic conditions remain stable for a longer time. Also, it may be a sound option to introduce fixed SFN patterns that are, for example, used at night time when the system load is known to be low.

A further option is to apply the concept in a multi-carrier HSDPA system where one of the available carriers is dedicated to SFN operation. By the usage of a dedicated carrier, it is possible to avoid the problems stated above since one carrier would be used as an anchor carrier guaranteeing connectivity and mobility of all devices, whereas SFN may be configured rapidly to improve the performance of certain users on the other carrier. In this study, however, the simulations are limited to single-carrier network, although similar gain levels can be expected if a dedicated carrier is used.

2.4 Summary

It has become obvious that special caution has to be exercised when designing resource allocation for MPTx techniques. Not only can a good design explicitly improve user throughput, but there can be several indirect positive consequences that efficient allocation can produce. For example, Multiflow enables load balancing between the cells and thereby releases system resources to other users. Accurate resource allocation is also mandatory with SFN-based methods, where

imprecise decisions may strongly reduce the system performance.

Resource allocation is often conceived as a method for sharing physical layer resources, but it also takes place in upper layers. Flow control in the RLC layer with Multiflow dictates the achievable throughput gain by estimating the data rates from the serving cells towards the user terminal and using that estimation to allocate new data to cells. An accurate flow control algorithm allows avoiding under-runs or extensive over-run situations that may produce a throughput penalty. A different flow control operation that relies on duplication of data to Multiflow cells instead of splitting may also be used for connections that have QoS dependent data. In such case, it is possible to let cells decide which one of cells has a better channel towards the UE and which one should transmit the PDU. This is made possible by the compound HS-DPCCH format specifically designed for Multiflow in Release 11.

It was discussed that especially SFN-based techniques are sensitive to signal transformations that occur in the air interface. Furthermore, when HS-SFN or M2P-SFN is used and cells transmit the same signal to the user, phase variation of the signal components may reduce or even eliminate the cumulative chip energy at the receiver. Possible enhancements for the transmitter and the receiver which aim to alleviate the air-interface issues with regard to HS-SFN operation were discussed.

The use of SFN-based methods influences the system by altering cells' identities via scrambling code changes and can cause confusion in mobility control. Changing the scrambling codes inevitably modifies the interference conditions in the network and may trigger extensive number of handovers. This increases signaling load and user terminal's battery consumption in addition to causing possible changes in network's mobility control parameters. Methods that are available for avoiding these issues, especially for M2P-SFN, were discussed.

As a conclusion, to maximize the benefit from MPTx and to minimize possible problems requires accurate design in the transmitter and receiver architectures. Also a pervasive system-wide planning is required to decide where and how multi-cell operation can be used.

3 SIMULATION RESULTS

The remainder of the dissertation presents solutions for the discussed issues and investigates their impact on the performance of each MPTx scheme. In order to understand the results and their validity, a detailed description of the simulation environment is given first.

3.1 Simulation Models

This chapter explains some of the most important properties of WCDMA and HSPA that influence MPTx. A description on how they were modeled in the simulator is also given. All simulations were executed on the same simulator environment; thus, regarding the main simulation features, the reader may refer to this chapter later in the thesis.

3.1.1 Overview of the Simulator Environment

A cell-based quasi-static network system simulator is used for modeling the HSDPA environment. The same simulator was used for preparing results for several 3GPP contributions before and simultaneously with this research. The features of the simulator have often been implemented according to well known models, and the functionality has been calibrated internally and against the results obtained from other 3GPP companies.

System simulations allow verification of network operations over a wide geographical area covering a large part of the network. Such simulations also reveal possible indirect implications in a wider scale if one part of the network is influenced by a certain phenomena. For example, if load balancing is applied around a highly congested area of the network, it will likely affect several tiers of the neighboring cells in some way. A downside of system simulations is that they may lack very detailed modeling of certain processes, a modeling that could be done with link level simulators. Including such models in a wider system

TABLE 2 Main simulation parameters

Parameter	**Value**
Cell Layout	Hexagonal grid, 19 NodeBs, 3 sectors per NodeB with wrap-around
Inter-Site Distance	1000 m
Carrier Frequency	2000 MHz
Bandwidth	5 MHz
Chip Rate	3.84 Mcps
Path Loss Model	L=128.1 + 37.6log10(R), R in kilometers [50]
Penetration Loss	10 dB
Log Normal Fading Standard Deviation Inter-NodeB Correlation Intra-NodeB Correlation De-correlation Distance Max BS Antenna Gain	 8dB 0.5 1.0 50m 14 dBi
2D Antenna Pattern	$A(\theta) = -min(12(\theta/\theta_{3dB})^2,\ Am)$, where $\theta_{3dB} = 70\ degrees,\ Am = 20dB$
Channel Model	ITU PedA 3 km/h, PedB 3 km/h, VehA 30 km/h
CPICH Ec/Io	-10 dB
UE Antenna Gain	0 dBi
UE Noise Figure	9 dB
UE Receiver Type	Type3 or Type3i, 2 Rx LMMSE equalizer
HS-PDSCH Spreading Factor	16
Maximum Sector Tx Power CPICH Transmit Power	43 dBm 10 %
Number of HARQ Processes	6
CQI	Ideal with 3 TTI delay

would become too costly with regard to simulation time, therefore simplified approaches are often used to keep the simulation time reasonable while still achieving reliable results. Information obtained from link level simulators is often used in system simulations by some type of link-to-system mapping to improve the accuracy of the simulations without incurring a high computational cost [48].

The model used introduces 7 or 19 NodeBs, each having three 120 degree sectors. Simulation parameters common to each study subject are introduced in Table 2, which mainly follows the assumptions defined by the 3GPP standardization [49].

For most simulations, users remain stationary during the simulation, although slow fading depends on the user's location and varies according to a log-normal distribution. Fast fading is modeled by reading fading values from an external trace file. For the study **PIV** focused on, the simulator was extended to support dynamic capabilities. The implemented mobility control for that study supports handover process by including handover timers, such as Time-to-Trigger (TTT), and signaling and processing delays, allowing realistic channel quality deterioration prior to a handover. The mobility model is required when evaluating the pre-handover communication, which usually can be unreliable due to high

signal attenuation and elevated interference.

In a hexagonal cell based scenario, the handover regions are formed quite monotonously between the cells' beam coverages. It is observed that, when a 6 dB handover margin is enabled, approximately 9 % and 36 % of the cell's users reside at softer and soft handover (HO) areas, respectively. The softer HO region is the border area between two sectorized beams originating from two cells that are controlled by the same NodeB, whereas the soft HO region is formed between cells that are controlled by different NodeBs with a significant geographic separation[1]. The users within the handover area are the primary targets for multipoint services. Nevertheless, it depends on the MPTx scheme which users are actually served from multiple cells.

Only the downlink part of the network is accurately implemented. Uplink related operations, such as transmission of HS-DPCCH, are realized by using static or simple statistical models to account for signaling delays or UL channel measurements.

3.1.2 Wraparound Model

A wraparound model for signal propagation is an essential part of confident simulations where simulated network is replicated around the center simulation area, as illustrated in Figure 15. The wraparound model allows creating logical copies of the transmitter or the receiver node and the link between them in the main area as well as in each of the replicated areas. From among these logical links the strongest is chosen as the effective one to be used between the transmitter and the receiver. The propagation calculation with wraparound is done for serving and interfering cells alike; thus a realistic interference level is offered also at the borders of the main area.

Regarding the user mobility with wraparound in **PIV**, a simple approach was taken where the user, upon reaching the border of the area, turns 180 degrees and continues moving with a mirrored trajectory. A more accurate mobility wraparound model would, for example, transit the UE, upon it leaving the main area, to the opposite side of the main area that matches the location where the user would move in the replicated network. Nevertheless, the simple model was deemed adequate for the studies.

3.1.3 Link Adaptation and AVI Tables

Link adaptation in HSDPA covers the selection of MCS for rapidly changing channel conditions [51]. It is based on the CQI report from the UE, which composes the report based on the received signal level on the CPICH. An example of channel measurement and MCS selection is illustrated in Figure 16.

CQI is a discrete index value, a logical representation of the maximum data rate that can be achieved with a given block error rate (BLER). The MCS, and further the transport format and resource combination (TFRC) in the figure, are

[1] Soft HO is often abbreviated as SHO.

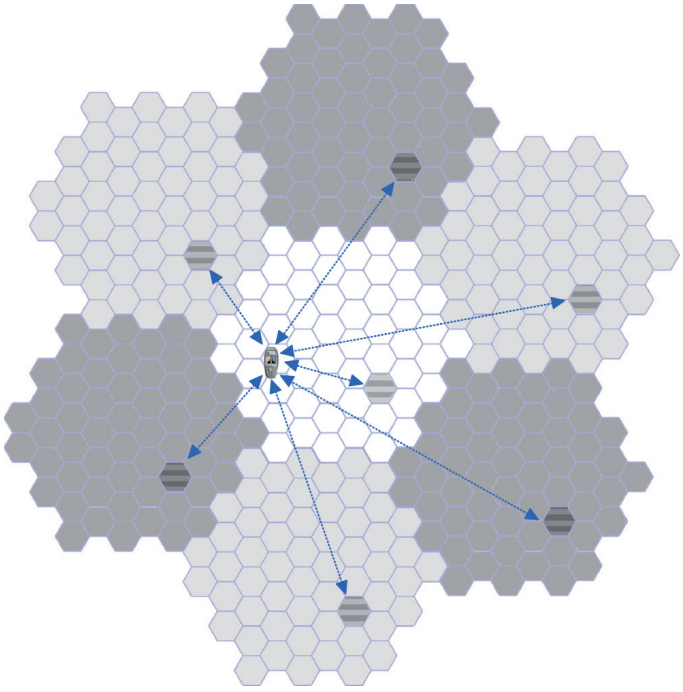

FIGURE 15 Wraparound network layout with seven link candidates between a UE and a cell

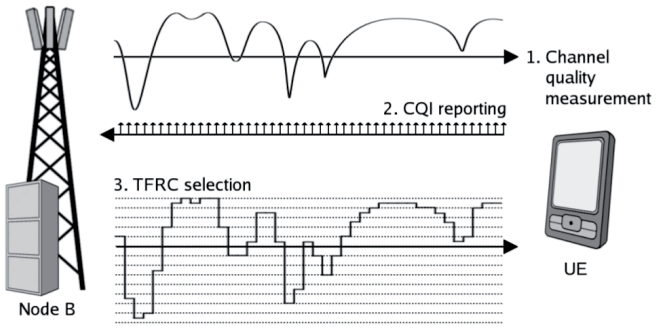

FIGURE 16 Discrete mapping of channel quality to transport block format [52]

then chosen based on the CQI-to-MCS mapping.

In the simulator employed, link adaptation, as well as the block error calculation, are based on an Actual Value Interface (AVI) lookup, in which accurate information obtained from a link level simulator is exploited [53]. Regarding link adaptation, the MCS is selected based on the CPICH SINR and AVI tables. In addition to MCS, the link adaptation determines the number of OVSF codes that can be reserved for the transmission. When decoding the packet, the AVI lookup is performed for the used MCS after the HS-PDSCH SINR is calculated as described in Chapter 3.1.4 and Chapter 3.1.5. In other words, the HS-PDSCH SINR

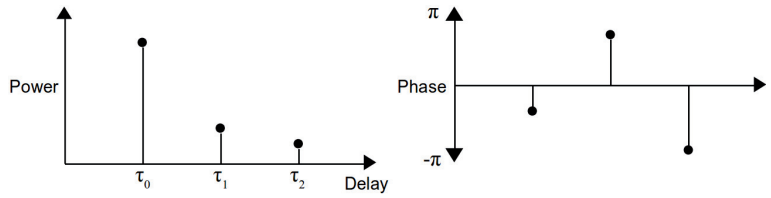

FIGURE 17 Power and phase of received multipath components

is matched to the block error probability of a given MCS.

3.1.4 Signal Model

After the signal has left the transmitter, it encounters several obstacles, such as buildings and various forms of terrain, as it propagates. The attenuation caused by them is called shadow (or slow) fading. In addition to attenuation caused by the obstacles, the signal is subject to reflections, scattering and other characteristics of radio wave which may cause the signal to disperse and travel along different paths. This is called fast fading: multipath components reach the receiver at different times, creating a received power delay profile. The components of the profile are known as taps, which represent the energy and phase of the signal copies (Figure 17). The multipath components often partially overlap with each other in time domain. At the receiver, the energy of the overlapping taps is combined. Depending on the phases of the taps, combining can be either additive or destructive, and in the worst case the taps can even eliminate each other. In conventional single-link communication, there is often one dominant multipath component which reduces the effect of any destructive combining. However, in single-frequency based multipoint communication, the phase-offsets may present a significant issue with non-zero cross-correlation between multiple strong signal elements. Thus it is essential to include the power delay profile in the model. Fast fading is modeled by obtaining values from a pre-constructed trace file.

The signal model presented below is a mathematical approach to introduce the discussed multipath propagation and its implications. As explained in [54], the received chip sequence can be expressed as

$$\mathbf{r}(m) = \mathbf{H}^T \mathbf{s}(m) + \mathbf{n}(m), \tag{4}$$

where $\mathbf{s}(m)$ is the transmitted signal

$$\mathbf{s}(m) = [s(m+F+L-D), \ldots, s(m), \ldots, s(m-D)]^T \tag{5}$$

and $\mathbf{n}(m)$ is the noise vector. In (5), D represents the delay variable ($0 \leq D \leq F$) and L is the delay spread of the channel, normalized to the chip interval. F denotes the linear filter length in the receiver. The $(F+L) \times (F \times N_{Rx})$ sized

channel matrix

$$\mathbf{H} = \begin{bmatrix} \mathbf{h} & 0 & \cdots & 0 \\ 0 & \mathbf{h} & \cdots & 0 \\ \vdots & \vdots & \ddots & \vdots \\ 0 & 0 & \cdots & \mathbf{h} \end{bmatrix}^T, \tag{6}$$

represents the convolution of a transmitted chip sequence and the channel impulse response originated from a single cell. The channel impulse response matrix

$$\mathbf{h} = \begin{bmatrix} \mathbf{h}_0(0) & \mathbf{h}_0(1) & \cdots & \mathbf{h}_0(\tau) \\ \mathbf{h}_1(0) & \mathbf{h}_1(1) & \cdots & \mathbf{h}_1(\tau) \\ \vdots & \vdots & \ddots & \vdots \\ \mathbf{h}_{N_{Rx}}(0) & \mathbf{h}_{N_{Rx}}(1) & \cdots & \mathbf{h}_{N_{Rx}}(\tau), \end{bmatrix} \tag{7}$$

expresses the impulse responses for each receive antenna at delayed time instances, where τ is the delay spread of the signal. In the simulations, the number of receiver antennas at the UE terminal (N_{R_x}) is two, while each cell transmits with single antenna. For single-frequency based transmissions, $\mathbf{H}$ is replaced by a compound channel matrix $\mathbf{H}_c$ that takes into account all cells jointly transmitting the same signal:

$$\mathbf{H}_c = \sum_{i=0}^{N_{SFN}-1} \sqrt{\frac{L_i P_i}{L_0 P_0}} \mathbf{H}_i, \tag{8}$$

where L_i represents the shadow fading and path loss from cell i to UE, P_i the transmission power of the same cell and $i = 0$ the primary serving cell of the UE.

Three different channel models were used in the simulations. The difference between them is with the power delay profiles as shown in Table 3. The profiles are modified versions of those given in [55].

TABLE 3 ITU channel model power delay profiles

	Pedestrian A		**Pedestrian B**		**Vehicular A**	
Tap	Delay (chips)	Power (dB)	Delay	Power	Delay	Power
1	0	0	0	0	0	0
2	1	-12.77	1	-2.8	1	-1.92
3	-	-	3	-5.97	2	-7.31
4	-	-	4	-11.43	3	-10.39
5	-	-	5	-10.91	4	-10.89
6	-	-	9	-9.35	-	-

3.1.5 Type 3 and Type 3i receivers

3GPP has studied the performance of different types of advanced receivers for HSPA with multipath interference canceling capabilities [56, 57]. The main types are listed in Table 4 [58, 7]. User terminals with both Type 3 and Type 3i chip-level

TABLE 4 Main 3GPP receiver types for HSPA

Type 1	Rx diversity with RAKE receiver
Type 2	Single antenna channel equalizer
Type 2i	Type 2 with interference awareness
Type 3	Rx diversity with channel equalizer
Type 3i	Type 3 with interference awareness

linear minimum mean squared error (LMMSE) equalizers are deployed in the simulations to mitigate the effect of Multiple Access Interference (MAI). MAI is observed when the orthogonality of the WCDMA signal is lost due to frequency-selective channel and the objective of the LMMSE receiver is to try to restore the orthogonality [52, 59]. An essential part of LMMSE is the calculation of the filter weight, w, which tries to maximize SINR with the obtained signal and interference matrices.

In single-frequency based simulations, Type 3 receiver is utilized in order to maximize the benefit from transmissions with macro-diversity. Multiflow, in which the parallel serving streams do not share physical layer parameters, achieves the best gain with a Type 3i receiver since the inter-cell interference can be minimized.

For Type 3 receiver with receive diversity, the weight w is calculated as follows [40]:

$$\mathbf{w} = \mathbf{C}_w^{-1}\mathbf{H}^H(\mathbf{H}\mathbf{C}_w^{-1}\mathbf{H}^H + \mathbf{I})^{-1}\delta_D. \tag{9}$$

Here, δ_D is a $\tau + F$ sized delay vector, where F denotes the length of the linear filter in the receiver, τ represents the previously mentioned delay spread and $\mathbf{C}_w$ is a $(F + N_{Rx}) \times (F + N_{Rx})$ sized interference matrix that represents the total downlink interference from the network, thermal noise and cell-specific interference after multipath propagation [54].

The Type 3i receiver tries to cancel the inter-cell interference with the knowledge of the strongest interferer cells. The weight calculation is done as

$$\mathbf{w} = \mathbf{C}_{rr}^{-1}(\mathbf{M_0})^{\mathbf{H}}\delta_D, \tag{10}$$

which utilizes an inverse of the covariance matrix $\mathbf{C_{rr}}$ to cater for the known interference from nearby cells. $\mathbf{M_0}$ contains channel impulse response matrices from each of the receive antennas. Details of the calculations can be found in [56] and [40].

The Carrier-to-Interference-plus-Noise ratio (C/I) of the signal can be calculated as

$$C/I = \frac{P_{0,HS\text{-}PDSCH} \cdot \left|\mathbf{w}^T\mathbf{H}^T\delta\right|^2}{I_{MAI} + I_{col} + I_{thermal}}, \tag{11}$$

where the denominator consists of MAI (12), colored inter-cell interference (13) and thermal noise (14):

$$I_{MAI} = \mathbf{w^T}\mathbf{H^T}\delta'\mathbf{H}^*\mathbf{w}^*, \tag{12}$$

$$I_{col} = \sum_{i=1}^{N_{cells}} P_i \mathbf{w}^{\mathbf{T}} \mathbf{H}_{\mathbf{i}}^{\mathbf{T}} \mathbf{H}_{\mathbf{i}}^{*} \mathbf{w}^{*}, \tag{13}$$

$$I_{thermal} = \mathbf{w}^{\mathbf{T}} \mathbf{C}_{thermal} \mathbf{w}^{*}. \tag{14}$$

δ' in (12) represents a $F \times F$ diagonal matrix

$$\delta' = \mathrm{diag}([\ 1 \quad \cdots \quad 1 \quad 0 \quad 1 \quad \cdots \quad 1\ ]). \tag{15}$$

P_i in the above equations refers to received signal power from the ith cell. The obtained C/I is finally matched to an AVI table containing the BLER values for different MCSs, as described earlier. More detailed information on the C/I calculations can be found in [52].

3.1.6 Modeling Extensions for M2P-SFN

The simulator is extended for M2P-SFN simulations with the features discussed in Chapter 2.3.2: propagation delay model, introduction of imperfect channel knowledge at the user terminal and DL-to-UL matching for channel estimation done by the NodeB.

User terminals in the M2P-SFN simulations utilize Type3 receivers with an LMMSE equalizer and receiver diversity with two receive antennas. The equalizer filter length here (τ) is 10 taps. The time between two taps is derived from the chip duration in WCDMA and equals

$$\Delta t_{tap}[s] = \frac{1}{3.84\ \mathrm{Mcps}}. \tag{16}$$

Thus, the maximum distance difference between two NodeBs that may transmit the same data and improve the received signal is

$$d_{max} = c \cdot \Delta t_{tap} \cdot \tau \approx 768\ \mathrm{meters}, \tag{17}$$

where c is the speed of light. Although there is a fairly short maximum allowed distance spread between the closest and the furthermost NodeB, it is likely that the signals from distant cells will be subject to high attenuation and therefore the 10 tap limit in the equalizer will not become influential. The cells transmitting beyond the maximum supported distance automatically produce interference at the receiver.

Imperfect channel estimation is modeled by adding zero-mean and Gaussian errors to the compound channel matrix before calculating the receive filter as in (9). The variance of the estimation error depends on the tap index j and receive antenna t and is given by

$$\sigma_t^2[j] = \frac{1}{P_{pilot} L_{corr}} \left(P_{tot} \sum_{k=0, k \neq j}^{L} |\mathbf{h}_t[k]|^2 + \sum_{n=1}^{N_{cell}-1} [\phi_n^{\mathrm{real}}]_t + \sigma^2 \right), \tag{18}$$

where p^{pilot} is the absolute pilot power transmitted by each cell and L_{corr} is the length of the pilot sequence multiplied by the number of consecutive pilot symbols used for channel estimation. The first term inside the parentheses represents

the fact that the spreading codes used for pilot transmission have a non-zero auto-correlation, meaning that a correlator-based channel estimation is subject to systematic inter-tap interference. In (18), this is modeled statistically by summing the power of all other channel taps multiplied with the overall transmit power per cell p^{tot}, as the error originates from pilot, control and data transmission in neighboring symbols. The second term introduces the impact of inter-cell interference to channel estimation, which is done by calculating the absolute interference covariance from cell n as observed by the terminal. $[\phi_n^{\text{real}}]_t$ refers to the diagonal elements of the covariance matrix and reflects the interference variance at terminal antenna t.

An uplink channel is not explicitly implemented in the simulator. Instead, uplink large-scale channel properties having a certain correlation with the actual downlink channels are randomly generated. In fact, as already covered in Chapter 2.3.2, it is enough to consider differences in shadow fading between UL and DL. The shadow fading correlation level between the channels can be up to 0.9, which is the value used in the simulations. The calculation of the UL shadowing based on the DL counterpart γ_{dl} is done as follows:

$$\gamma_{ul} = r \cdot \gamma_{dl} + \sqrt{1 - r^2} \cdot X \cdot \sigma, \tag{19}$$

where r denotes the correlation factor mentioned above, X is a normally distributed random variable and σ the standard deviation of the shadow fading.

3.2 Multiflow

The throughput gain obtained with Multiflow, compared to conventional communication, is determined by the network load and channel imbalance, as shown in Figure 18. According to the figure, the average throughput (burst rate) improvement by SF-DC Multiflow with ideal flow control can be up to 50 %. Multiflow does not impose penalty to non-Multiflow users that cannot utilize the additional data flow since the scheduling guarantees that assisting Multiflow transmission never blocks a cell's primary UEs from being served. The primary negative effect that Multiflow creates is the additional interference from the assisting cell. Occasionally, however, having constant transmission from the strong interferer might in fact stabilize the SINR level and therefore improve the accuracy of link adaptation.

Table 5 shows how the average temporal utilization rates of cells change after enabling Multiflow, indicated by the *Cell utilization rate* column. The table is showing results for low to high network loads with the per-UE load being approximately 200 kbps. According to [60], a white paper published in 2012, an average cell utilization rate over a 48-hour period in real HSPA network approximately matches the results with four UEs/cell in the table. With such network load, the cells are transmitting on average only in 12 % of TTIs without Multiflow and 14.4 % with Multiflow. This indicates that the spectral efficiency in an average

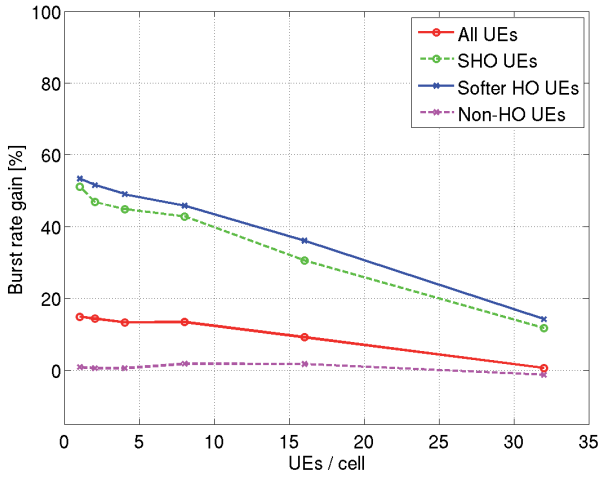

FIGURE 18 Throughput gains with Multiflow, 200 kbps/user traffic load, PedA channel model, Type 3i receiver

TABLE 5 Utilization rates of cells and Multiflow links

	Cell utilization rate [%]		Utilization of Multiflow links [%]	
UEs/cell	**Reference**	**Multiflow**	**Primary link**	**Assisting link**
1	4.4	4.3	97.9	96.5
2	6.6	7.2	95.9	92.8
4	12.0	14.4	91.7	84.8
8	25.6	31.2	81.5	68.0
16	59.6	68.3	54.9	30.7
32	97.6	99.6	9.7	0.2

network can be significantly improved by utilizing assisting traffic flows. In fact, according to the table, SF-DC Multiflow is explicitly increasing the cell utilization until the saturation point. The *Utilization of Multiflow links* column in the table shows average percentages of TTIs when data is transmitted over primary and assisting traffic streams when Multiflow is enabled. The activity is defined as the ratio between scheduled TTIs and the TTIs when the stream could be scheduled, i.e., when there is data in the transmission buffer. Surprisingly, the assisting serving cell can serve the user with significant granularity also at higher loads. For example with a mediocre load of 16 UEs/cell, the user can be scheduled over the second traffic flow in 30 % of the schedulable TTIs. This basically leads to efficient load-balancing that also implicitly helps other users by freeing cell's resources.

3.2.1 Flow Control

Ideal RLC layer flow control was assumed in the results shown in the previous chapter, which means that both primary and assisting cells have access to a common transmission buffer. In reality though, it is the RNC that has to provide the

data to NodeBs according to NodeB's requests. The accuracy of the request then defines how efficiently Multiflow can be utilized, since with too small a request the cell's buffer may become empty although it could still transmit and too large a request results in a prolonged file transmission. These two conditions are called buffer under-runs and over-runs. In order to avoid them, cell needs to estimate how many user-specific RLC PDUs it can transmit in the next flow control period and send the request to the RNC accordingly. This was explained in higher detail in Chapter 2.1.1.

In this work, the estimation is based on a UE-specific target buffer, which stores the actual amount of data transmitted in previous TTIs. The overall flow control algorithm, which is later used with the simulations, works as follows:

- In the beginning of the call a same (moderate) number of PDUs is delivered to primary and assisting serving NodeBs. It is best to avoid over-filling the buffer in the beginning without prior knowledge of the channel conditions, thus the buffers are filled with 33 % of the maximum capacity that could be transmitted within the duration defined by the target buffer length.
- Target Buffer (TB), residing in the NodeB and measured in TTIs with a parameter Target Buffer Delay (TBD), is updated in every TTI. Each entry in the TB contains the number of bits that was transmitted in previous TTIs. It will be observed that the TBD should be longer than the flow control period in order to have protection against under-runs.
- NodeB calculates the residual PDU capacity in the transmission buffer by summing up the bits in the whole TB and comparing the result to current transmission buffer size. The remainder determines the number of new PDUs the NodeB requests from the RNC at next flow control period.

Figure 19 depicts the effect of different flow control periods and accordingly changing TBD. The handover margin for Multiflow is set to 6 dB and the RLC PDU size is 1250 bytes. Other parameters match those given in the previous section and Table 2. The CDF presents throughputs from the cell-edge Multiflow users. By allowing more frequent PDU requests, the NodeB is effectively able to minimize over-runs and under-runs. A drawback is an increased Iub signaling load, which is the main reason that prevents even more frequent requests. Using a longer flow control interval, changing air interface conditions may lead to empty buffer before it can be refilled in the next period. The presented 10 TTI flow control period provides a good trade-off between the accuracy and moderate signaling load.

In addition to flow control interval, the performance of the discussed flow control algorithm is dependent on TBD, impact of which is presented in Figure 20. It can be observed that a longer TBD can guarantee the avoidance of under-runs. Nevertheless, long TBD is often not the best option since the PDUs may reside in the buffer for extensive time periods. For instance with delay-sensitive data, this would definitely introduce QoS issues. The effect is even more present in highly mobile environments, where channel quality may deteriorate fast. Regarding Multiflow, this may even lead to a certain level of starvation if the UE is

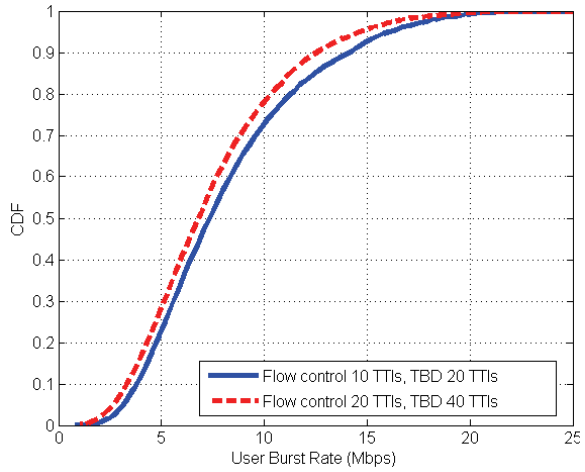

FIGURE 19 Impact of flow control frequency on user throughput

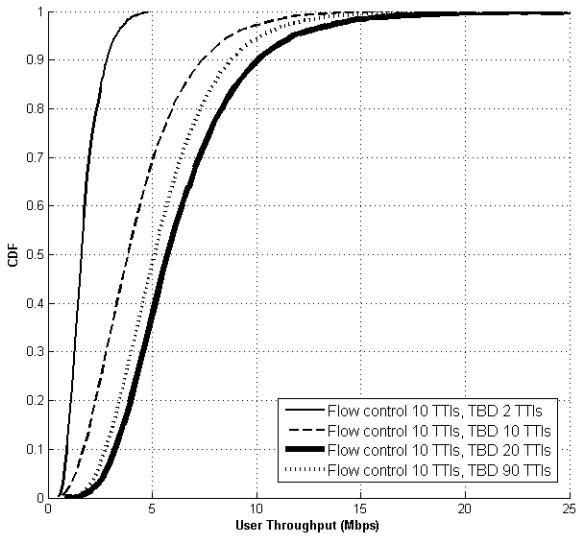

FIGURE 20 Impact of target buffer delay on user throughput

continuously scheduled only from the better cell while there still remains data in second cell's buffer. At least spectral efficiency will be reduced if the 'worse' serving cell is forced to transmit the remaining buffered packets to avoid starvation. Therefore, from the presented set of TBDs, 20 TTI length, i.e. double the length of the flow control period is providing the best result.

3.2.2 Split Control

Flow control defines how many PDUs are sent to each serving cells, while split control refers to in which order PDUs are sent to them. The need for split control

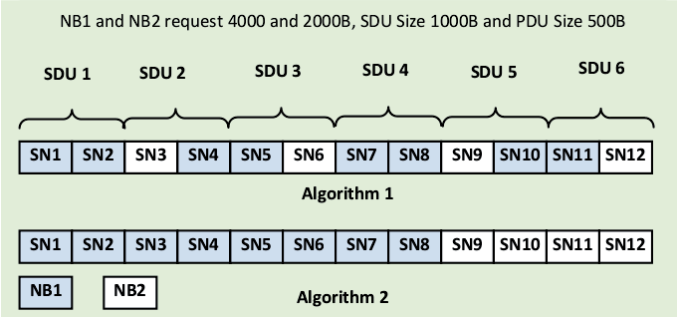

FIGURE 21 PDU split control example for Multiflow

was explained in Chapter 2.1.2. Three split control algorithms are evaluated:

1. PDU distribution ratio between the primary and the assisting serving cell is determined linearly by the cells' reported capacity allocations that are based on the flow control algorithm. Weighted Round Robin is then applied to allocate PDUs to both cells based on the ratio. The absolute number of subsequent PDUs allocated to a cell depends on how many PDUs form one logical Service Data Unit (SDU) block.
2. Based on the cells' capacity allocations, PDUs are first allocated in order to primary serving cell until its capacity is fulfilled. After that the allocation is done for the assisting serving cell.
3. Similar to Algorithm 1, except the weight for the primary serving cell is squared. This algorithm is less dependent on the assisting serving cell, which is an advantage in case the cell becomes occupied by its own UEs, possibly blocking the assisting Multiflow stream.

An example of distribution differences with Algorithms 1 and 2 is given in Figure 21. In the example, the primary serving cell (NB1) has two times higher estimated capacity than the assisting serving cell (NB2). Thus the distribution ratio with Algorithm 1 is 2:1 that is used with both algorithms.

The algorithms are evaluated by the amount of *negative* skew they produce and by the number of additional RLC layer retransmissions. As explained in Chapter 2.1, *negative* skew occurs when two consecutive PDUs are received in disorder. The skew reflects how delayed is the PDU transmission from one buffer compared to another and may, if extensive enough, trigger an RLC layer retransmission. In a reference system without Multiflow, skew occurs due to HARQ retransmissions and is usually very small and it was observed in the simulations to stay below 20 ms. Table 6 shows how big portion of PDUs have skew longer than 50 ms and 200 ms, which are typical values for HARQ T1 timer and *Release 11* RLC reordering timer, respectively, although the values are implementation specific. In case of Multiflow, an expired RLC reordering timer triggers a PDU retransmission. Increase of the RLC layer retransmissions are given in Table 7. The reference is a simulation without Multiflow. In the reference system HARQ can eliminate almost all RLC layer retransmissions. With Multiflow, a few retrans-

TABLE 6 Skew probability

	Flow control algorithm		
Skew	**Algorithm 1**	**Algorithm 2**	**Algorithm 3**
> 50 ms, 1 / 4 UEs/cell	0.4777 % / 0.5806 %	0.4163 % / 0.4784 %	0.4144 % / 0.4825 %
> 200 ms, 1 / 4 UEs/cell	0.0015 % / 0.0060 %	0.0024 % / 0.0053 %	0.0020 % / 0.0070 %

TABLE 7 Increase in RLC layer retransmissions with realistic flow control

	Flow control algorithm		
Load level	**Algorithm 1**	**Algorithm 2**	**Algorithm 3**
1 UE/cell	170 %	184 %	177 %
4 UE/cell	247 %	235 %	262 %

missions are triggered by the skew. Since a retransmission in the reference case is an extremely rare situation, the relative percentages seem very high with Multiflow, even though the probability to exceed 200 ms skew, as shown in Table 6, is also very small. Nevertheless, none of the algorithms provide distinctively better results over other algorithms. However, taking into consideration that Algorithm 3 is least dependent on the assisting serving cell and its traffic condition changes, it may provide the best performance especially in highly mobile network conditions. The results show that in general it is important to design the flow control and receiver (timer) configurations such that excessive skew and unnecessary RLC layer retransmissions can be minimized as the retransmission is always a rather undesired operation due to resulting signaling load and delay extensions.

3.2.3 RLC Layer Bicasting

As explained in Chapter 2.1.3, bicasting covers the scenario where the same data is delivered from both cells, or only from the conditionally selected *best* Multiflow cell, in order to increase the probability of correct reception of PDUs. A simple PDU duplication algorithm was used in **PIII** that consumes excessive amount of cell's resources, especially since each PDU was transmitted from both cells, often without a need for such robustness. Two objectives were identified with regard to efficient voice service with Multiflow:

- Minimize the power used for transmitting a PDU related to voice traffic.
- Avoid double transmission of the same packet over PHY layer.

This section presents a conditional bicasting approach that allows a duplication-free PHY layer PDU transmission only from the instantaneously best serving cell.

It was discussed in Chapter 2.1.3, that with constant low data rate communication power control can replace AMC to some extent. The implemented power control mechanism adjusts the transmission power of the cell according to the Channel Quality Indication (CQI) message obtained from the UE. To fulfill the objective of power minimization and to enable a singleton PDU reception, a method is used where the RNC duplicates the PDUs to both cells and the cells

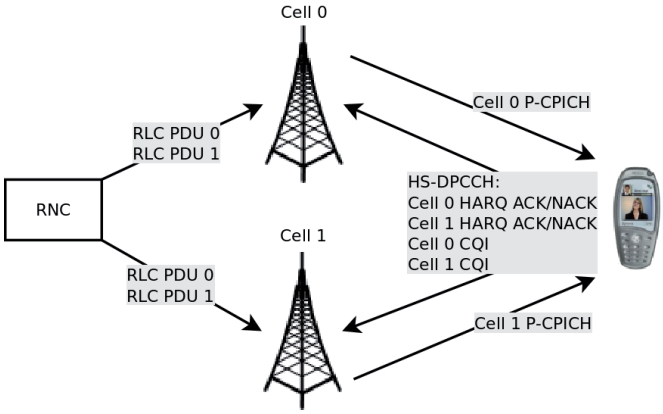

FIGURE 22 PDU duplication and composite HS-DPCCH

decide whether they should transmit the PDU to UE. The method is depicted in Figure 22. Multiflow utilizes so-called composite HS-DPCCH reporting, which alleviates the cell's decision making on whether is should transmit the packet. When configured with Multiflow, a UE includes CQI and Hybrid Automatic Repeat Request (HARQ) information for both data flows in a single HS-DPCCH message which is received by both primary and assisting cells, resembling channel quality reporting with Dual-Cell HSDPA and MIMO [61, 62]. In fact, Multiflow re-uses the previously defined HS-DPCCH format and just changes its usage logic suitable for multi-cell reporting. Upon decoding the message, both cells obtain not only the information of their own channel but also of the neighboring channel. This, in fact, enables the above-mentioned power control that is dependent on the CQI information, also in the assisting serving cell. As both cells have access to the same information on both channels, they may apply similar calculations at the point when they receive a PDU from the RNC and accordingly drop or enqueue the PDU.

Upon decoding the HS-DPCCH from UE n, the cell (primary or assisting serving cell) calculates the relative quality of the serving channels by

$$\Delta r_n(l) = r_{n,0}(l) - r_{n,1}(l). \tag{20}$$

l denotes the TTI number, $r_{n,i}(l)$ the transport block size according to the CQI report and $i = \{0, 1\}$ refers to the primary and assisting serving cells. In addition to the relative quality, the cells trace the trend in both cells' channel slopes. In case the absolute channel qualities are similar, the preferred cell to transmit the PDU has an increasing channel slope, which means that the channel is likely improving in coming TTIs. The slope calculation is based on linear estimation from the two latest reports as

$$m_{n,i}(l) = r_{n,i}(l) - r_{n,i}(l-1). \tag{21}$$

Since the CQIs are already based on filtered measurements, two reports are adequate for making the estimation. Moreover, forming the estimation from short time period allows better accuracy in terms of following the effects of small scale

fading. In case the superiority of the cells cannot be distinguished from the slopes, the primary serving cell will transmit the PDU.

As a side note, making the decision at NodeB on whether it should transmit a PDU could be applied to split control Algorithm 2. that was presented in Chapter 3.2.2. In fact, moving the responsibility from RNC to NodeB could be used to minimize the skew and imperfect buffer fills that are somewhat inevitable when RNC splits the data.

AMR 12.2 kbps voice traffic model is used for the evaluation. Figure 23 shows the CDF of power that is used for voice data transmissions. The evaluation was done with simulations where terminals were uniformly distributed over the network. Terminals move either with the velocity of 3 km/h (PedA) or 30 km/h (VehA). Type 3i with receive diversity is again utilized in the terminal receivers. As a result of conditional bicasting, the average required power can be reduced

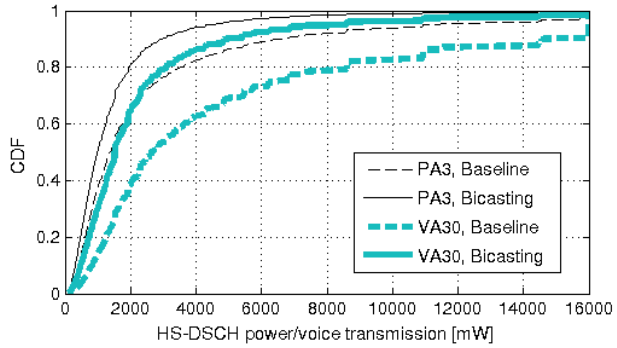

FIGURE 23 Aggregate HS-PDSCH and HS-SCCH power allocated for voice transmission in HO region

approximately by 50 % from the baseline single-cell operation. This is due to both cells being able to adapt to varying channel conditions fast enough. Average residual cell throughput levels are given in Figure 24. They are also improved by up to 25 % depending on the number of voice users in the network

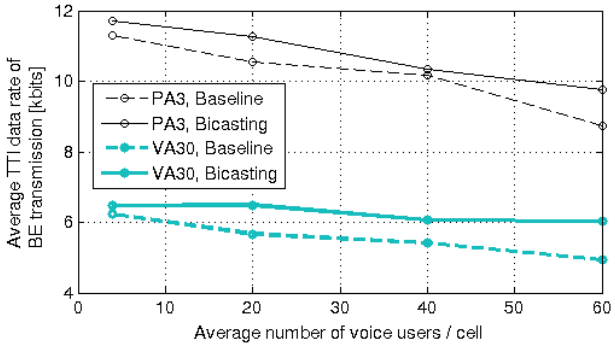

FIGURE 24 Average TTI data rates for BE users

Although the transmission power for voice transport block is reduced significantly, the outage level actually is not affected negatively. Regarding the reference simulations, the highest load level, the 60 voice UEs/cell, is the only scenario that leads to 2 % outage. A terminal encounters an outage when at least 2 % of its packets are dropped. Lower loads had no significant packet drop rates. With Multiflow, the outage percentage with 60 UEs/cell also drops to 0 %. Thus, the proposed traffic and power control mechanisms with Multiflow seem to provide a comprehensive performance improvement with no architectural penalty on the terminal side and with only software-based updates required in the access network.

3.3 HS-SFN

Chapter 2.2.1 presented the need for HS-SFN-specific scheduling algorithm. In this study a unified performance metric for the whole site is calculated for selecting whether each cell in the site should transmit or not. Since the cells are controlled by and located in the same NodeB unit, forming a combined metric is assumed possible. Notice that it is mainly the lack of direct inter-NodeB interface in the HSPA system that limits HS-SFN to an intra-NodeB operation only. Utilizing remote baseband units that control multiple cell sites would also enable inter-site HS-SFN, but it is left out-of-scope of this work. Since the scheduling decisions are made by one entity for several cells, by using the information obtained from those cells, the scheduling is called *coordinated*.

Proportional fair ([63]) is used as a basis for the coordinated scheduling. First, for each individual user n that can be scheduled in TTI t, a dedicated metric P_n based on single-cell transmission is calculated as

$$P(n,t) = \frac{D_{est}(n,t)}{S(n,t)}, \tag{22}$$

where $D_{est}(n,t)$ is the estimated data rate in the next TTI based on the CQI report and $S(n,t)$ denotes the mean data rate from past TTIs calculated with an exponential weighted moving average (EWMA):

$$S(n,t) = (1-\alpha)S(n,t-1) + \alpha R(n). \tag{23}$$

The forgetting factor α is a constant scalar while

$$R(n) = \begin{cases} D_{real}(n,t-1) & \text{if scheduled} \\ 0 & \text{otherwise} \end{cases} \tag{24}$$

contains the actual data rate from the previous TTI.

In the next step, a combined metric for each HS-SFN capable user is calculated by using the compound CQI report with the above calculations. Compound CQI, which contains information for both primary and assisting cells, is a non-standardized report that was discussed in Chapter 2.2.1. Pilot measurement and

CQI formation is made possible by the usage of cells' original scrambling codes for CPICH and other common control channels.

Once all dedicated and combined metrics are available from all cells, a brute force algorithm can be used to find the maximum aggregate metric within the whole site, which finally determines who shall be served and in which mode the cells operate. Notice that the brute force method may soon become too time-consuming in case the network congestion raises or the number of sectors in the site is increased, since the number of possible scheduling combinations grows exponentially in both cases. In such cases, heuristic rules can be applied to reduce the number of possible transmission combinations.

It should be noted that the utilization of a secondary contributing interferer stipulates an amendment in the LMMSE receiver model described in Chapter 3.1.5; the MAI component in (11) needs to be broken into data and control parts as explained in **PV**, since different scrambling codes are used for data and control channels in the assisting serving cell.

With optimal DL channel measurement, low traffic load and without transmitter or receiver enhancements, HS-SFN provides up to 25 % throughput gain for users in softer HO region with a 3 dB handover margin. However, the benefit decreases as the network traffic load increases. Although a relatively high throughput improvement is seen for softer HO, there is only a marginal penalty for other users with regard to average data rates which is shown in [40]. Nevertheless, scheduling might be improved by not allowing HS-SFN assistance from a cell that could serve its own UE. For current study, the coordinated scheduler maximizes the metric throughout the site, which might result in a cell becoming assistant to the neighbor cell's user even though it could transmit to its own user (user becomes blocked). Referring to [60], the networks are often underloaded; an average network load over a 48-hour period was only 12.2 % from the maximum capacity, which means that the HS-SFN utilization rate could still be kept at a high level most of the time even if blocking is avoided. Although this would decrease HS-SFN usage, at the same time overall network interference would also reduce.

The introduction of the enhanced LMMSE equalizer for Type 3 receiver that was discussed in Chapter 2.2.2 increases the accuracy of the channel estimation, which translates into higher C/I. The effectiveness of the equalizer algorithm depends strongly on the imbalance of the channels in relation to both cells, which is in other words the relative distance and position of UE towards the cells. When the imbalance is small, the terminal gets higher "interfering" power from the assisting cell, which results in a higher equalization accuracy. The results included in **PVI** show that with very low load network an average softer HO throughput gain rose to up to 40 % compared to non-HS-SFN networking from 4.5 Mbps to 6.5 Mbps. The improvement compared to simple LMMSE with HS-SFN remained between 15 to 10 %.

The second improvement for HS-SFN is the phase adjustment explained in Chapter 2.2.3. After the phase correction, signals arrive in the same phase at the receiver, effectively improving the C/I. The results published in **PVII** and [40]

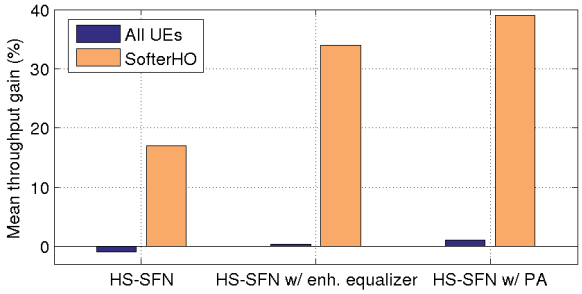

FIGURE 25 Mean softer HO user throughput gain with HS-SFN, 1 Mbps cell traffic load, PedA channel model, Type 3 receiver

show that phase adjustment has approximately similar effect on the throughputs than the enhanced equalizer. Improvement of the cell edge throughput is up to 2 Mbps compared to case without HS-SFN and up to 1 Mbps compared to normal HS-SFN, although the result depends on the load of the network and channel strength imbalance between the two serving links. The percentual gain remains between 40 and 10 % for non-HS-SFN and 20 and 5 % for normal HS-SFN with both ITU Pedestrian A and B channel models. System simulations show that there is little penalty to non-HS-SFN terminals, which is expected as phase adjustment does not alter the interference conditions towards other terminals. Although phase adjustment seems like a sound amendment that can be used with HS-SFN, a further study with non-ideal PCI reporting and channel measurements would be needed to determine a more accurate ratio of throughput gain and penalty originating from additional signaling.

Figure 25 summarizes the throughput gains achieved with HS-SFN, with and without improvements at receiver and transmitter sides. The offered load level in the compared scenarios is approximately 1 Mbps per macro cell and the channel model is ITU Pedestrian A, 3 km/h. The target softer HO group is formed by the terminals within the 3 dB handover area between the cells. In [40], system simulations were performed when both the enhanced equalizer and phase adjustment were enabled at the same time. The throughput gain was raised to approximately 50 % compared to classical single-cell operation with the same parameters that were used for the comparison in the Figure 25.

Impact of different channel models is discussed in **PVII** with ITU Pedestrian A, 3 km/h and Pedestrian B, 3 km/h models. Deeper investigation was conducted in [40] which also includes ITU Vehicular A, 30 km/h model. Both studies show that there is only marginal throughput gain difference between the channel models in softer HO region with baseline HS-SFN. The difference increases in favor of Pedestrian A after introducing enhanced equalizer and phase adjustment, which is somewhat expected as the channel estimation becomes more inaccurate with Pedestrian B and Vehicular A.

3.4 M2P-SFN

It was discussed in Chapter 2.3, that the performance of M2P-SFN is based on how precisely the clustering can be conducted. It is assumed that the central control of multiple geographically-separated transmitters is possible via Remote Radio Heads (RRHs) or baseband hotels, where the network control logic and Radio Resource Management (RRM) functions are located in a common network entity.

The proposed SFN clustering starts with the selection of candidate UEs for scheduling from each of the controlled cells. Depending on the reconfiguration interval, one or several UEs can be selected from one cell, but in this study the candidate set is limited to one per cell. The next step is to create the clusters for the selected UEs. It should be noted that each cell added to a particular SFN will likely be beneficial for the users served by the SFN but will cause interference to other users that are not within the same SFN area. A combinatorial approach, where each combination represents a constellation of scrambling codes used by cells over the whole SFN area, is taken. By pre-allocating scrambling codes for the cells, one may estimate the achievable SINR for each UE within the SFN by utilizing UL channel measurement explained in Chapter 2.3, and a maximization of achievable throughput can then be performed. If the area controlled by the central unit covers multiple cells and UEs, the number of possible scrambling code constellations might become very large; thus the combination pool should be reduced in order to perform the configuration within an acceptably short period of time. Heuristic rules can be defined to exclude the combinations that clearly would perform badly if applied, and the search space of possible combinations can be greatly limited. For instance, it does not make sense to transmit to a user from a very distant cell. Once the combination candidates have been sought out, a brute force method can find the combination to maximize the metric within the SFN area. Channel bit rate is estimated after the scrambling codes are pre-allocated by calculating the geometry factor (G-factor) and applying it to a modified Shannon capacity formula given in [64]:

$$C = BW * \eta * log_2 \left(1 + \frac{SINR}{SINR_{eff}}\right), \tag{25}$$

where η is the correction coefficient having a value 0.75. The $SINR_{eff}$ will be set to 1, since the given G-factor as SINR does not contain the processing gain from despreading. Otherwise, η would be set to 16, which is the spreading factor of the HS-PDSCH channel. Bandwidth (BW) is the chip rate in WCDMA, namely 3.84 Mcps.

The same hexagonal layout that was used with other models is also used with the new M2P-SFN simulations, with the exception that SFN configuration and transmission can be done only within the 7-site area (see Figure 26) that is controlled by a central unit. The outer ring of cells produces interference and is excluded from the area from which statistics are gathered. The SFN reconfigu-

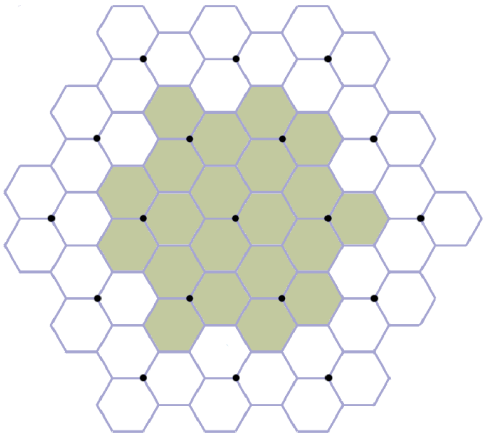

FIGURE 26 A configurable SFN area consisting of seven sites

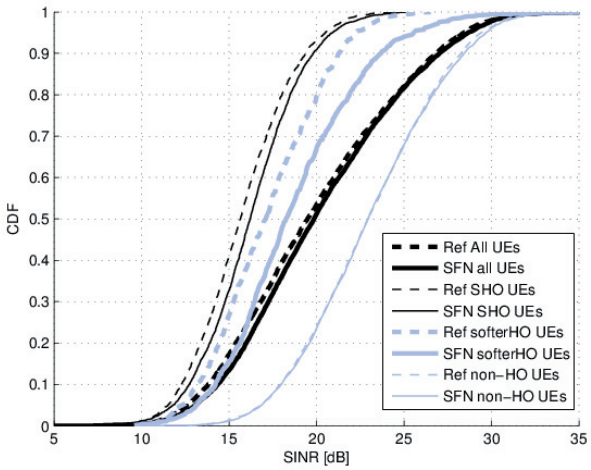

FIGURE 27 SINR distributions of different user groups in the SFN area, 1 Mbps cell traffic load, PedA channel model, Type 3 receiver

ration interval is set to 250 milliseconds. As described in Chapter 2.3, very fast reconfiguration cycle would likely be unrealistic due to issues it poses with the mobility control. Imperfection models presented in Chapter 3.1.6 are applied. Other simulation parameters are based on 3GPP assumptions widely used in HSPA studies [49].

An SINR distribution from the simulations is depicted in Figure 27, where standard single-cell communication results (*'Ref'*) are compared to those obtained from SFN simulations. The grouping of terminals is done according to their locations in the network with respect to conventional cellular deployment without modified cell identities; soft HO and softer HO areas are inter-site and intra-site cell borders, respectively. A 6 dB handover margin is used. As with HS-SFN,

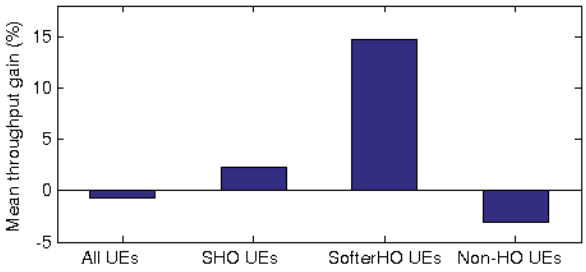

FIGURE 28 Mean user throughput gain in the SFN area, 1 Mbps cell traffic load, PedA channel model, Type 3 receiver

NGMN traffic model with 1 megabit file size is utilized.

Terminals in the softer HO region have most likely two primary contributor cells in the same site, with relatively equal channel strengths and distances to the terminal. This shortens the delay spread and reduces the occasions when destructive over-the-air combining happens. At the same time, the strongest interfering link originating from a different site may have a large attenuation due to long distance to the receiver, which also explains the highest gain among the depicted user groups. However, the non-HO UEs that do not have strong secondary contributors are slightly encumbered by possible cutback of scheduling opportunities as more UEs share the air interface resources within the SFN cluster.

An average throughput gain from the same scenario is shown in Figure 28. It is noticeable that, although for each group of users the SINR distribution is not deteriorated after applying SFN, the throughput results remain rather tepid. On average, albeit the clusters might become suboptimal for the target UEs after the configuration phase, the received signal can still be enhanced. In the light of this, converting the signal improvement into a higher bit rate is prevented mostly by the reconfiguration cycle during which UEs within an SFN have to share the network capacity and scheduling opportunities. Knowing that the higher softer HO gain can mostly be explained with small channel imbalance, it may be beneficial to utilize a more distinctive limitation as regards which cells may co-operate with each other in order to improve the applicability of M2P-SFN also for inter-site communication as well as to minimize interference for UEs that cannot benefit from MPTx.

As explained earlier, the practical impairments presented in Chapter 2.3.2 were applied for the above results. Figure 29 shows a step-by-step effect of each of those impairments to simulation results. Clearly, the reconfiguration cycle length is the primary factor that limits the performance. This is understandable when the network conditions are highly dynamic due to user movement or the traffic mainly consisting of short calls. To overcome the reconfiguration granularity limitation would require that SFN is configured on a carrier that is not the anchor carrier for mobility. However, as stated in Chapter 2.3.3, in dual-carrier system the secondary carrier can be fully DTXed, which means that the reference system

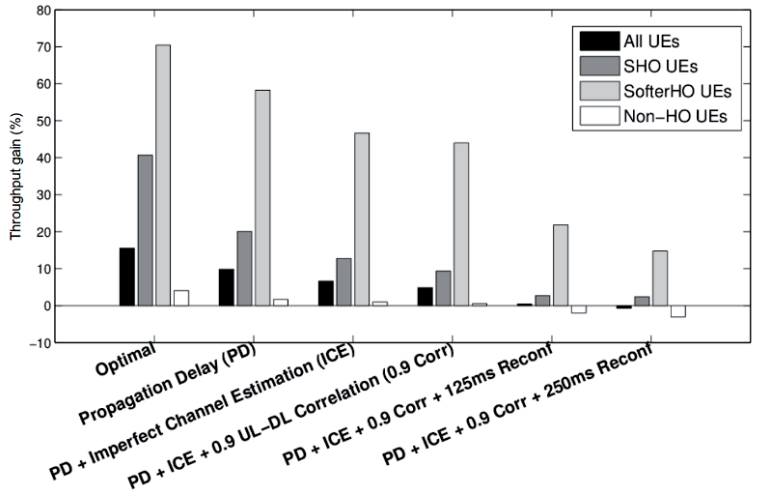

FIGURE 29 Mean user throughput gain in SFN area with different impairments, 1 Mbps cell traffic load, PedA channel model, Type 3 receiver

performance already approaches that of highly dynamic M2P-SFN. Therefore, in order to make M2P-SFN clearly more beneficial, it might make sense to first tackle the channel estimation accuracy or the phase incoherence issue.

3.5 Reciprocal Performance of the Techniques

Some of the results presented in previous sections were obtained with slightly different simulation parameters than others. In order to assess the reciprocal performance of the MPTx schemes, some new simulation results are presented in this section. Common parameters for the new simulations are given in Table 8, in addition to those listed in Table 2. HS-SFN operates without enhancements,

TABLE 8 Common simulation parameters

Parameter	**Value**
UE receiver type	Type3i, 2 Rx LMMSE equalizer
Channel model	PedA, 3 km/h
Flow control for Multiflow	Realistic, period=10 ms, TBD=20 ms
Clustering period for M2P-SFN	250 ms
Number of UEs/cell	[1, 4]. UEs dropped randomly across the system
Handover reporting threshold	3 dB
Traffic	
Traffic model	Bursty traffic source model
File size	Fixed at 1 megabit
File inter-arrival time	Exponential, mean 5 seconds

i.e. phase adjustment and enhanced equalizer. The comparison is done against

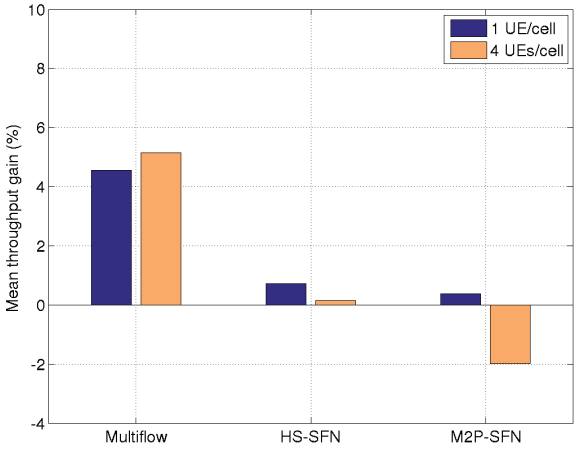

FIGURE 30 Mean user throughput gain, All UEs

baseline simulations without MPTx communication. Performance numbers are given for four user pools:

- All UEs in the network, representing the overall impact.
- Softer handover area UEs located between two cells from the same site.
- Soft handover UEs located between two cells from different sites.
- Non-handover UEs usually residing in the cell center. UEs who do not belong to soft(-er) HO groups.

Figure 30 shows how much enabling multipoint transmission benefits on average. A 3 dB handover reporting threshold results in approximately 25 % of UEs being in the cell-edge and thus available for MPTx. Softer HO covers a modest 5 % and soft HO approximately 20 % of network's terminals. This explains Multiflow's superiority, as it explicitly reaches all cell-edges, which is confirmed also in the following figures where the results for HO UEs are separated. HS-SFN is limited to softer HO and thereby will not have a great influence on the overall performance. M2P-SFN suffers slightly from ineffectiveness in cell-center areas, which can be seen in the network-wide scope. Still the degradation remains quite small.

Throughput gains are shown for Softer HO UEs in Figure 31. In comparison with Figure 18, in which ideal flow control was used, Multiflow's performance degrades significantly after realistic flow control is introduced, which is visible with 4 UEs/cell. The reasons for this were already discussed in Chapter 3.2.1. These new Type 3i results for HS-SFN and M2P-SFN are more or less in line with the Type 3 results shown in the previous sections, with the difference that Type 3i provides slightly worse softer HO gains. It was already covered in [40], that in case of HS-SFN, although Type 3i outperforms Type 3 in absolute performance, the interference awareness that Type 3i provides already in baseline simulations partially limits the achievable MPTx gain.

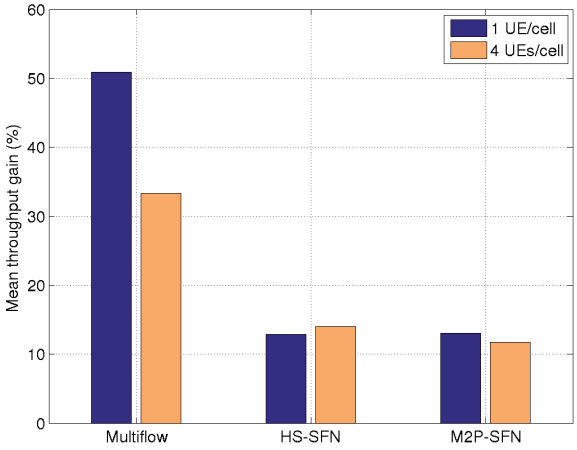

FIGURE 31 Mean user throughput gain, softer HO UEs

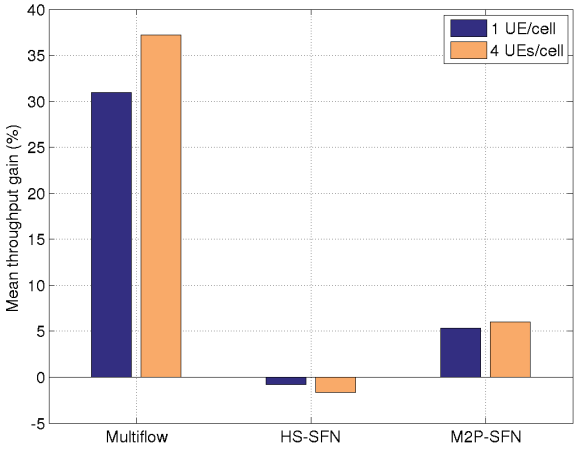

FIGURE 32 Mean user throughput gain, soft HO UEs

The next figure, Figure 32, depicts throughput gains for soft HO UEs. Again, Multiflow explicitly targets soft HO which explains the high gain. Soft HO UEs are out-of-scope for HS-SFN but they are also affected negatively only to a very small extent. The soft HO performance with M2P-SFN was discussed in Chapter 3.4. It was described that high distance and path loss variation between the serving cells restricts the effectiveness of over-the-air combining. Moreover, inter-site interference might be very strong and originating from multiple sources in soft HO region in case the terminal resides in the edge of its own SFN cluster.

Results for the last group of users, residing in the cell center (non-HO) areas, are presented in Figure 33. Samples included in the figure are obtained from users

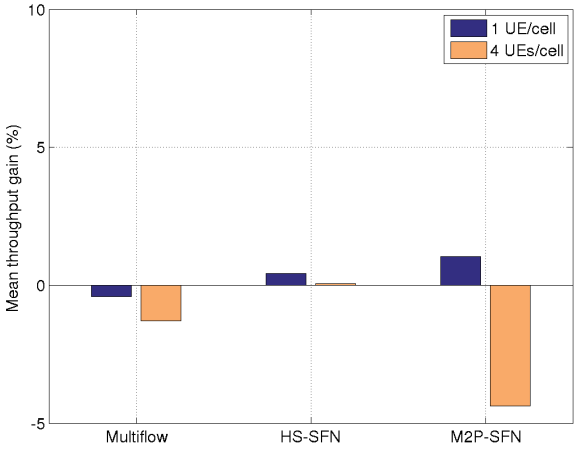

FIGURE 33 Mean user throughput gain, non-HO UEs

that are not part of soft(-er) HO. This group is not directly affected by Multiflow nor HS-SFN. For M2P-SFN, clusters will not be formed for cell center UEs, but they may be explicitly affected due to TDM during a SFN reconfiguration period. Besides the fact that Multiflow and HS-SFN do not reduce the performance in those parts of the network that they cannot explicitly reach, another observation to note is the relatively high negative gain with M2P-SFN. The main reason is the long clustering period during which the UEs in the same cell-cluster have to share common air resources of multiple cells in TDM manner. Cell-center nodes also achieve only low benefit from additional signals from neighbor cells. Therefore the main benefit from M2P-SFN for cell-center UEs is the possible reduction of strongest interfering cells. In order to explain the weak cell-center performance, configured cluster sizes are their frequencies are depicted in Figure 34. The clusters are not clearly of different sizes with 1 and 4 UEs/cell. This is the outcome of the used clustering algorithm that forms the clusters around single users selected from each cell, without taking into consideration how other active UEs in the cells are affected until the next configuration step takes place. As the load level of the network increases, it is likely that the formed cluster is not perfectly suitable for increasing amount of UEs. Based on these results, a more comprehensive evaluation of the performance prediction based on which the clustering is conducted should be used.

3.6 Summary

The performance evaluation of each MPTx technique was done with a quasi-static system level simulator, in which a hexagonal network with cell sectorization was deployed. It was shown that when the primary objective is user throughput im-

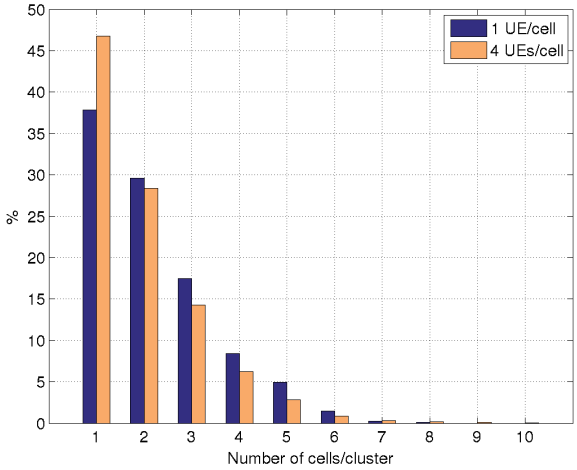

FIGURE 34 Configured cluster sizes with M2P-SFN

provement, Multiflow can provide consistent enhancement in both intra- and inter-site border areas. The maximum average throughput gain in those locations is around 50 % with ideal flow control compared to conventional networking. However, the gain depends on the load level of the network and the flow control algorithm used in the RLC layer. Compared to ideal flow control, a performance loss of approximately 15 % is observed after applying realistic flow control, as shown in **PII**. This is mainly due to imprecise filling of NodeB's transmission buffer and resulting over- and under-runs. In a low-load network, a throughput gain of 30 % is still achieved compared to single-cell transmission.

The second presented use case for Multiflow is the bicasting of QoS-dependent voice data. It was shown that, conditional usage of two data streams can considerably decrease the required transmission power for voice traffic and thereby improve the residual data rate for best effort data connections. It was discussed that only software-based modifications in the network side are needed to allow selection of the best of two cells for each PDU transmission. The effectiveness is seen especially prior to handover when the old channel may quickly decline while the neighboring cell provides more reliable communication.

HS-SFN is limited to co-operation between cells in the same site, which greatly confines the user group who can benefit from dual-cell service. Still, the data rates in the handover area can be raised by approximately 15 to 40 % depending on the usage of signal processing enhancements in the transmitter and the receiver.

Although M2P-SFN can be applied over a large geographical area, the most suitable target according to the simulation results is the intra-site softer HO area where the average throughput was elevated by up to 15 % with the presented clustering algorithm. General M2P-SFN performance is degraded by the scrambling code reconfiguration that has to be done in low frequency in order to avoid

issues with user mobility control and signaling loads. Furthermore, it is known that SFN-based transmission is sensitive to signal phase mis-alignment that may eliminate most of the over-the-air combining gain. According to the results, accurate selection of clustering algorithm, preferably tailored to the environment where it is applied, and means to maximize the coherence of signal components are the key elements for higher performance.

In the comparison of the concepts, Multiflow is unsurprisingly superior compared to the SFN-based schemes. HS-SFN and M2P-SFN perform equally well in softer HO areas in terms of throughput improvement but since M2P-SFN can be applied to inter-site regions, it is much more capable of improving the fairness of the network than HS-SFN. Utilizing M2P-SFN also requires no modifications in the terminal equipment than HS-SFN, so in case the negative influence of M2P-SFN to cell-center communication can be minimized, the final verdict would lean towards M2P-SFN.

4 CONCLUSION

High peak bit rates are no longer the main motivation in the development of modern wireless broadband networks. Instead, network operators want to provide a consistent networking experience regardless of customer's location. One way to achieve this in downlink communication is to utilize multiple cells that transmit data to the same user.

This thesis presented three multi-cell transmission methods for High-Speed Downlink Packet Access communication protocol, their principal difference being in the employment of scrambling codes that are used for distinguishing the cells from each other. It was shown that the three concepts, Multiflow, High-Speed Single-Frequency Network, and Multipoint-to-Point Single-Frequency Network, can each improve the cell edge performance, which is one of the main concerns when discussing consistent networking. Depending on the technique, the usage of multiple transmitters may have major implications on large-scale interference conditions and mobility control as well as direct impact on other terminals in the form of reduced resource allocation opportunities. Several network and terminal side features to minimize such negative influence and to improve the achievable gain have been presented in this dissertation.

A vast majority of the evaluations were carried out with system simulations. This is also a slight limitation of the study, as analytical background for feature development was left for lesser attention. Nevertheless, the research reflects parts of the industrial viewpoint on standard evolution.

Research on Multiflow concentrated on throughput and voice traffic improvements. Applying the technique for efficient delivery of video content could be an interesting topic for future, as increasing amount of network capacity will be consumed by resource-demanding high-definition audiovisual traffic. According to the results presented in the dissertation, SFN-based many-to-one communication could have potential in certain use-cases, for example in the improvement of wireless communication in rural, sparsely populated areas. Further study and ideas are however needed in order to minimize the issues that arise from cell identity variation. Moreover, according to the input obtained from this study there seems to be room for scheduling improvements for both HS-SFN and

M2P-SFN.

The development of fourth and fifth generation networks has rapidly increased its foothold in the industry and in academic research. Although the multi-cell schemes can extend the life-cycle of HSPA networks in a cost-efficient way, the applicability of the discussed methods on next generation networks could be worth studying. The technologies have anyway several commonalities, for example in resource allocation. The application of the methods on 5th generation networking is particularly interesting due to the ambitious objectives related to ubiquity, speed and reliability of future communication.

YHTEENVETO (FINNISH SUMMARY)

Modernien langattomien laajakaistaverkkojen kehityksessä ei nykyään ole tärkeintä saavuttaa suuria maksimidatansiirtonopeuksia. Verkko-operaattorit haluavat sen sijaan tarjota yhdenmukaisen ja tasaisen kommunikaatiokokemuksen riippumatta asiakkaan sijainnista verkossa. Yksi keino tavoitteen saavuttamiseen on hyödyntää useita soluja yhden käyttäjän datan lähettämiseen.

Tämä väitöskirja, jonka nimi on *HSDPA-yhteyden suorituskyvyn parantaminen monipistelähetysmenetelmien avulla*, esittelee kolme HSDPA-verkossa käytettävää monipistelähetysmenetelmää, joiden olennaisin ero liittyy solut identifioivien sekoituskoodien käyttöön. Työssä osoitettiin, että kaikki kolme konseptia, Multiflow, High-Speed Single-Frequency Network ja Multipoint-to-Point Single-Frequency Network, tehostavat solujen reunoilla tapahtuvaa tietoliikennettä, mikä on yksi tärkeimmistä kohteista yhdenmukaisen kommunikaation saavuttamisessa. Riippuen menetelmästä, useiden lähettimien käytöllä voi olla merkittäviä vaikutuksia verkon häiriöolosuhteisiin, käyttäjien mobiliteetin hallintaan ja resurssien allokointimahdollisuuksiin. Työssä esiteltiinkin useita tapoja näiden negatiivisten seurausten minimointiin ja lähetysmenetelmistä saatavien hyötyjen edistämiseen.

Suurin osa menetelmien evaluoinnista suoritettiin järjestelmäsimulaatioilla. Tämä on myös lievä puute, sillä analyyttinen tausta ominaisuuksien kehityksessä jätettiin siten vähemmälle huomiolle. Tutkimus kuitenkin osittain kuvastaa teollisuudessa tapahtuvaa standardien kehitystä.

Tässä työssä Multiflow-tutkimus keskittyi tiedonsiirron nopeuden ja ääniliikenteen parannuksiin. Menetelmän käyttö videosisällön siirtoon voisi olla mielenkiintoinen tulevaisuuden tutkimuksen aihe, sillä kasvava osa verkon kapasiteetista tullaan käyttämään korkeatarkkuuksisen äänen ja videon lähetykseen. Väitöskirjassa esiteltyjen tulosten perusteella yksitaajuusverkkoihin perustuvilla lähetysmenetelmillä voisi olla käyttöpotentiaalia tietyissä tilanteissa, kuten tiedonsiirron parantamisessa harvaan asutuilla alueilla. Lisätutkimuksia ja ideoita tosin tarvitaan solujen identiteettien vaihtumisesta syntyvien ongelmien ratkaisemiseksi. Tutkimuksesta saadun tiedon myötä selvisi myös, että sekä HS-SFN:n että M2P-SFN:n tapauksessa skeduloinnin tehostamisella olisi mahdollista nostaa verkon suorituskykyä.

Neljännen ja viidennen sukupolven verkkojen kehittäminen on nopeasti kasvattanut jalansijaa teollisuudessa ja akateemisessa tutkimuksessa. Vaikka monipistelähetysmenetelmät voivat pidentää HSPA-verkkojen toiminta-aikaa kustannustehokkaasti, väitöskirjassa käsiteltyjen menetelmien soveltuvuus seuraavien sukupolvien verkkoihin voisi olla tutkimisen arvoinen kohde. Etenkin, kun verkkotekniikoista löytyy useita yhteisiä piirteitä muun muassa resurssien kohdentamisessa. Menetelmien käyttö olisi mielenkiintoista nimenomaan tulevaisuuden viidennen sukupolven verkoissa niihin kohdistuvien korkeiden saatavuuteen, nopeuteen ja luotettavuuteen liittyvien tavoitteiden johdosta.

REFERENCES

[1] Ericsson. Mobility Report. White paper, Nov 2015.

[2] 4G Americas. Global mobile broadband market shares, Jan 2015. 4G Americas statistics, based on Ovum, December 2014 Subscriber Estimates, http://www.4gamericas.org.

[3] The METIS 2020 Project. https://www.metis2020.com.

[4] Cisco. Cisco Visual Networking Index: Global Mobile Data Traffic Forecast Update, 2013-2018. White paper, Feb 2014.

[5] The 3rd Generation Partnership Project. http://www.3gpp.org.

[6] 3GPP. Overview of 3GPP Release 11, Mar 2014.

[7] H. Holma and A. Toskala. *WCDMA for UMTS - HSPA Evolution and LTE*. John Wiley & Sons, Ltd, West Sussex PO19 8SQ, England, 4th edition, 2008.

[8] 3GPP TS 25.346. Introduction of the multimedia broadcast/multicast service (MBMS) in the radio access network (RAN); stage 2, Mar 2011.

[9] H. Holma and A. Toskala. *HSDPA/HSUPA for UMTS - High Speed Radio Access for Mobile Communications*. John Wiley & Sons, Ltd, West Sussex PO19 8SQ, England, 2007.

[10] C. A. Jotten, C. Sgraja and H. Schoneich. Performance Evaluation of Multicast/Broadcast Single Frequency Network Operation for WCDMA. In *Proceedings of the IEEE International Symposium on Spread Spectrum Techniques and Applications (ISSSTA)*, pages 79–84, Bologna, Italy, Aug 2008.

[11] J. Bergman, M. Ericson, D. Gerstenberger, B. Göransson, J. Peisa and S. Wager. HSPA Evolution – Boosting the performance of mobile broadband access. *Ericsson Review*, 85(1), 2008.

[12] T. Kratochvil and V. Ricny. Simulation and experimental testing of the DVB-T broadcasting in the SFN networks. In *Proceedings of the 18th IEEE International Conference Radioelektronika*, Prague, Czech Republic, Apr 2008.

[13] M. Tormos, C. Tanougast, A. Dandache, D. Masse and P. Kasser. Evaluation performance analysis of DVB-T2 in a SFN network. In *Proceedings of the 5th IEEE International Symposium on I/V Communications and Mobile Network (ISVC)*, Rabat, Morocco, Sep 2010.

[14] 3GPP TR 25.800. Study on UMTS heterogeneous networks (Release 12), Dec 2013.

[15] 4G Americas. 4G Mobile Broadband Evolution: 3GPP Release 11 & Release 12 and Beyond. White paper, Feb 2014.

[16] 3GPP TR 36.814. Evolved Universal Terrestrial Radio Access (E-UTRA); Further advancements for E-UTRA physical aspects, Mar 2010.

[17] Minghai Feng, Xiaoming She, Lan Chen and Yoshihisa Kishiyama. Enhanced Dynamic Cell Selection with Muting Scheme for DL CoMP in LTE-A. In *Proceedings of the IEEE Vehicular Technology Conference (VTC 2010-Spring)*, Taipei, Taiwan, May 2010.

[18] Binbin Wang, Bingbing Li and Mingqian Liu. A Novel Precoding Method for Joint Processing in CoMP. In *Proceedings of the IEEE International Conference on Network Computing and Information Security (NCIS)*, pages 126–129, Guilin, Guangxi, China, May 2011.

[19] R. Irmer, H. Droste, P. Marsch, M. Grieger, G. Fettweis, S. Brueck, H. P. Mayer, L. Thiele and V. Jungnickel. Coordinated multipoint: Concepts, performance, and field trial results. *IEEE Communications Magazine*, 49:102–111, 2011.

[20] S. Barbera, K. Pedersen, P. H. Michaelsen and C. Rosa. Mobility Analysis for Inter-Site Carrier Aggregation in LTE Heterogenous Networks. In *Proceedings of the IEEE Vehicular Technology Conference (VTC 2013-Fall)*, Las Vegas, NV, USA, Sep 2013.

[21] S. C. Jha, K. Sivanesan, R. Vannithamby and A. T. Koc. Dual Connectivity in LTE small cell networks. In *Proceedings of the IEEE Globecom Workshops*, pages 1205–1210, Austin, TX, USA, Dec 2014.

[22] Aimin Sang, Xiaodong Wang, M. Madihian and R. D. Gitlin. Coordinated Load Balancing, Handoff/Cell-site Selection, and Scheduling in Multi-cell Packet Data Systems. In *Proceedings of the 10th ACM International Conference on Mobile Computing and Networking (MobiCom)*, pages 302–314, Philadelphia, PA, USA, Sep 2004.

[23] GSMA. MIMO in HSPA: the Real-World Impact. White paper, Nov 2010.

[24] K. Johansson, J. Bergman, D. Gerstenberger and M. Blomgren. Multi-Carrier HSPA Evolution. In *Proceedings of the IEEE Vehicular Technology Conference (VTC 2009-Spring)*, Barcelona, Spain, Apr 2009.

[25] 3GPP R1-110479. Multiflow performance evaluation, Jan 2011.

[26] 3GPP R1-110477. HS-SFN performance evaluation, Jan 2011.

[27] Radio-Electronics.com. UMTS 3G History. http://www.radio-electronics.com/info/cellulartelecomms/umts/3g-history.php.

[28] Ge Weiyan, R. Kapoor, Zhang Danlu, S. Sambhwani and M. Scipione. System performance of Inter-NodeB MF-HSDPA with RLC and MAC enhancements. In *Proceedings of the IEEE International Conference on Communication (ICC)*, pages 6071–6075, Ottawa, Canada, Jun 2012.

[29] A. Yaver, P. Marsch, K. Pawlak and F. S. Moya. On the joint usage of MIMO and Multiflow in evolved HSPA networks. In *Proceedings of the IEEE International Conference on Communication (ICC)*, pages 6076–6080, Ottawa, Canada, Jun 2012.

[30] 3GPP TSG-RAN, RP-111375. HSDPA Multiflow data transmission, Sep 2011.

[31] Qualcomm Incorporated. HSPA+ Multiflow. White paper, Feb 2014.

[32] 3GPP TSG-RAN, RP-150288. New WI proposal: Multiflow Enhancements for UTRA, Mar 2015.

[33] T. Nihtilä, J. Kurjenniemi and E. Virtej. System Level Analysis of Interference Aware LMMSE Chip Equalization in HSDPA Network. In *Proceedings of the 10th IEEE Symposium on Computers and Communications (ISCC)*, pages 133–138, Aveiro, Portugal, Jul 2007.

[34] H. Holma, A. Toskala and P. Tapia. *HSPA+ Evolution to Release 12: Performance and Optimization*. John Wiley & Sons, Ltd, West Sussex PO19 8SQ, England, 2014.

[35] 3GPP TS 25.308. High Speed Downlink Packet Access (HSDPA); Overall description; Stage 2, Sep 2014.

[36] 3GPP TS 25.321. Medium Access Control (MAC) protocol specification, Sep 2014.

[37] H. Holma and A. Toskala. *WCDMA for UMTS - OFDMA and SC-FDMA Based Radio Access*. John Wiley & Sons, Ltd, West Sussex PO19 8SQ, England, 2009.

[38] O. Ozturk, R. Kapoor, V. Chande, J. Hou and B. Mohanty. Circuit-Switched Voice Services over HSPA. In *Proceedings of the IEEE Vehicular Technology Conference (VTC 2010-Spring)*, Taipei, Taiwan, May 2010.

[39] 3GPP TSG-RAN, RP-101439. Proposed study item on HSDPA multipoint transmission, Dec 2010.

[40] Oleksandr Puchko. *Multipoint Transmission Scheme for HSDPA*. PhD thesis, University of Jyväskylä, Finland, 2013. ISBN 978-951-39-5476-5.

[41] R. Tresch, C. Mehlfuhrer and M. Guillaud. LMMSE channel estimation for MIMO W-CDMA with out-of-cell interference mitigation. In *Proceedings of the 42nd IEEE Asilomar Conference on Signals, Systems and Computers (SSC)*, pages 331–335, Pacific Grove, CA, USA, Oct 2008.

[42] C. Mehlfuhrer, S. Caban, M. Wrulich and M. Rupp. Joint throughput optimized CQI and precoding weight calculation for MIMO HSDPA. In *Proceedings of the 42nd IEEE Asilomar Conference on Signals, Systems and Computers (SSC)*, pages 1320–1325, Pacific Grove, CA, USA, Oct 2008.

[43] T. Nihtilä and V. Haikola. HSDPA Performance with Dual Stream MIMO in a Combined Macro-Femto Cell Network. In *Proceedings of the IEEE Vehicular Technology Conference (VTC 2010-Spring)*, Taipei, Taiwan, May 2010.

[44] J. Peisa, S. Wager, M. Sågfors, J. Torsner, B. Göransson, T. Fulghum, C. Cozzo and S. Grant. High Speed Packet Access Evolution – Concept and Technologies. In *Proceedings of the IEEE Vehicular Technology Conference (VTC 2007-Spring)*, pages 819–824, Dublin, Ireland, Apr 2007.

[45] E. Perahia and D. C. Cox. Shadow Fading Correlation Between Uplink and Downlink. In *Proceedings of the IEEE Vehicular Technology Conference (VTC 2001-Spring)*, pages 308–312, San Jose, CA, USA, May 2001.

[46] S. Ariyavisitakul. Effects of Slow Fading on the Performance of a CDMA System. *IET Electronics Letters*, 29:1533–1534, 1993.

[47] 3GPP TS 25.304. User Equipment (UE) Procedures in Idle Mode and Procedures for Cell Reselection in Connected Mode, Jan 2013.

[48] M. Moisio and A. Oborina. Comparison of Effective SINR Mapping with Traditional AVI Approach for Modeling Packet Error Rate in Multi–state Channel. In *Proceedings of the 6th International Conference on Next Generation Teletraffic and Wired/Wireless Advanced Networking (NEW2AN)*, pages 461–473, St. Petesburg, Russia, May 2006.

[49] 3GPP TR 25.872. High speed packet access HSDPA multipoint transmission, Sep 2011.

[50] 3GPP TS 25.942. Radio frequency (rf) system scenarios, Sep 2012.

[51] M. Nakamura, Y. Awad and S. Vadgama. Adaptive Control of Link Adaptation for High Speed Downlink Packet Access (HSDPA) in W-CDMA. In *Proceedings of the 5th IEEE International Symposium on Wireless Personal Multimedia Communications (WPMC)*, Honolulu, Hawaii, Oct 2002.

[52] T. Nihtilä. *Advanced Receivers and Antenna Diversity in WCDMA HSDPA*. PhD thesis, University of Jyväskylä, Finland, 2007. ISBN 978-951-39-2853-7.

[53] S. Hämäläinen, P. Slanina, M. Hartman, A. Lappeteläinen, H. Holma and O. Salonaho. A Novel Interface Between Link and System Level Simulations. In *Proceedings of the ACTS Mobile Communication Summit*, pages 509–604, Aalborg, Denmark, Oct 1997.

[54] T. Nihtilä, J. Kurjenniemi, M. Lampinen and T. Ristaniemi. WCDMA HSDPA Network Performance with Receive Diversity and LMMSE Chip Equalization. In *Proceedings of the 16th IEEE International Symposium on Personal, Indoor and Mobile Radio Communications (PIMRC)*, pages 1245–1249, Berlin, Germany, Sep 2005.

[55] Recommendation ITU-R M.1225. Guidlines for evaluation of radio transmission technologies for IMT-2000, 1997.

[56] 3GPP TR 25.963. Feasibility study on interference cancellation for UTRA FDD User Equipment (UE), Sep 2014.

[57] Motorola. 3GPP HSxPA Solutions. Technical solution paper, 2007.

[58] E. Dahlman, S. Parkvall, J. Skold and P. Beming. *3G Evolution: HSPA and LTE for Mobile Broadband*. Academic Press, 32 Jamestown Road, London NW1 7BY, United Kingdom, 2010.

[59] J. Landre and A. Saadani. Receive Diversity and LMMSE Equalization Benefits for HSDPA: Realistic Network Throughputs. In *Proceedings of the 25th IEEE International Symposium on Personal, Indoor and Mobile Radio Communications (PIMRC)*, Athens, Greece, Sep 2007.

[60] Nokia Siemens Networks. Efficient resource utilization improves the customer experience. White paper, Jan 2012.

[61] T. Chapman, E. Larsson, P. von Wrycza, E. Dahlman, S. Parkvall and J. Skold. *HSPA Evolution: The Fundamentals for Mobile Broadband*. Academic Press, 32 Jamestown Road, London NW1 7BY, United Kingdom, 2014.

[62] D. M. de Andrade, A. Klein, H. Holma, I. Viering and G. Liebl. Performance Evaluation on Dual-Cell HSDPA Operation. In *Proceedings of the IEEE Vehicular Technology Conference (VTC 2009-Fall)*, Anchorage, AK, USA, Sep 2009.

[63] A. Jalali, R. Padovani and R. Pankaj. Data throughput of CDMA-HDR a high efficiency-high data rate personal communication wireless system. In *Proceedings of the IEEE Vehicular Technology Conference (VTC 2000-Spring)*, pages 1854–1858, Tokyo, Japan, May 2000.

[64] P. Mogensen, Wei Na, I. Z. Kovacs, F. Frederiksen, A. Pokhariyal, K. I. Pedersen, T. Holding, K. Hugl and M. Kuusela. LTE Capacity Compared to the Shannon Bound. In *Proceedings of the IEEE Vehicular Technology Conference (VTC 2007-Spring)*, pages 1234–1238, Dublin, Ireland, Apr 2007.

ORIGINAL PAPERS

PI

INTRODUCTION OF MULTIFLOW FOR HSDPA

by

Vesa Hytönen, Oleksandr Puchko, Thomas Höhne and Thomas Chapman 2012

Proceedings of the 5th IFIP International Conference on New Technologies, Mobility and Security (NTMS)

Introduction of Multiflow for HSDPA

Vesa Hytönen, Oleksandr Puchko
Department of Mathematical Information Technology,
P.O.Box 35 (Agora), FI-40014,
University of Jyväskylä, Finland
{vesa.a.hytonen, oleksandr.puchko}@jyu.fi

Thomas Höhne
CEF CTO Research,
Nokia Siemens Networks,
Espoo, Finland
thomas.hoehne@nsn.com

Thomas Chapman
Roke Manor Research Ltd.,
Hampshire, SO51 0ZN, United Kingdom
thomas.chapman@roke.co.uk

***Abstract*—This paper introduces a multi-cell transmission scheme for High-Speed Downlink Packet Access (HSDPA) networks, called Multiflow. In this concept, downlink data is transmitted to a user terminal at the border of two cells from one or both of the cells. The cells may belong to same NodeB or to two different NodeBs. The data flows are separated by different scrambling codes used by each associated cell, thus the flows can be treated independently. This provides increased multi-user diversity by means of flexibility in downlink resource management, in addition to the spatial diversity of multiple transmission locations. Another important gain mechanism for this scheme is realized by short-term load balancing between neighboring cells. We evaluate the performance of Multiflow by semi-static system level simulations. The presented results reveal high throughput gains for users in handover areas and also a slight improvement to overall network performance.**

***Index Terms*—Multipoint transmission, HSDPA.**

I. Introduction

Satisfying the growing requirements of mobile networking customers, telecommunication companies and service providers are seeking new ways to improve the capacity of their networks. Enhancements for WCDMA based HSDPA are especially of interest for operators as the next generation mobile networks, such as LTE, are just starting to be rolled out, whereas HSPA has already been deployed worldwide. Over time, the evolvement of the networks has changed from providing increased peak data rates to focusing more on serving the customers with improved fairness. The concept discussed in this paper is well positioned to do so as it is applicable to all cell-edge users and is able to improve their throughput and thereby user experience in low to medium load scenarios.

The family of Multiflow schemes for HSDPA has been approved as a 3GPP work item ([1]). There, the traffic is forwarded to the User Equipment (UE) from two sectors controlled by the same or different NodeBs. In Multiflow, downlink transport blocks containing different data can be transmitted independently, at different times or simultaneously, from two cells over separate flows. As the concurrent flows are not orthogonal, an interference aware receiver is mandatory at the UE side. By the usage of two data streams UE throughput could be, in theory, doubled. True gain levels are however lower due to channel imbalance between the cells and suboptimal interference cancellation at the UE. In this study the focus is on Multiflow applied in single-carrier network, where all the cells share a common carrier frequency, and transmissions are separated by dedicated scrambling codes for each cell.

Due to its novelty, literature about Multiflow other than 3GPP study item reports is scarce. However, multipoint transmission concepts have not been studied only for HSDPA. A considerable amount of research has been done for Coordinated Multipoint Transmission (CoMP) in LTE-Advanced (LTE-A). In LTE-A, as in HSDPA, the main reason for utilizing multi-cell transmission schemes is to elevate cell edge and possibly system throughput. There are two sub-schemes of CoMP in downlink: Joint Processing and Coordinated Scheduling/Coordinated beamforming (CS/CB) [2]. Further, Joint Processing can be divided into two categories. First, so called Dynamic Cell Selection where data is transmitted from one eNodeB at a time [3]. This technique is quite similar to Single-Frequency Dual-Cell (SF-DC) Switching in HSDPA, one of the multi-cell transmission schemes evaluated during the study item phase of the current work item. In the second category, Joint Transmission, downlink transmission occurs from multiple eNodeBs to a single UE simultaneously, thus having strong resemblance with Multiflow scheme studied in this paper [4].

The rest of the document is organized as follows. Section II gives an overview of Multiflow describing the gain mechanisms and requirements for the deployment. In Section III the simulator environment together with the achieved results are discussed. Section IV concludes the paper.

II. The concept

Users at the cell borders are usually subject to low signal level due to strong path loss caused by long distance to NodeB or a location that is not in the cell's antenna beam direction. They also suffer from high interference from other sites in the network. As the center cell terminals enjoy good signal quality, the overall fairness in terms of user experience in the network might be low. This can be corrected by the scheduler but at a cost of cell capacity.

Multiflow will help cell edge UEs as they are able to receive data from two transmitting cells, located either in the same site or different sites. Depending on the scheduler employed this can be achieved by using resources of the neighbor cell which would otherwise be used there for cell-center users, or by restricting assisting transmissions from the neighbor

978-1-4673-0229-6/12/$31.00 ©2012 IEEE

cell to TTIs where the neighboring cell has free resources, thereby enabling short-term load-balancing. In theory, the cell edge UEs utilizing two transmissions may even double their throughput if the channel conditions to both cells are in balance.

Assuming that no scheduling coordination between the transmitting cells is established, data blocks can be transmitted from two cells to a single user concurrently and they will present interference to each other at the UE. In order to mitigate the interference, a type3i receiver with antenna diversity is required in the user equipment which provides interference cancellation with a chip level equalizer. This type of receiver calculates an equalizer filter that maximizes the overall SINR by using the knowledge of the colored interference of neighboring transmissions [5].

A. Gain mechanisms

The gain mechanism for UEs in the network with enabled Multiflow is two-fold. First, utilization of the second data stream increases per-UE data rates. The amount of extra throughput depends on the post-receiver SINR of both links and load levels of the cells. Second, Multiflow directly helps users at the cell borders by which they are able to finish their data transfer events faster, offering increased opportunities to resource utilization for other users in the network. Since cell-edge users usually remain in the network long due to high signal losses and inter-cell interference, reduction of their activity time in the network improves the throughput fairness across the UEs in the system. As demonstrated later this can be achieved without a negative impact on cell-center users.

A Multiflow capable UE may be allocated resources from both cells in Multiflow active set independently which thereupon increases the utilization rate of low load cells while enhancing scheduling opportunities for UEs in highly loaded cells.

B. Flow control and signaling

In Multiflow, the source data packets are divided onto separate data flows, routed over separate NodeBs and received (potentially) in parallel by the UE. Once the data packets have been decoded successfully, they will be re-ordered and delivered to higher layers. The data can be split at different layers in the network or NodeB. The best way of doing so is an active area of research.

Intra-site Multiflow enables the use of fast data flow split on MAC-ehs layer at the NodeB, whereas for inter-site operation the split needs to be performed on the PDCP or RLC layer in the Radio Network Controller (RNC), see Fig. 1. In HSDPA, there is no direct link for communication between the NodeBs, thus the split operation in RNC is the only option for inter-site NodeBs, if a possible core network operation is excluded [6].

At the receiver side, two MAC-ehs entities are needed for the RLC PDU reception of the primary and secondary transmission, in case of inter-site Multiflow. Similarly, one MAC-ehs entity is sufficient in case only intra-site Multiflow is supported by the network.

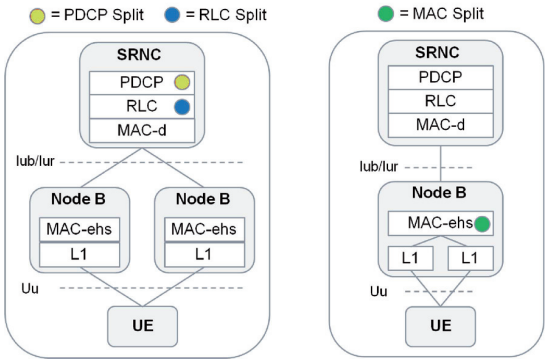

Fig. 1. Data flow split options for Multiflow

The Radio Network Controller (RNC) is responsible for enabling and disabling Multiflow on user-by-user basis. It informs the UEs which cells they should monitor for transmission and consequently provide Channel Quality Indication (CQI) feedback messages for. The CQI operation in Multiflow would closely follow that of Dual-Cell HSDPA and HSDPA MIMO, where several CQIs are reported to the nodeB per TTI [7]. Likewise, for Multiflow the amount of CQIs transmitted in UL would be adjusted according to the number of configured carriers in DL. As with existing schemes, the feedback may be reported in compound messages or in time-multiplexed fashion (see 3GPP Technical Specification 25.212, Table 15C.4). Similar to CQI signaling, also the Hybrid Automatic Repeat Request (HARQ) acknowledgments need to be reported in UL for all flows.

In addition to selecting which UEs should enable or disable Multiflow support, the RNC decides which sectors in the network may participate the multi-cell transmission operations. However, it is a matter of NodeB scheduler to dynamically decide based on the feedback messages which cells from those selected by the RNC may apply a Multiflow transmission on each TTI. As for the other operations, additional higher layer (L2, L3) signaling will support the activation of Multiflow as well as data flow control [8].

III. System Model

A semi-static cell-based network simulator is used to model Multiflow in an HSDPA environment. The model introduces 57 NodeBs, each having three sectors covering 120 degree angles. Simulation parameters are introduced in Table I. They follow the assumptions defined by 3GPP standardization [9]. Both inter- and intra-site Multiflow operation are enabled, applying dual data flow possibility for users located at each cell border where the signal strength imbalance between two cells falls within 6 dB.

During a simulation UEs are stationary. However, fast fading is introduced to produce channel variation. Shadowing is modeled by running several simulation sets with different seeding where UEs are dropped randomly in the simulation

TABLE I
SIMULATION PARAMETERS.

Parameter	Value
Cell Layout	Hexagonal grid, 19 NodeBs, 3 sectors per NodeB with wrap-around
Inter-site distance	1000 m
Carrier Frequency	2000 MHz
Path Loss	L=128.1 + 37.6log10(R), R in kilometers
Penetration Loss	10 dB
Log Normal Fading	
Standard Deviation	8dB
Inter-NodeB Correlation	0.5
Intra-NodeB Correlation	1.0
Correlation Distance	50m
Max BS Antenna Gain	14 dBi
Antenna pattern	
2D Pattern	$A(\theta) = -min(12(\theta/\theta_{3dB})^2,\ Am)$, where $\theta_{3dB} = 70\ degrees,\ Am = 20dB$
Channel Model	PedA 3 km/h
CPICH Ec/Io	-10 dB
Total Overhead power	30 %
UE Antenna Gain	0 dBi
UE noise figure	9 dB
UE Receiver Type	Type3i with 2 Rx antennas
Spreading factor	16
Maximum Sector Transmit Power	43 dBm
Handover reporting threshold	6 dB
Multiflow operation	Inter- and intra-site
Number of HARQ processes	6
Number of UEs/cell	1, 2, 4, 8, 16 and 32. UEs dropped randomly across the system
Traffic	
Traffic model	Bursty Traffic Source Model
File size	Fixed at 1 Mbit
File inter-arrival time	Exponential, mean 5 seconds
Flow control on Iub	Ideal and instantaneous
HS-DPCCH Decoding	ACK decoded on UL; C2P used: 2 dB for Intra-NB, 4 dB for Inter-NB
CQI	Ideal with 3 TTI delay

area. The used bursty FTP traffic model has a constant file size but the file inter-arrival time for a UE follows exponential distribution with a mean value of 5 seconds. Each UE has an own traffic generator with an independent arrival probability.

A Multiflow capable UE that is located at the cell border may receive transport blocks from two cells. For modeling purposes this type of UE may be divided into two conceptual entities which are independent from each other: class A UE entity that is served by the strongest (primary) cell and class B UE entity that is served by the second strongest (secondary) cell. The received amount of data is aggregated from both of these entities in the end of the simulation so as to attain the total amount of data received by a single Multiflow user. Although each UE has an independent data buffer, class A and B Multiflow entities share a common traffic generator so as not to have doubled amount of files for one Multiflow UE.

Following the user entity division, the basic proportional fair scheduling (see e.g. [10]) is extended for Multiflow regarding the transmit opportunities from the secondary cell to class B UE entity. In case the Multiflow UE is in soft or softer handover area, the class B UE is scheduled only if there are no active class A UEs in that cell. This results in reduced usage of Multiflow when the load level of the network increases. It is observed that Multiflow can provide gains until the network load corresponds to virtually user full-buffer traffic, a rare situation in real HSDPA networks. Class A UEs are treated normally as other non-Multiflow UEs in each cell.

A 6 dB handover margin is used which results approximately in 9 % and 36 % UE percentages in softer handover (softer HO) and soft handover (SHO) area, respectively. In our simulations, all of these UEs are Multiflow capable. It has been noted by different studies that legacy UEs who are not capable of receiving two data flows concurrently and who may not use interference aware receivers do not suffer from Multiflow, thus for simplification they are left out from our tests (see e.g. [11][12]).

We assume ideal time and frequency synchronization of Multiflow transmissions regardless whether the cells are controlled by the same or different NodeBs. Also the Doppler shift is assumed similar. The I_{ub} interface flow control is ideal as both cells participating Multiflow acquire bits from a common user-specific buffer of data that is comprised of queued files.

A. Simulation Results

Fig. 2 presents cumulative distribution function (CDF) of UE burst rates (throughputs) for the case where on average eight UEs are present in each cell in the network. Total amount of UEs in the network is thus $57 \times 8 = 456$. These curves include results from all UEs in the network. In the figure, the ”Reference” curve displays the results where Multiflow was switched off and UEs can receive data only from their primary cell. The curve labeled ”Multiflow” show the case where Multiflow was enabled and the UEs within the HO margin may receive transmissions over both primary and secondary link. Fig. 3 provides separated results for three user terminal groups: users in the soft handover area (i.e. users who reside at the border of two cells served by different NodeBs), users in the softer handover area (i.e. users who reside at the border of two cells served by the same NodeB) and non-HO users who do not reside at cell borders.

The first observation from Fig. 2 is that low and medium burst rate UEs achieve biggest gain when using Multiflow, which is due to the fact that many of these UEs reside in the handover region and therefore may utilize two data flows from two cells. The burst rate distribution can be easily seen from Fig. 3 by looking at the burst rates of softer HO and SHO area UEs. On average, UEs in SHO region have the lowest burst rate among the groups due to high inter-site interference and long distance to their serving cell site, and softer HO area UEs achieve mostly low or medium burst rates. Therefore, gains for high burst rate UEs stay at a very low level. Thus the throughput fairness across UEs is enhanced.

By evaluating the Multiflow gains from Fig. 3, it is evident that handover area UEs in all burst rate levels levels have equally gained from receiving assistance on the secondary link. An important characteristic of Multiflow is that a large pool of UEs is benefiting in equal manner. By increasing

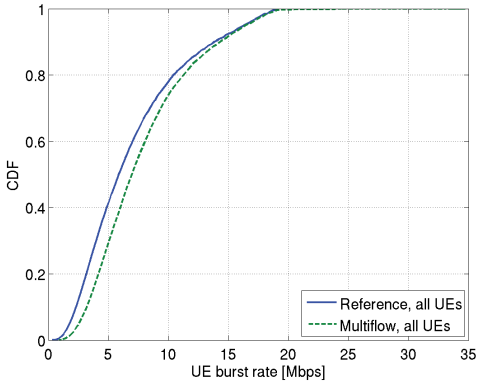

Fig. 2. Burst rate CDF of all UEs, 8 UEs/cell

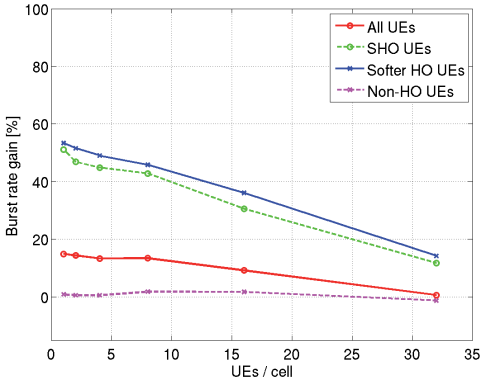

Fig. 4. Burst rate gains for various load levels

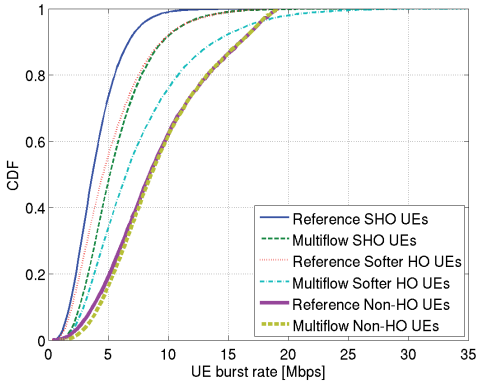

Fig. 3. Burst rate CDF of HO and non-HO area UEs, 8 UEs/cell

the handover threshold margin the pool could be even larger, however defining too large a margin would result in reduction of Multiflow performance due to increased imbalance between the primary and secondary link. Also, the UL control signaling would need to be dimensioned to be reliably received by both cells. Equivalently, having smaller margin allows the link balance to approach 1:1 ratio for all handover area users, but with a cost of a smaller user pool size.

Fig. 3 also presents burst rates for non-handover UEs who usually reside closer to cell center or cell site and will not be able to receive Multiflow transmissions from two cells, but who are served normally by a single cell. As seen from the figure, there is no negative impact from Multiflow to these UEs, and even a slight improvement is visible. Although Multiflow does not affect the non-HO area UEs directly, the implicit impact can be both negative and positive. Total interference in the network might be increased as Multiflow UEs may activate otherwise empty cells (negative impact). However, improved burst rates and by that reduced activity times of Multiflow UEs allow more scheduling opportunities for all other UEs, which affects positively to burst rates of non-HO area terminals.

Percentual burst rate gains for all simulated load levels are shown in Fig. 4. UEs in handover region, either in softer HO or SHO, have high gains starting from over 50 %, then decreasing towards high loads. The degradation is caused by fewer opportunities to schedule a transmission on the secondary link since there is a higher probability for a cell to have active class A UEs of its own as the number of UEs per cell increases.

One should notice that the burst rate gain for non-HO area UEs stays close to 0 %, demonstrating that there is no overall negative impact from Multiflow. This is ensured by the non-blocking scheduling operation where class A UEs are favored over class B UEs.

Absolute mean burst rates for all UEs in the simulations are presented in Fig. 5. This is an alternative representation of the burst rate gains for all UEs in the network displayed in Fig. 4, but in addition showing that a larger number of UEs results in extended UE activity times and thus decreased absolute data rates.

To support and explain the burst rate gains presented in Fig. 4, cell and user activity ratios are gathered in Table II. The cell TTI usage numbers provide information on how many TTIs cells transmit data during the simulations, i.e.

$$cellTTIusage[\%] = \frac{Num_{activeTTIs}}{Num_{allTTIs}} \times 100. \qquad (1)$$

The numbers are gathered from both reference and Multiflow simulations. The table contains also activity statistics for Multiflow users, separated into activity levels of primary and secondary link. These are the ratios between the number of TTIs when users are scheduled over the number of TTIs when users could be scheduled, i.e. when there is data for those users in the transmission buffers. It can be observed that for low

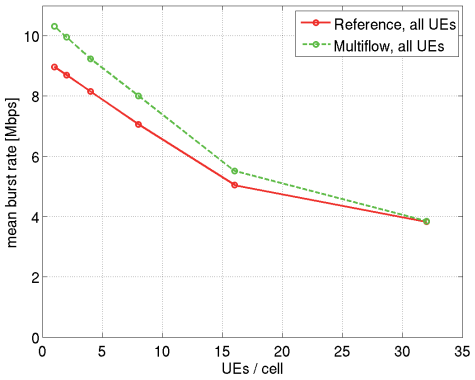

Fig. 5. Mean burst rates for various load levels

TABLE II
TTI ACTIVITY

	Cell TTI usage [%]		Multiflow user TTI activity [%]	
UEs/cell	Reference	Multiflow	Primary link	Secondary link
1	4.4	4.3	97.9	96.5
2	6.6	7.2	95.9	92.8
4	12.0	14.4	91.7	84.8
8	25.6	31.2	81.5	68.0
16	59.6	68.3	54.9	30.7
32	97.6	99.6	9.7	0.2

loads cells remain silent over 90 % of the time, and Multiflow users can be scheduled almost always over both primary and secondary link. The average cell activity level in the Multiflow simulations is higher than in the reference simulations, which is expected as two flows can be utilized instead of one. Also in the user activity statistics we see that the utilization rate of the secondary link declines towards higher loads, as expected. However, even for moderately high load, such as 8 or 16 UEs per cell, there is still a high probability that the secondary cell will not serve its class A UEs, and therefore could schedule a class B UE. Indeed, by looking at Fig. 4, the gains (for all UEs) approach zero only for 32 UEs per cell when the network offered load leads to UEs having very few transmission opportunities and effectively having full-buffer traffic. However, some gains are still visible for handover area terminals.

IV. Conclusion

In this paper an HSDPA multi-cell transmission scheme called Multiflow is presented. A discussion on the requirements and solutions for the concept is provided together with simulation results gathered with semi-static network simulations.

In Multiflow, two sectors under the control of one or two NodeBs transmit independent data blocks to a user. To support Multiflow, user terminal equipment requires an interference aware type3i receiver with spatial diversity in order to reduce the interference between the two received flows. Enhanced flow control is needed in the network as well as data splitting to each participating cell before the transmission in either the Radio Network Controller or the NodeB. Data combining is alike necessary at the user terminal when merging the flows back together.

The simulation results show that Multiflow provides substantial gains of around for 40% for cell edge users who otherwise may reach only low or mediocre data rates. The gains are realized primarily by utilizing free transmission resources in neighboring cells, amounting to short-term load balancing. This directly results in improved mean user throughput as the users may finish their data transmissions and leave the network earlier, which in part helps other existing users by releasing more resources for them. Although Multiflow may create additional interference to the network, the advantages from the concept are predominant.

Acknowledgment

The authors would like to thank Petri Jolma and Jani Moilanen from Nokia Siemens Networks for their valuable contributions to the Multiflow work. Also special thanks to Michal Maternia, Krystian Pawlak and Patrick Marsch from Nokia Siemens Networks for their assistance with the development of the network simulator.

References

[1] 3GPP TSG-RAN, RP-111375, "HSDPA multiflow data transmission," Sep 2011.
[2] 3GPP TR 36.814 v9.0.0, "Further advancements for E-UTRA physical aspects," Mar 2010.
[3] Minghai Feng, Xiaoming She, Lan Chen and Yoshihisa Kishiyama, "Enhanced Dynamic Cell Selection with Muting Scheme for DL CoMP in LTE-A," in *Vehicular Technology Conference Spring, 2010*, Taipei, Taiwan, May 2010.
[4] Binbin Wang, Bingbing Li and Mingqian Liu, "A Novel Precoding Method for Joint Processing in CoMP," in *Network Computing and Information Security, 2011*, Guilin, China, May 2011.
[5] T. Nihtilä, J. Kurjenniemi and E. Virtej, "System Level Analysis of Interference Aware LMMSE Chip Equalization in HSDPA Network," in *IEEE Symposium on Computers and Communications, 2007. ISCC 2007*, Aveiro, Portugal, Jul 2007, pp. 133–138.
[6] 3GPP TSG-RAN WG1, R1-111141, Nokia Siemens Networks, Nokia, "Multiflow performance evaluation," Feb 2011.
[7] D.M. de Andrade, A. Klein, H. Holma, I. Viering and G.Liebl, "Performance Evaluation on Dual-Cell HSDPA Operation," in *Vehicular Technology Conference Fall, 2009*, Anchorage, USA, Sep 2009.
[8] 3GPP TSG-RAN WG1, R1-111775, Nokia Siemens Networks, Nokia, "Signaling and configuration for the multi-point transmission schemes," May 2011.
[9] 3GPP TSG-RAN, R1-111116, TR 25.872, V0.1.3, "HSDPA multipoint transmission," Mar 2011.
[10] A. Jalali, R. Padovani and R. Pankaj, "Data throughput of CDMA-HDR a high efficiency-high data rate personal communication wireless system," in *Vehicular Technology Conference Proceedings, 2000*, Tokyo, Japan, May 1997, pp. 1854–1858.
[11] 3GPP TSG-RAN WG1, R1-111539, QUALCOMM Incorporated, "System Performance Evaluation of SF-DC Inter NodeB Aggregation in Uniform Loading Scenario Assuming Realistic RLC and Flow Control (30% Penetration)," May 2011.
[12] 3GPP TSG-RAN WG1, R1-112627, Nokia Siemens Networks, Nokia, "Text proposal on the performance of multiflow (SF-DC aggregation) in legacy deployments (30% multiflow penetration)," Aug 2011.

PII

FLOW CONTROL FOR MULTIFLOW IN HSPA+

by

Ali Yaver, Thomas Höhne, Jani Moilanen and Vesa Hytönen 2013

Proceedings of the 77th IEEE Vehicular Technology Conference
(VTC2013-Spring)

Flow Control for Multiflow in HSPA+

Ali Yaver
Radio Systems,
Nokia Siemens Networks,
Wroclaw, Poland
ali.yaver@nsn.com

Thomas Höhne
Radio Systems,
Nokia Siemens Networks,
Espoo, Finland
thomas.hoehne@nsn.com

Jani Moilanen
Radio Systems,
Nokia Siemens Networks,
Espoo, Finland
jani.moilanen@nsn.com

Vesa Hytönen
Department of Mathematical
Information Technology
University of Jyväskylä, Finland
vesa.a.hytonen@jyu.fi

***Abstract*—Multiflow is a major enhancement envisioned as part of evolved HSPA. As 3GPP Release 11 is nearing its conclusion, Multiflow forms an integral element of the new set of standards. 3GPP compliant simulation studies from various stakeholders have shown a cell-edge throughput gain in the order of 40%. 3GPP simulation assumptions for Multiflow in release 11 however targeted an ideal scenario to quantify upper bound on achievable throughputs. Some of the key challenges related to Multiflow that have been identified as part of 3GPP work item include flow control between RNC and participating nodeBs, scheduling and distribution of data among the links, dynamic buffer management and the skew arising from an imperfect data split. Although, these issues have been widely discussed in the 3GPP context, there have been no extensive system level simulations so far to accurately study the constraints. This paper highlights such aspects by means of system level simulations. The paper also presents a framework for dynamic buffer management with flow control and the performance of different data split algorithms to combat skew. A comparison of the achievable throughput when an ideal data split is replaced with a realistic one is also investigated.**

***Keywords*—HSPA Evolution, Multiflow, SHO. Flow Control, Skew, RLC**

I. INTRODUCTION

Although LTE (Long Term Evolution) has already been standardized and first LTE compliant smart devices have already hit the shelves, the disproportionate presence of UMTS networks and devices is driving continuing evolution of HSPA both in terms of pushing the peak rates and optimizing the overall network efficiency. Many stakeholders have agreed to continue the standardization work for new features in HSPA for 3GPP release 12. 3GPP standardization work in HSPA evolution can be roughly categorized into two broad areas. In the first area of research, 3GPP aims to add new features which are targeted at raising the peak data rates. MIMO, Multicarrier, higher order modulation and coding are examples of such enhancements. On the other hand, new features are being added to increase the efficiency of the network and improving user throughput using existing spectrum and power resources. SON (Self Organizing Networks) and Multiflow are examples of these features [1].

Multiflow is targeted at performance improvements for cell-edge users and the 3GPP work item was initiated in 2011 [2]. Cell-edge users are among the most challenging group due to their high physical distance from the transmitter. At the same time, cell-edge users also experience a high level of interference due to their close proximity to the neighbouring transmitters. In contrast to spatial diversity schemes such as MIMO diversity, Multiflow uses transmitters from two different cells (or two sectors belonging to the same cell) to enable independent streams of data. As a result, the user experiences a higher throughput since from the transmitter's perspective each data stream is scheduled as an independent entity [3][4].

Initial simulation studies for performance analysis presented in 3GPP technical documents [5] are meant to observe absolute gains possible by means of employing Multiflow. One of the limiting assumptions of these simulations is the absence of RNC (Radio Network Controller) based flow control mechanisms. Since the nodeBs are not synchronized like in LTE and there is a lack of a direct interface between two nodeBs in a UMTS network, the RNC itself is responsible for an optimal data split between the two entities. The adaptation of the data split ratio based on the performance of the two links is the central theme of flow control. In this paper, we have conducted system level simulation studies which take into account flow control mechanisms and the results are compared against an ideal split scenario. The data streams from two different nodeBs undergo not only uncorrelated channel conditions but they also pass through independent schedulers. Thus at the receiving end, these data units may arrive in a different order leading to skew. Three different split scheduling schemes for combating skew at RLC (Radio Link Controller) level are also studied by means of simulations. Moreover, different optimizations are also discussed which focus on varying flow control frequency and target buffer sizes at nodeB.

The rest of the paper is organized as follows. Section II describes the theoretical concepts of Multiflow and flow control along with a description for the design of a dynamic buffer. Section III defines the system model and lists key simulation assumptions and parameters. Section IV presents a commentary on simulation results with proposals for possible optimizations. Concluding remarks are presented in Section V.

II. FLOW CONTROL IN MULTIFLOW

HSDPA does not support soft handover, however the users residing in a soft handover region are prime candidates for Multiflow transmission. Due to comparatively worse

978-1-4673-6337-2/13/$31.00 ©2013 IEEE

propagation conditions than the cell centre users, the UEs (user equipments) at the cell-edge require more resources in terms of transmission power and spectrum to be served equally well. A possibility of having an additional link available from a neighbouring nodeB proves to be advantageous as these UEs can have access to additional capacity offered by the assisting link. Being at the edge of the cell also means that the received power from the assisting link would not be considerably lower than their serving cell. If a part of the data is scheduled through the assisting link, it also frees resources at the serving cell thereby improving the overall system efficiency. However, it is important that the additional resources offered by the assisting cell do not deprive its primary users. Therefore, a simplistic scheduling assumption is that the Multiflow users are only scheduled on the assisting link when there are free TTIs [5].

The data split between participating nodeBs for a common Multiflow UE takes place at the RNC at the level of the RLC protocol [6 reference to be updated: e.g. 25.308 specifies to MAC-ehs entities]. An important aspect of the scheme is that the nodeBs are scheduling the data independently. This also means that the UE must be able to simultaneously receive data from both nodeBs. These data flows are then re-ordered and combined.

In case of ideal split described earlier in section I in the context of 3GPP's ideal simulation assumptions for Multiflow, the data split is happening at the level of MAC-ehs. That is, in effect the idealistic assumption is that RNC is performing scheduling each TTI based on instantaneous channel state information. In practice, however, flow control takes place between the RNC and the nodeB at intervals of tens of TTIs, and the actual TTI-to-TTI CQI-based scheduling of data is done by the nodeB. For the flow control the nodeB is maintaining a local buffer from which it schedules its packet data. That buffer is kept filled by the RNC according to feedback by the nodeB, see Fig.1. Depending on the flow control period the buffer may be kept large, with the risk of having to discard data at times of handover, or may be kept small, with the penalty of additional flow control signaling overhead.

The proposed flow control algorithm works as follows:

- In the initial state when a UE starts a packet call Multiflow, RNC transmits equal number of bits to both links. These bits are a fraction of the total capacity possible. Thus, a "slow start" for filling the nodeB buffers is achieved
- A target buffer size with a fixed queuing delay is defined. It is updated every TTI according to the achieved link speed.
- NodeB requests new data from RNC at each predefined flow control period based on the difference between the total capacity of the buffer and the amount of data still waiting to be transmitted.
- No new data are requested if the untransmitted bits at the nodeB MAC buffer are equal or more than the estimated target buffer capacity. This situation is referred to as an 'over-run'
- If the buffer is emptied fully before the next flow control period is due, an 'under-run' occurs: the nodeB cannot transmit even if there is data waiting at the RNC

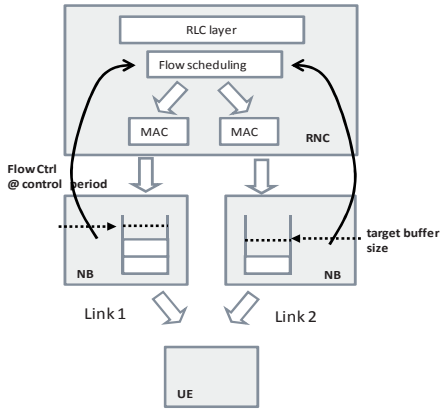

Figure 1: Flow Control Block Diagram

One of the receiver functions performed by the UE is the reordering of RLC PDU prior to delivering them to higher layers. Reordering of RLC PDUs becomes necessary for instance in case of retransmissions. In Multiflow reordering becomes even more important, as the PDUs may arrive out-of-order not only because of retransmissions, but also because they were travelling through nodeBs with different transmission rates and overall different path delays. Note that the nodeB transmission rate and path delay for a user comprises not only the raw achievable link speed but is also influenced by the load of other users present in the cell.

The different path delays in general will lead to skew – a difference in arrival times of successive packets at the UE.

$$s_{PDU} = t_{arrival}(PDU_{SN}) - t_{arrival}(PDU_{SN-1})$$

The skew – when large enough – will not only cause costly RLC layer retransmissions of the skewed PDUs, but when large enough may also affect the performance of higher layer protocols such as TCP.

In order to minimize skew, Multiflow split scheduling schemes are investigated on top of flow control. Flow control determines the amount of data fed to each link whereas the split scheduling schemes distribute RLC PDUs over the two links in a specified manner. In this paper, three split scheduling schemes have been analyzed:

- In algorithm 1, weighted round robin is applied to PDUs until both links run out of credits
- In algorithm 2, PDUs are first assigned to serving link until it has reached its capacity and

later the PDUs are assigned to assisting link until it reaches its capacity.

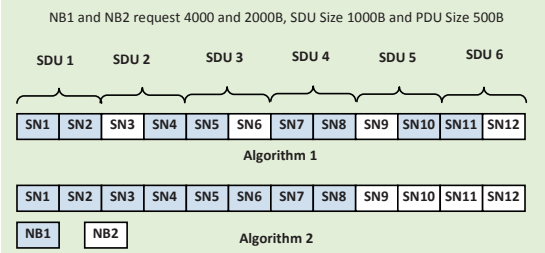

Figure 2: Example of Multiflow Split Scheduling Schemes

III. Simulation Model

A semi-static system level simulation capable of modeling fast fading, nodeB-based channel aware scheduling, and RNC-nodeB flow control has been used for this study. The network consists of 19 sites with three sectors each leading to a deployment of 57 cells. A uniform user distribution is assumed. The region of soft handover is defined to be within a power margin of 6dB leading to a total Multiflow share of above 40% of all users. A bursty FTP based traffic model is used, where for each user files of size 1 Mbit are generated according to a Poisson arrival process with an exponentially distributed inter-arrival time between consecutive files of 5 seconds. Each file is divided into PDUs which are then scheduled over Multiflow links based on schemes described earlier. The data is forwarded to nodeB based on the capacity reported by the flow control algorithm. The following table lists the key simulation parameters.

TABLE I: Simulation Parameters

Parameter	**Value**
ISD (inter-site distance)	500 m
Carrier Frequency	2000 MHz
Path loss	128.1+37.6log(R in km)
Shadowing	Log-normal dist.
Shadow fading standard dev.	8 dB (log normal)
UE Velocity	3 kilometers/hour
Ideal CQI delay	3 TTIs
De-correlation distance	50 meters
Inter-site Correlation	0.5
Intra-site Correlation	1.0
Tx Antenna Gain	14dB
2D Antenna Pattern	$A(\theta) = -\min(12(\theta/\theta 3dB)2, Am)$, $\theta 3dB = 70$ degrees, $Am = 20dB$
Noise figure at the UE	9 dB
Spreading factor Codes in use	16 15
Multiflow HO Margin	6 dB
PDU Size	1250 bytes
Flow Control Period	2, 10 and 20 TTIs
Initial Buffer State	33% of maximum capacity
Number of HARQs	6 Processes
Number of HARQ processes	6

IV. Simulation Results

Simulations were performed for different degrees of cell loading, highlighting different aspects of flow control in the context of Multiflow. The results are presented in the following order: First, the operation of the flow control is illustrated by plotting buffer of a nodeB over time. Next, the user throughput achieved with the proposed flow control algorithm is benchmarked against ideal flow control described earlier. Then the effect of varying the flow control period is shown. Last, a comparison of skew is presented based on two split algorithms.

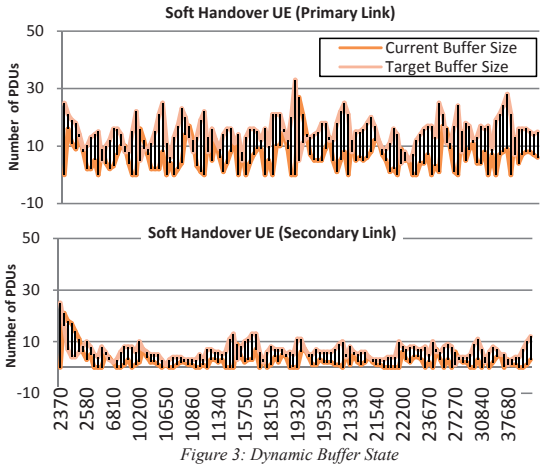

Figure 3: Dynamic Buffer State

Figure 3 illustrates a snapshot view over several time slots (1 time slot = 0.667 ms) of the amount of data in the nodeB and the dynamically changing target buffer size in terms of PDUs for a randomly chosen UE. The target buffer size is changing as the target delay is constant but the achievable transmission rate is varying. Also over- and under-runs are visible. They are highly dependent on estimation accuracy and the reporting frequency of flow control. The difference in link quality between serving and assisting links can also be seen.

Figure 4 shows the relative throughput losses when comparing ideal Multiflow case with flow control based (realistic) simulations for 1 UE/cell. Flow control is carried out every 10 TTIs with a target buffer delay (TBD) of 20 TTIs, i.e., the target buffer size is determined by the transmission history from the previous 20 TTIs. It can be seen that the impact of modeling flow control is minimal in the baseline case with no Multiflow enabled. However, when enhancing Multiflow simulations with flow control a performance loss of about 15% becomes visible for Multiflow users. This can be attributed to the fact that the data distribution to the nodeB buffers is imperfect, and hence the transmission to a UE may be continuing in one

nodeB while the other has already emptied its buffer and is idle, and hence the throughput is reduced.

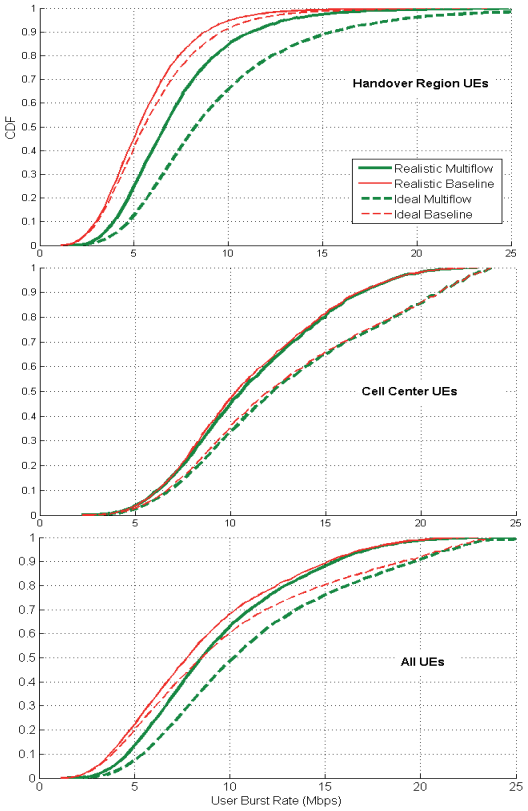

Figure 4: Ideal versus Realistic Multiflow for one user per cell

Figure 5 shows the performance of ideal and realistic multiflow scenarios with a higher system load. In this case we are assuming 4 users per cell. Similar flow control and target buffer delay is assumed as in the case of one UE per cell. It can be observed that the relative trends are consistent with the single UE case. In both cases, the overall performance gain in terms of user burst rate gain for multiflow enabled handover users is close to 30%.

Figure 6 illustrates the impact of reducing flow control frequency. Ideally, the nodeB should be able to request data every TTI. In practice however such high signaling load is not tolerable and flow control periods of e.g. 10 TTIs are assumed. Here, the effect of further reducing the period to 20 TTIs is shown. Unsurprisingly, the overall user throughput is negatively impacted. At lower flow control frequencies, the buffer has a reduced adaptability to changing radio environment. This leads to more frequent under-run periods where the data is available at the RNC but the nodeB buffer is empty and cannot be refilled until the next flow control request. Similar behavior is observed for individual UE classes such as soft, softer and non handover UEs and also for different load scenarios. It can be concluded that increasing the flow control frequency even further would result in higher gains and we can approach the ideal performance with a flow control frequency of one TTI.

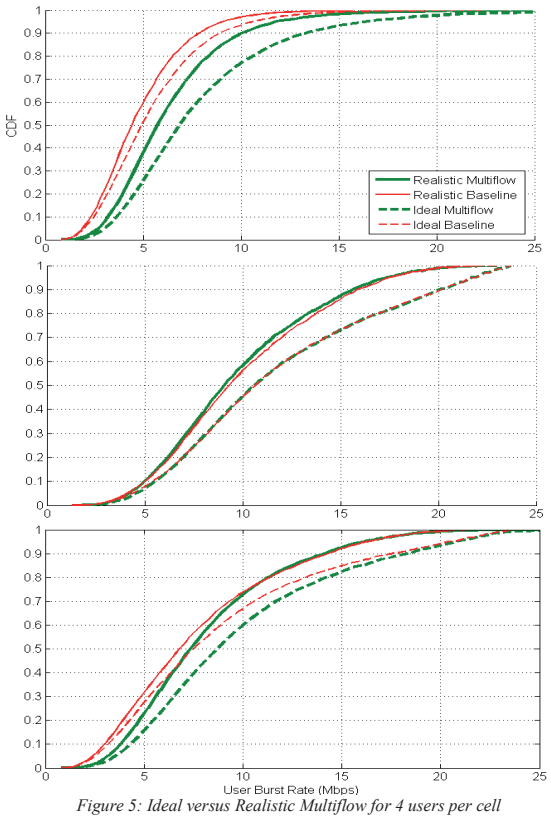

Figure 5: Ideal versus Realistic Multiflow for 4 users per cell

Figure 7 compares several values for fixed target buffer delay for all multiflow UEs. The target buffer delay (TBD) is chosen to be a multiple of flow control period in order to optimize link imbalance and under-runs. A higher value of TBD would reduce under-runs at the cost of causing more link imbalance between serving and assisting link. A lower TBD ensures balanced links but may result in higher percentage of under-runs. In the following figure, for a fixed flow control period of 10 TTIs, four delay values of 2, 10, 20 and 90 TTIs are compared. The values of 2 and 10 TTIs are presented in order to illustrate the throughput trend. In practice however, a buffer delay less than the flow control period itself would not make sense. Even a value that equals the flow control period would encounter under-runs on a frequent basis. Our studies show that a value of buffer delay which is twice as much as the flow control frequency provides an optimal balance between avoiding excessive under-runs and balancing the data transmission.

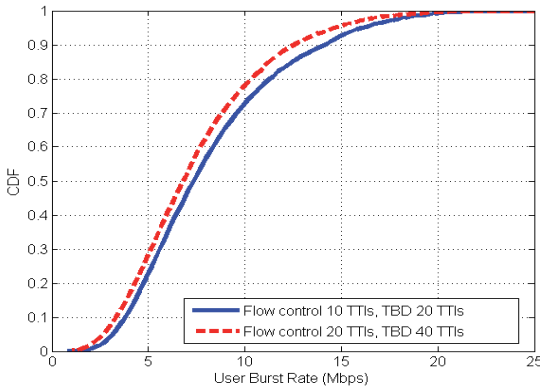

Figure 6: Impact of flow control frequency

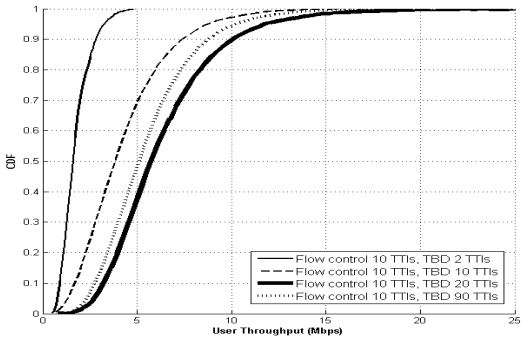

Figure 7: Impact of Target Buffer Delay

In legacy operation, negative and positive skew arise from different reasons. Positive skew, where PDU with sequence number n (SN(n)) arrives before PDU SN(n+1), is naturally produced from PDUs transmitted in correct order but at different times. Negative skew is caused by the HARQ operation, where PDU SN(n) is first dropped and followed by a successful reception of PDU SN(n+1). After the HARQ retransmission delivers the PDU SN(n) successfully, a negative skew is observed. An HSDPA terminal implements a so called re-ordering release timer (hereafter referred to as T1 timer) which stalls the delivery of the received MAC-ehs PDU to upper layers in case a PDU with a smaller SN was not received yet [6]. After the expiration of T1 timer the MAC-ehs PDU will be marked as lost, which triggers a RLC layer retransmission. In normal operation this is a rare event, but with Multiflow the skew will be larger such that the T1 timer is not adequate. Therefore, a new timer called RLC PDU Timer_reordering [6] is enabled in the Multiflow terminals which has a longer duration than the T1 timer, preventing the RLC retransmission in case of a long negative skew.

The durations for the T1 timer and the Timer_reordering are not defined in the specifications, instead they are vendor specific values. In our simulations, values of 50ms and 200ms are used for the T1 timer and the Timer_reordering, respectively. In Table 2, we show the relative increase of RLC layer retransmissions for Multiflow users utilizing two flows when compared to users with single traffic flow. In Multiflow simulations, the RLC retransmission rate consists of permanently failed HARQ processes (residual Packet Error Rate, PER) and PDUs that are correctly received but have a large skew such that Timer_reordering duration is exceeded. In the baseline simulations, the retransmission rate is composed only from the residual PER, as even the lowest negative skew can be handled already by the T1 timer.

TABLE II: INCREASE OF RLC LAYER RETRANSMISSIONS WITH MULTIFLOW

	Flow control		
Load level	**Algorithm 1**	**PER_SDU**	**Algorithm 2**
1 UE/cell	170 %	177 %	184 %
4 UEs/cell	247 %	262 %	235 %

From the table it is evident that applying Multiflow not only creates additional load with the redundant RLC messages, but it may also have an impact on the RLC layer performance if an excessive amount of retransmissions are triggered. The presented numbers are valid for the simulation scenario of on average balanced load among cells. In hotspot scenarios where neighbouring cells may have large difference in load, larger skews with consequently larger amount of RLC retransmissions can be expected. The employed flow control algorithms also perform without noticeable differences in low load scenarios. However, the selection of the algorithm is assumed to have an impact when the load increases.

V. CONCLUSIONS

In this paper, we have presented the impact of realistic flow control on the user throughput in HSDPA Multiflow operation by studying different flow control related parameters and PDU division algorithms. Further, RCL PDU skew incurred by the usage of two traffic flows was discussed. It was concluded that although Multiflow may create larger skew between two PDUs, the introduction of RLC PDU Timer_reordering is required to reduce the need for additional RLC layer retransmissions of PDUs. Our future work will concentrate on studying advanced flow control algorithms for further reduction of skew.

REFERENCES

[1] 3GPP, http://www.3gpp.org
[2] 3GPP TSG-RAN, RP-111375, “HSDPA Multiflow data transmission”, September 2011
[3] Yaver, A.; Marsch, P.; Pawlak, K.; Moya, F.S.; , "On the joint usage of MIMO and Multiflow in evolved HSPA networks," Communications (ICC), 2012 IEEE International Conference on , vol., no., pp.6076-6080, 10-15 June 2012
[4] Hytönen, V.; Puchko, O.; Höhne, T.; Chapman, T.; , "Introduction of Multiflow for HSDPA," New Technologies, Mobility and Security (NTMS), 2012 5th International Conference on , vol., no., pp.1-5, 7-10 May 2012
[5] 3GPP TSG-RAN WG1, R1-111141, Nokia Siemens Networks, Nokia, “Multiflow performance evaluation,” Feb 2011.
[6] 3GPP TS 25.321, Medium Access Control (MAC) protocol specification.

PIII

DOWNLINK BICASTING WITH MULTIFLOW FOR VOICE SERVICES IN HSPA NETWORKS

by

Vesa Hytönen, Pavel Gonchukov, Alexander Sayenko and Subramanya Chandrashekar 2013

Proceedings of the 6th IEEE International Workshop on Selected Topics in Wireless and Mobile computing (STWiMob)

2013 Sixth International Workshop on Selected Topics in Mobile and Wireless Computing

Downlink Bicasting with Multiflow for Voice Services in HSPA networks

Vesa Hytönen, Pavel Gonchukov
Department of Mathematical Information Technology,
University of Jyväskylä,
Finland
{vesa.a.hytonen, pavel.y.gonchukov}@jyu.fi

Alexander Sayenko
CTO, Industrial Environment,
Nokia Solutions and Networks,
Espoo, Finland
alexander.sayenko@nsn.com

Subramanya Chandrashekar
Mobile Broadband, WCDMA,
Nokia Solutions and Networks,
Bangalore, India
subramanya.chandrashekar@nsn.com

***Abstract*—The latest 3GPP Rel-11 is characterized by a number of new features, where a few of them specifically address UE performance at the cell edge. In particular, the Rel-11 downlink Multiflow improves noticeably the cell edge performance as a UE receives simultaneously data from two neighboring cells. Even though Multiflow caters for the cell edge performance and increased data rates there, this feature can also ensure more robust reception of the voice CSoHS and VoHS packets at the cell edge in the heavily loaded scenarios. In this paper, we study and simulate voice services in conjunction with Multiflow, where we utilize the latter to bicast data from two neighboring Node Bs.**

***Keywords*—HSPA, Multiflow, CSoHS, VoHS.**

I. Introduction

Even though recent advances in the area of the wireless communication are usually associated with Long Term Evolution (LTE), it is worth noting that High-speed Packet Access (HSPA) system is been continuously developed and improved, sometimes even outpacing the development and commercial deployment of similar features on the LTE side. According to the latest statistics, the overall number of the LTE subscriptions constitute 1% of the global market, whereas 90% belong to the HSPA terminals [1]. Facing the fact that HSPA will be dominant wireless broadband technology for many years, a number of new features were introduced for HSPA in the latest 3GPP Rel-11. Some of them cater for improved peak rates, such as downlink 4x4 MIMO, uplink MIMO, and a possibility to aggregate up to eight carriers (resulting in the total bandwidth of 40 MHz). At the same time, there are a few features that address specifically the cell edge challenges and problems.

One of the new features, called Multiflow [2], aims at improving the cell edge performance in downlink, whereupon a user equipment (UE) receives data from its main serving cell and a neighboring cell. Even though this scheme logically reminds the LTE cooperative multipoint (CoMP), it is simpler in its design in a sense that base stations (Node Bs) do not have to coordinate their transmissions and schedule data in a completely independent way based on their own internal performance and scheduling metrics. By transmitting data from two Node Bs, the cell edge throughput and performance almost doubled as different data is sent over each Node B.[1]

[1]There is an ongoing Rel-12 study item in LTE [3] aiming at developing the inter-Node B aggregation scheme similar to the HSPA Multiflow.

At the same time, there is an unexplored possibility of applying the Multiflow feature not only for the throughput demanding applications, but also to voice services to increase their robustness and performance at the cell edge. In case of the Rel-99 WCDMA system, the so-called DCH channel is configured for the circuit-switched (CS) voice to deliver data, whereupon all the cells in the UE active set can send the same data thus ensuring a high reliability level. However, as will be explained later, the DCH channel is not resource efficient when compared to the HSDPA channels, which can also carry voice data. On the other hand, prior to Rel-11 Multiflow, the HSDPA transmission could take place only from the serving cell. Thus, in this paper, we study further the combination of Multiflow with voice services. In particular, we exploit bicasting where we use Multiflow to send the *same* data from two Node Bs. Such an approach allows to benefit from reception of the same data from several sources as in the legacy DCH case, at the same time being capable of using advanced HSDPA features, such as HARQ, link adaptation, high-order modulation and coding schemes, etc. It must be also noted that unlike the downlink direction, the HSPA uplink is characterized by a possibility of receiving data from all the Node Bs in the E-DCH active set and data combining. This is partially the reason why this paper tackles downlink improvements only.

Yet another motivating factor to study further the reliability of the packet voice transmission in HSPA, in particular voice-over-IP (VoIP), is the wider availability of the Voice over LTE (VoLTE) service. As the call can be originated inside the LTE radio system, after which the terminal can simply move out of the LTE coverage, the whole Internet Multimedia Subsystem (IMS) call should be moved as the IMS voice session into HSPA. If an operator does not deploy VoLTE at all, then upon the CS fallback to the WCDMA system, the operator can also configure the call over HSPA.

Several scientific studies have been conducted over Multiflow, such as [4] and [5], to name a few. However, the previous research have mainly concentrated on analyzing the performance of Multiflow with packet switched data services, yet applying Multiflow for delivering voice over HSPA has not been investigated deeply.

The rest of the article is organized as follows. Section II presents at a cursory level the downlink Multiflow feature and basic concepts of the voice data transmission over the HSPA networks, in particular CSoHS and VoHS. This section also elaborates about a rational behind applying Multiflow for the

978-1-4799-0428-0/13/$31.00 ©2013 IEEE

voice data transmission. Simulation scenarios are presented in Section III. In Section IV, results, as well as analysis and discussions about the advantages and drawbacks of each scheme are presented. Finally, Section V concludes the article and outlines further research directions.

II. Overview of Concepts

In this section, we provide a brief overview of the downlink Multiflow feature as well as basic principles behind combining it with bicasting of voice data.

A. Multiflow

As already mentioned earlier, the downlink Multiflow feature improves noticeably the cell edge performance because a UE receives simultaneously data from two neighboring cells. In other words, the interfering neighbor now turns into the source of data transmission. The basic design principles and performance number can be found in [6] and [7] respectively. As per Rel-11 functionality, Multiflow is supported in various forms capable of aggregating up to four carriers over two different frequencies that can reside in the same or different bands [2].

Of course, to receive data independently from two cells and cancel interference, a UE would need typically at least two receive antennas and the type3i receiver. However, all these techniques are already in the commercial use by many UE vendors that make dual-cell HSDPA chipsets (DC-HSDPA), which becomes the common baseline not only for USB dongles, but also for smartphones. In fact, common availability of DC-HSDPA in the mobile terminals makes it possible to deploy also Multiflow because the latter is functionally close to DC-HSDPA. Two receive chains are tuned to receive data from two cells residing at the same frequency, as opposed to two different frequencies as in DC-HSDPA case.

Being a cell edge feature, Multiflow is mostly beneficial for the UEs with small channel imbalance between its current serving cell and a neighboring cell. At the same time, Multiflow can provide gains with the link imbalance of up to 6dB.

B. Voice over HSPA

Conventionally, voice calls are carried over the so-called circuit switched (CS) services, mapped to the DCH radio bearer as per WCDMA Rel-99 functionality. This is a resource hungry approach as the DCH channel constantly occupies resources despite pauses in the speech and despite the fact that voice data may need to be delivered only sparsely. To address those inefficiencies, a more advanced scheme was introduced in Rel-7 called circuit switched voice over HSPA (CSoHS). The premise idea is that the same voice payload is sent over the RLC unacknowledged mode (UM) mapped to the HSDPA channel. Such an approach allows for allocating resources only when they are needed and, more importantly, it allows for applying advanced techniques such as HARQ, link adaptation, higher order modulation and coding schemes. Starting from Rel-9, the HSPA system supports VoIP over HSDPA (VoHS) solution, which is conceptually similar to the LTE VoIP (VoLTE). In particular, voice payload is carried over RTP/UDP/IP protocol stack, over the RLC UM mode, which is mapped to the HSPA packet service (PS) bearer with

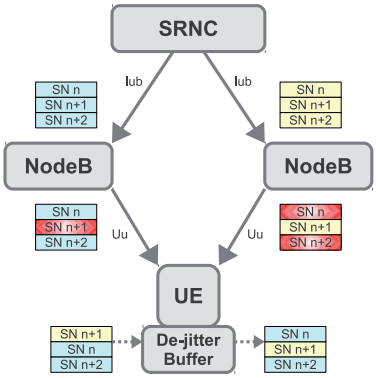

Fig. 1. Voice packet bicasting

the appropriate QoS parameters to differentiate it from the normal best-effort PS connections. The session signaling and management are done through IMS as in LTE. It is important to note that from the Node B point of view there is absolutely no difference whether to schedule CSoHS or VoHS data as both of them are carried over the RLC UM mode. Thus, the Node B just observes arriving RLC UM packets, which it schedules irrespective of whether they belong to CS or PS radio access bearer.

As mentioned briefly in the Introduction part, the drawback of the CSoHS/VoHS services is that a UE can receive data only from *one* cell in the downlink direction, which is a limitation of the baseline HSDPA design. As opposed to that, the Rel-99 WCDMA voice service can receive data from *all* the cells in the active set, making it quite robust in the cell edge environment. With Rel-11 Multiflow, one can combine CSoHS/VoHS services with Multiflow to achieve the best trade-off between the link efficiency provided by HSDPA and robustness ensured by Multiflow.

C. Voice data bicasting with Multiflow

In this section, the principle of improving the CSoHS/VoHS performance by applying data bicasting in conjunction with Multiflow operation is discussed. As opposed to delivering different data over two traffic flows, the same information bits are transmitted over both streams in case of with CSoHS/VoHS. Fig. 1 depicts a simplified functional model with two data flows that bicast data to a UE. Firstly, the RNC duplicates the generated RLC UM PDUs containing AMR voice payloads and sends them over the Iub/Iur interface to both Node Bs serving the UE (it should be noted that in case of normal data the RNC does not duplicate data, but rather splits it between the Multiflow links based on their speeds and quality). Then, those RLC UM PDUs are transmitted independently by two Node Bs over the physical channel to increase the probability of correct reception of each individual RLC PDU. Each Node B schedules independently RLC UM PDUs with voice payloads, which makes this scheme much simpler when compared to the LTE CoMP, where tight synchronization between eNode Bs over the X2 interface is needed.

Since the same PDU can be received by a UE over both flows, the duplicated one should be discarded by the UE at the RLC layer after a notification of an already existing sequence number (SN). In fact, this is an already existing functionality inside a UE because in case of CSoHS/VoHS services, RLC UM PDUs with voice data may arrive in different order due to wrongly decoded transport blocks which results in retransmissions of the data and varying HARQ process durations. Thus, in order to prevent unnecessary issues in the upper layers, a UE supporting CSoHS/VoHS implements a so-called de-jitter buffer that allows for reordering and duplicate detection of the received data before delivering froward the AMR frames. This is done based on the RLC UM sequence number that is part of the RLC layer [8], [9]. Such an approach does not require architectural or functional changes at the UE side and is completely transparent with regards to the CSoHS or VoHS service.

III. Simulation Model

The simulation results presented in this paper are obtained by means of a quasi-static system level simulator, which follows the general 3GPP simulation methodology and captures all the essential aspects of the HSDPA PHY and MAC layers. Exactly the same tool has been used to study and contribute on various HSPA multi-point transmission schemes, simulation results for which are already captured in [6].

The main simulation parameters are presented in Table I. The physical abstraction of the links between UEs and Node Bs is based on the ITU PedA profile. A seven site wrap-around layout was utilized in the current study. To study voice performance under heavy load conditions, we create a scenario with low- and high-loaded cells. The low-loaded cells are able to provide additional bicasting transmissions for Multiflow capable UEs located in the high-loaded cells. In our simulations we conduct three cells in the center of the network that have considerably higher load than others, with a load ratio varying from 2:1 to 4:1. This models, for instance, a congested downtown area or a hot spot surrounded by cells with a moderate amount of UEs. In the low-loaded cells, 20 CSoHS/VoHS UEs are dropped uniformly, whereas the high-loaded cells accommodate from 40 to 80 CSoHS/VoHS UEs. As will be presented later, the saturation point, at which the 80ms voice packet delay budget is starting to be inadequate, is reached already with 50 to 55 CSoHS/VoHS UEs/cell, which is explained by the limitation of available cell resources. Certainly, by increasing the number of UEs up to 80 will result in a heavily loaded environment. Furthermore, we add four best effort (BE) UEs with the full buffer traffic to each cell in the network to study the remaining capacity.

It makes sense to mention explicitly the Node B target delay of 80ms applied for all the voice packets. If the Node B cannot schedule a packet within this time, then it is dropped from an internal buffer. As will be presented later, the Node B target delay is one of the reasons for packet drops caused in turn by the lack of scheduling opportunities. It also bears mentioning that in our implementation this delay does not interrupt the ongoing HARQ processes. As will be shown later, this is a reason why certain packets have a delay of up to 90ms.

The scheduler deployed in the simulator prioritizes delay-sensitive traffic over best effort. The scheduling order of

TABLE I. Simulation parameters.

Parameter	Value
Cell Layout	Hexagonal grid, 7 Node Bs, 3 sectors per Node B with wrap-around
Inter-Site Distance	1000 m
Path Loss	L=128.1 + 37.6log10(R), R in kilometers
Penetration Loss	10 dB
Log Normal Fading	
Standard Deviation	8dB
Inter-Node B Correlation	0.5
Intra-Node B Correlation	1.0
De-correlation Distance	50m
Max BS Antenna Gain	14 dBi
2D Antenna Pattern	$A(\theta) = -min(12(\theta/\theta_{3dB})^2,\ Am)$, where $\theta_{3dB} = 70\ degrees,\ Am = 20dB$
Channel Model	PedA 3 km/h
CPICH Ec/Io	-10 dB
UE Antenna Gain	0 dBi
UE Noise Figure	9 dB
UE Receiver Type	Type3i, 2 Rx ant. LMMSE equalizer
Maximum Sector Transmit Power	43 dBm
Total Sector Overhead Power	30 %
CPICH Transmit Power	10 %
Traffic Model	AMR 12.2 kbps voice, 0.5 voice activity ratio
SID	Every 160ms during voice inactivity
Voice packet delay budget	80ms
Flow Control on Iub	Ideal and instantaneous
Maximum number of parallel HS-SCCH channels/cell	4
CQI	Ideal with 3 TTI delay

CSoHS/VoHS UEs is determined by the Head-of-Line (HoL) delay, which gives higher priority to queues, whose packet buffering time gets closer to the maximum delay limit. In case there are remaining resources in the cell after scheduling the voice traffic, one additional BE UE can be scheduled who will be allocated all residual transmission power and the number of OVSF codes it requires. In addition to that, the bicasting scheduling rule was introduced such that cells always prioritize their primary voice traffic flows over the assisting flows. This ensures that CSoHS/VoHS UEs having a primary data flow with a cell will never be blocked by an existing assisting flow. The applied scheduling, however, favors the assisting voice flows over best effort traffic, due to which the residual cell capacity slightly suffers from bicasting. The target of such approach is, first of all, to show the upper bound improvement of call quality of CSoHS/VoHS UEs, and secondly, provide the worst case scenario regarding how bicasting affects the remaining cell capacity after scheduling all available voice traffic. As mentioned earlier, best effort traffic consists only of full buffer data, which inevitably will be subject to lower amount of available cell capacity due to such a greedy resource allocation.

Yet another scheduling enhancement we use is a power control mechanism applied for voice traffic, which tries to ensure adequate call reliability by adjusting the transmission power according to channel quality. Node B estimates the power requirement based on the channel quality indication (CQI) received from the UE, from which the achievable data rate is measured. The theoretical maximum transport block size is then matched to the number of bits in transmission in

order to determine the final power requirement that matches a certain block error rate (BLER) target. The same power control method is used for the HS-SCCH and HS-PDSCH channels. Although power consumption for HS-SCCH is modeled, decoding of HS-SCCH is assumed ideal. For HS-PDSCH, a BLER of 10% after the first HARQ transmission is targeted. The aggregate cell transmission power in the simulator consist of pilot channel (CPICH), other common control channels and UE dedicated HS-SCCH and HS-PDSCH channels:

$$P_{\text{tot}} = P_{\text{CPICH}} + P_{\text{common}} + \sum_{i}^{n} (P_{\text{HS-SCCH},i} + P_{\text{HS-PDSCH},i}), \quad (1)$$

where i refers to one scheduled UE and n is the total number of scheduled UEs per transmission time interval (TTI).

As mentioned briefly earlier, Multiflow should and cannot be enabled to all the UEs in the system since only the UEs residing in the handover area can really benefit from it. Based on the previous simulation results from this feature [6], we limit Multiflow only to those UEs that have a link imbalance of less than 6dB.

It is also worth noting that in our simulations we do not make a distinction between the CSoHS and VoHS services. Their difference is partially in the area of the call establishment and handling, which is anyway not modeled in the simulator. Even though VoHS is carried over IP/UDP/RTP protocol stack, which results in much larger packet sizes, it is usually the case that an operator turns on the robust header compression making the resulting packet size almost identical to CSoHS.

IV. Simulation Results and Analysis

To assess the voice call quality in the heavily loaded parts of the network, the amount of dropped packets from UEs is measured. The packet drop ratio is calculated separately for all the UEs based on the number of dropped voice packets out of all transmitted packets. The obtained statistics is separated into two groups: all UEs served by the heavy-load cells (see Fig. 2a), and UEs residing at the edge of the heavy-load cells whose second strongest cell is not among the heavy-load cells (see Fig. 2b). The purpose of presenting the second group is to show the explicit improvement from voice bicasting. When bicasting is enabled, the packet drop ratio of Multiflow capable UEs declines significantly. As mentioned before, although the assisting channel may be up to 6dB weaker than the primary channel, the power control algorithm is able to reduce the HARQ drops to minimum, as long as there are enough free resources in the cell. Thereby the drops are mainly caused by reaching the queuing delay limit. By looking at Fig. 2b, always-on bicasting of voice traffic ensures that the cell edge UEs will greatly benefit from bicasting, practically leading to 0% of UEs being in an outage situation.

Fig. 3 presents a different view on the packet drop statistics, where we present CDF curves based on the packet drop rate samples taken from all the connections. For the sake of clarity, only three load levels are shown that are the most interesting ones from the viewpoint of the estimation of the voice capacity. As can be seen from the figure, voice bicasting improves noticeably the performance by decreasing the drop error rate. In fact, the performance improvement can be also understood as the voice capacity increase. Referring to [10], at least 98%

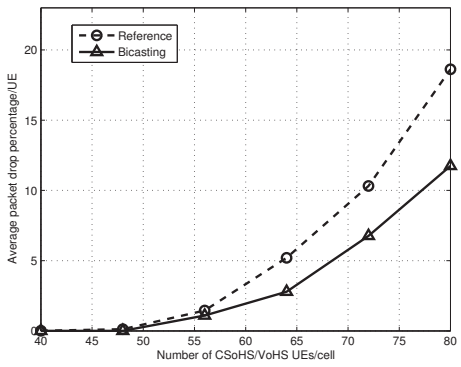

(a) All UEs

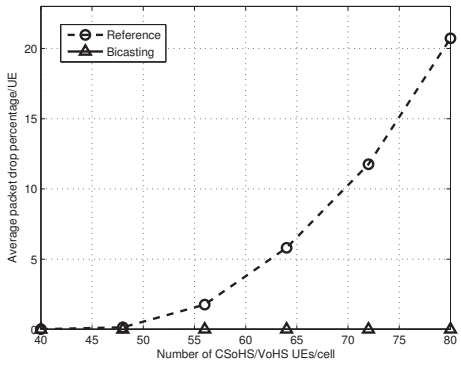

(b) Multiflow capable UEs

Fig. 2. Average packet drop percentage/UE in the heavily loaded cells

of packets should be delivered successfully within 50ms delay limit in order to avoid having a UE in an outage condition.[2] Moreover, overall capacity of the network with regards to VoIP defined in [10] says that at most 2% of UEs should be in outage before full voice capacity is reached, while other proponents use to relax this requirement as well. Nevertheless, it can be seen that regardless of the outage criteria, the overall capacity of the network could be extended by using bicasting. As an example, considering a tight outage definition of 2% of unsuccessful packets, bicasting improves the maximum voice capacity by approximately 7%.

Similar to packet drop statistics, delays of the successfully received packets are divided into two parts. Mean packet delays for all UEs residing in the heavy-load cells are shown in Fig. 4a and for UEs affected by bicasting from low-load cells in Fig. 4b. A reason for high improvement of the packet delays is that even in moderately loaded cells, where 20 primary CSoHS/VoHS UEs share cell resources, the cell capacity is

[2]Some performance evaluation assumptions relax this requirement to 97%, as for instance presented in [11].

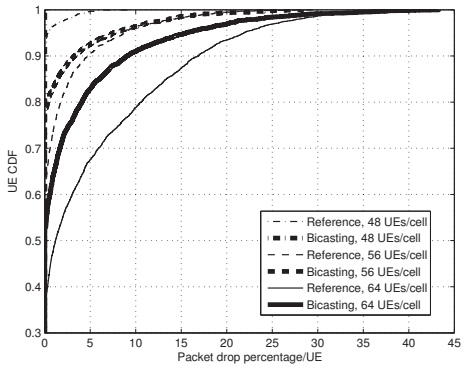

Fig. 3. Packet drop percentages of UEs in the heavily loaded cells

not fully consumed with regards to the transmission power or OVSF codes. In addition to improving the voice quality, reducing the average packet delay in the access network by even 35 milliseconds allows for greater flexibility and delay tolerance also in the core network.

In Fig. 5, we present delays of successfully received packets in the heavy-load area for the three most important load levels in the from of the CDF curves. Similarly to Fig. 3, there is a clear observable trend that bicasting decreases packet delays, which is in fact a reason for lower drop rates, and as a result a possibility of having a higher capacity of voice flows that a system can admit. It should be noted that the tails after the 80ms maximum delay limit are caused by pending HARQ processes, which we do not terminate once the transmission starts. As can be seen, it results only a quite limited number of packets that violate the delay boundary of 80ms reaching the maximum delay of 90ms.

As mentioned before, the scheduler deployed in the cells is very greedy considering voice traffic, as it always prioritizes traffic queues of CSoHS/VoHS UEs over those of best effort UEs. The reason for the selection of this type of resource allocation was to observe theoretical maximum improvement of performance with bicasting. Certainly, this has a negative impact on the residual cell capacity that can be used for best effort UEs. In Fig. 6, the remaining cell throughput is depicted in both, low- and high-load cells. During the simulations, bicasting was not limited to the edge of unequally loaded cells, but instead it was possible in the whole simulated network. Naturally, the capacity of the low loaded cells is negatively affected by the extremely frequent usage of the second flow near the group of heavily loaded cells, but it is also slightly reduced by dual-flow operation among UEs purely served by two low-load cells.

Partially due to the same reason, the capacity in heavy-load cells significantly drops. Now, bicasting is possible also between two high-load cells as well as a high load cell operating as an assisting cell to UEs outside the congested area. As the number of assisting flows increases, the saturation point regarding the available transmission power of OVSF codes is

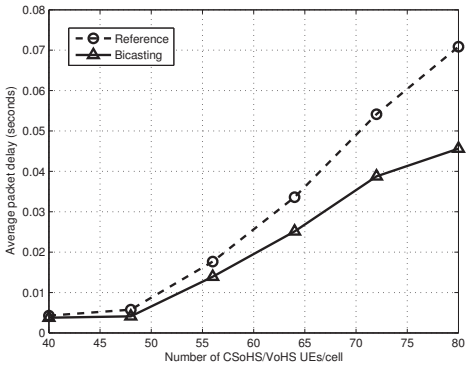

(a) All UEs

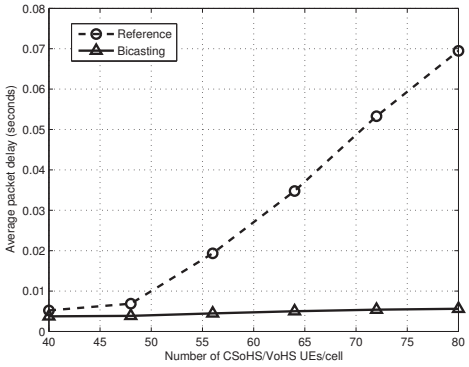

(b) Multiflow capable UEs

Fig. 4. Average packet delays in the heavily loaded cells

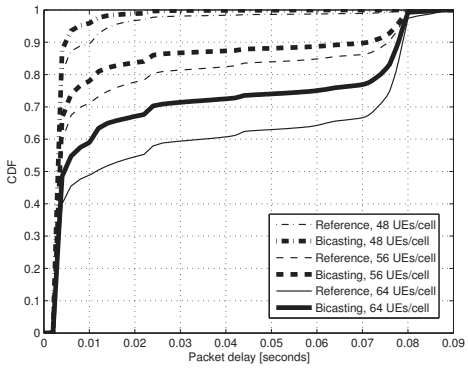

Fig. 5. Packet delays of UEs in the heavily loaded cells

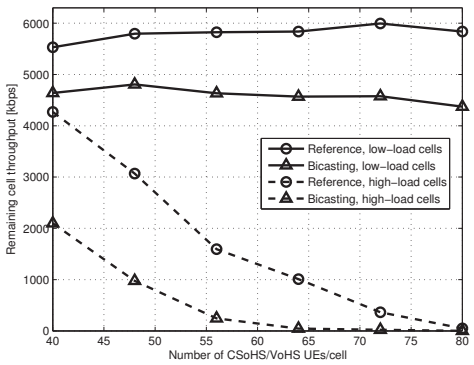

Fig. 6. Remaining cell throughput

reached earlier. As mentioned before, the lack of resources is beginning to be insufficient when the number of primary voice flows is around 50 to 55. With bicasting, similar capacity is realized already with 40 to 45 primary data flows due to serving of additional assisting flows.

V. Conclusions

In this paper, we have presented and studied a combination of the downlink Multiflow feature with the CSoHS/VoHS services to provide the continuous bicasting of voice data to the UEs residing at the cell edge. Due to the architectural modularity, such a combination does not cause any additional implementation complexity at the UE side: the data bicasting is a network side decision, as a CSoHS/VoHS capable UE anyway has to be able to perform duplicated data detection and avoidance.

Based on the presented simulation results, in uneven traffic conditions where a part of the network is highly congested, a large part of UEs with voice traffic suffering from the lack of scheduling opportunities can be very effectively served over an additional flow from neighboring cells having available resources. Voice data bicasting with Multiflow can improve significantly performance of the cell edge UEs leading to almost zero packet drop error rate. The packet delays are also reduced noticeably. It should be noted that the presented results and findings can be applied to LTE. Its voice service architecture is identical to the HSPA VoHS service, and it has an ongoing Rel-12 study item on the dual-connectivity [3], solutions for which are close the Rel-11 HSPA Multiflow.

It should be noted that we presented the upper-bound performance improvement for voice traffic by intentionally asking the scheduler to prioritize always the voice traffic, even the assisting flows over the primary BE connections. According to the results, the service of voice traffic with bicasting actually became redundantly robust, leaving room for further studies with more relaxed and smart division of cell's resources. The dual flow scheduling could be optimized such that high benefits for voice UEs are achieved while the decrease in best effort traffic is minimized. In particular, it is not absolutely necessary to perform bicasting all the time, but only when the voice connection in the serving Node B starts to experience heavy packet drops. One possible solution for this case would be to ask the assisting Node B to monitor the UE uplink HARQ feedback channel and transmit packets only when NACKs are observed. An alternative option would be to follow the reported CQI values. In fact, since a UE transmits a single HS-DPCCH feedback channel in the uplink direction, the assisting Node B always has an access to HARQ and CQI information for the serving Node B.

Acknowledgment

The authors would like to thank Eric Bouton, Jeroen Wigard, Matthias Hesse, Thomas Höhne and Karri Ranta-Aho from Nokia Solutions and Networks for their contribution and guidance.

References

[1] "Global mobile market shares," Dec 2012, 4G Americas statistics, based on Informa Telecoms & Media WCIS+. [Online]. Available: http://www.4gamericas.org

[2] 3GPP TS 25.308, "High Speed Downlink Packet Access (HSDPA); Overall description; Stage 2," Mar 2013.

[3] 3GPP TR 36.842, "Study on small cell ehancements for E-UTRA and E-UTRAN – higher layer aspects," Jun 2013.

[4] A. Yaver, P. Marsch, K. Pawlak and F. S. Moya, "On the Joint Usage of MIMO and Multiflow in Evolved HSPA Networks," in *IEEE International Conference on Communications (ICC), 2012*, Ottawa, Canada, Jun 2012, pp. 6076–6080.

[5] Weiyan Ge, R. Kapoor, Danlu Zhang, S. Sambhwani, M. Scipione, "System performance of Inter-NodeB MF-HSDPA with RLC and MAC enhancements," in *IEEE International Conference on Communications (ICC), 2012*, Ottawa, Canada, Jun 2012, pp. 6071–6075.

[6] 3GPP TR 25.872, "High Speed Packet Access (HSDPA) Multipoint Transmission (Release 11)," Sep 2011.

[7] V. Hytönen, O. Puchko, T. Höhne, T. Chapman, "Introduction of Multiflow for HSDPA," in *IEEE Fifth IFIP International Conference on New Technologies, Mobility and Security*, Istanbul, Turkey, May 2012, pp. 1–5.

[8] H. Holma and A. Toskala, *WCDMA for UMTS - OFDMA and SC-FDMA Based Radio Access*. West Sussex PO19 8SQ, England: John Wiley & Sons, Ltd, 2009.

[9] 3GPP TS 25.322, "Radio Link Control (RLC) protocol specification," Mar 2013.

[10] Report ITU-R M.2134, "Requirements Related to Technical Performance for IMT-Advanced Radio Interface(s)," Nov 2008.

[11] 3GPP R1-131704, "System Simulation Assumptions for VoHSPA," Qualcomm Incorporated, Apr 2013.

PIV

VOICE TRAFFIC BICASTING ENHANCEMENTS IN MOBILE HSPA NETWORK

by

Vesa Hytönen 2014

Proceedings of the 11th IEEE International Symposium on Wireless Communication Systems (ISWCS)

Voice Traffic Bicasting Enhancements in Mobile HSPA Network

Vesa Hytönen
Department of Mathematical Information Technology,
University of Jyväskylä, Finland
vesa.a.hytonen@jyu.fi

***Abstract*—This paper discusses methods for improving the effectiveness of delivering voice traffic over High-Speed Downlink Packet Access (HSDPA) network by employing transmission diversity with Single-Frequency Dual-Cell (SF-DC) Aggregation that is part of the Multiflow specification. SF-DC Aggregation allows the user to be served at the same time by two different cells. The enhancements discussed in the paper capitalize strongly on the availability of the composed Channel Quality Indication (CQI) feedback at both serving cells. According to the results obtained from the network simulations, the ability to select the better channel for each voice transmission significantly decreases the required transmission power of the cell, thus also improving the residual cell capacity available for best effort (BE) traffic. The required updates are completely software-based and are applied only in the access network, making them transparent to user terminal.**

Keywords*—*HSPA, Multiflow, SF-DC Aggregation, Bicasting, CSoHS, VoHS.

I. Introduction

According to [1], the growth in the number of High-Speed Packet Access (HSPA) subscriptions will increase in the coming years along with the volume of real-time communication in mobile networks. In addition to growing amount of video content delivered in the network, there is an interest towards extending the usage of HSPA to deliver voice traffic originating from circuit switched network or IP Multimedia Subsystem (IMS), creating a demand for an efficient control of real-time traffic delivery over the wireless channel [2].

One of the recent entrants in the HSPA+ standard, developed by the 3rd Generation Partnership Project (3GPP), is a multipoint transmission concept called Multiflow that was introduced in the Release 11 for HSDPA [3]. Resembling Cooperative Multipoint (CoMP) concept in Long Term Evolution (LTE), Multiflow aims to improve the data plane performance particularly in cell edge areas by utilizing additional traffic flows towards user terminal (UE). In its simplest form, SF-DC Aggregation, a UE can be served concurrently by two cells, known as the primary and secondary serving cells. Multiflow is conventionally designed to elevate the user-specific data rate in Downlink direction. However, network operators have an option to enable duplication of user plane data over the primary and secondary data flows, which is useful especially with traffic, such as voice traffic, that demands a higher level of quality of service (QoS) [4]. Transmission diversity with multiple low- or uncorrelated channels provided by Multiflow enables protection against multipath attenuation as well as shadow fading, and transmitting the same data over these channels greatly improves the likelihood of a successful packet reception.

978-1-4799-5863-4/14/$31.00

The current study aims at improving the effectiveness of voice calls delivered over HSPA network by utilizing SF-DC Aggregation related methods. Specifically, enhanced voice-traffic flow management and scheduling are examined and evaluated by network simulations. Some of the recent efficiency improvement studies related to voice over HSPA have concentrated on the Enhanced Serving Cell Change (E-SCC) ([5]) as well as duplication of voice data flow by utilizing connections with different network operators ([6]). Research on using Multiflow for improving voice service is, however, exiguous, mainly due to the novelty of the multipoint transmission concept. Many of the principles presented in this paper can also be applied for DL CoMP in LTE Advanced. However, the existing X2 interface between eNodeBs in LTE already enables an efficient dynamic cell selection, making the applicability of certain parts unnecessary. In a network with non-saturated voice capacity, the presented voice traffic control, in conjunction with an efficient power control operated by the NodeB, is capable of saving significant amount of transmission resources at the NodeB which also results in an extended residual cell throughput. One should notice that the methods proposed should be completely software-based that can be taken into use by a firmware update, and that the updates can be enabled in the access network devices, NodeB in particular, which makes the changes transparent to UEs.

The remainder of the paper is organized as follows. The proposed flow management mechanisms are discussed in Section II. The system model and scenarios for simulations are described in Section III, and the obtained results are presented in Section IV. Section V concludes the paper.

II. Voice Bicasting Enhancements

Two fundamental targets regarding voice traffic service are tackled in this paper. First, the data should be delivered to UE as reliably as possible while complying the temporal limitations in order to maintain a good call quality and to avoid outage condition. Second, the resource requirements of voice users ought to be minimized to achieve a better residual network capacity. Employment of SF-DC Aggregation allows the above to be performed by operations related to flow management and scheduling in NodeB.

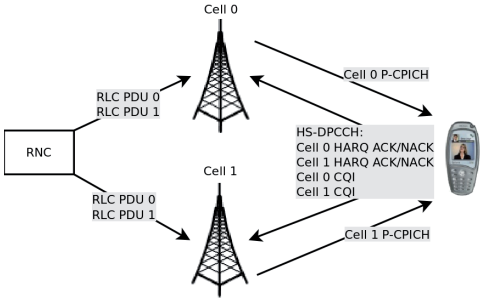

Fig. 1. PDU duplication and composite HS-DPCCH

A. Traffic Flow Utilization

This section concentrates on discussing the rules based on which the two traffic streams in SF-DC Aggregation should be used or deactivated in relation to voice bicasting. The underlying target is to serve the UE over the channel that is likely to be the better from the two available channels. The roles of Radio Network Controller (RNC) and NodeB and their suitability for participating the flow control process are considered.

1) The role of RNC in enhanced voice traffic management: RNC supporting Multiflow is responsible for either splitting or duplicating the user plane data between the flows in the Radio Link Control (RLC) protocol layer [7], [4]. With conventional unspecified bit rate (UBR) QoS traffic (e.g. FTP, web browsing), RNC splits the information for the Multiflow cells, and the cells forward all the data to UE according to their internal scheduling operation. Applying a slightly different approach for voice traffic, the RNC can duplicate each Protocol Data Unit (PDU) to both serving Multiflow cells [4].

It is possible to augment the responsibilities of RNC in bicasting process so that it may either duplicate or split the voice data based on certain conditions. The RNC would have to rely upon the channel measurement reports from UEs, for example, to deliver the user data to the serving cell with a stronger channel for downlink transmission. A disadvantage of this approach relates to the accuracy of how the ”best” cell can be selected. First of all, this approach assumes that periodical measurement reports are available to the RNC, which can be enabled by the network service provider. Assuming periodical reporting is enabled, channel measurement reports are usually filtered over a longer period of time, which means that they represent the average quality level of the channel. This will rule out the possibility of fast adaptation to channel fluctuation, especially since the reporting interval may range from hundreds of milliseconds to several seconds. Since the enhanced traffic control by RNC would likely lead to very ineffective voice bicasting, the function of RNC in this study is restricted to simple duplication of each voice-traffic related RLC PDU to both cells, as depicted in Fig. 1, leaving further flow control to be performed by NodeBs.

2) NodeB controlled flow management: The primary control of the voice traffic flows is assigned to NodeB. As concluded in the previous section, RNC will duplicate all data to both Multiflow cells and the cell decides whether it should serve the UE or not in certain Transmission-Time-Interval (TTI). The actual advantage of this method originates from the fact that the UE will report a composite CQI and Hybrid Automatic Repeat Request (HARQ) acknowledgement of both serving cells on one High-Speed Dedicated Physical Control Channel (HS-DPCCH) that can be decoded by both cells (see Fig. 1), allowing a cell to estimate the second Multiflow link quality and compare it to the cell's own link [8].

For achieving the best performance from the viewpoint of overall resource consumption, each RLC PDU should be transmitted only from one cell. Sending the same packet from both cells always dissipates the remaining capacity. Since the RNC duplicates all data over both Iub interfaces, it is the cell's responsibility to ensure no duplicate transmission takes place, unless explicitly desired. Therefore, the cell needs to discard the PDUs that it should not transmit from its queue. The PDU extraction will be done immediately when the cell receives a new packet from the RNC. By applying the same rules on both Multiflow cells and assuming the primary serving cell knows which PDUs are deliverable also to the secondary serving cell, it can be guaranteed that each PDU will be transmitted exactly from one cell. This method is selected for the study, as it allows a controlled way of handling PDUs in both Multiflow cells.

The cell relies on the uplink CQI reports when deciding whether to discard a packet. When a cell receives a new PDU on the Iub and detects that the Multiflow operation is enabled, it inspects the composite HS-DPCCH including the CQI report for both flows. Upon the CQI lookup, the cell calculates a relative channel quality between both serving cells by

$$\Delta r_n(l) = r_{n,0}(l) - r_{n,1}(l). \tag{1}$$

Since the CQI report received in TTI l from UE n contains only the index of the supported Modulation and Coding Scheme (MCS), the cell may match the index to transport block size, which is here denoted by $r_{n,i}(l)$. Subscripts 0 and 1 represent the current cell and opposite Multiflow cell, respectively. Both serving cells will also trace the slope of the channel by utilizing channel quality information from previous TTIs. As most of the physical layer errors take place during an adverse channel progression (assuming a constant interference level), i.e. channel quality decreased between the creation of CQI report and the data transmission, a favorable condition would be to switch the data flow if the opposite flow has an increasing trend in quality. A simple linear estimation of the slope for cell i is performed as follows:

$$m_{n,i}(l) = r_{n,i}(l) - r_{n,i}(l-1). \tag{2}$$

It can be assumed that the CQI already includes a filtered representation of the channel, therefore a direct subtraction of two subsequent data rate values based on supported CQIs will suffice. Another reason for not tracing the CQIs from a longer period is that the algorithm needs to follow the small-scale fading of the channel as well as possible, which would not be possible with averaging CQIs over a long duration.

After performing the steps above, cells that receive bicasted PDUs from the RNC follow simple heuristic rules for discarding the packet. In case the cell observes that the CQI related to its own channel is worse than the CQI of the second Multiflow channel, it discards the packet. When the CQIs are equal, which often can be the case as the CQI is a discrete variable,

the cell makes the decision based on the calculated channel slopes and discards the packets if the own slope is smaller than the opposite slope. Moreover, only the primary serving cell enqueues the new PDU if the slopes are also similar. In other form, set the discard flag as follows:

procedure CELL::DISCARDPDU(psc)
▷ psc = primary serving cell
  $discard \leftarrow$ `False`
  if $\Delta r_n(l) < 0$ **then**
    $discard \leftarrow$ `True`
  else if $\Delta r_n(l) = 0$ **then**
    if $m_{n,0}(l) < m_{n,1}(l)$ **then**
      $discard \leftarrow$ `True`
    else if $m_{n,0}(l) = m_{n,1}(l)$ **and** $psc =$`False` **then**
      $discard \leftarrow$ `True`
    end if
  end if
  return $discard$
end procedure.

The rules should guarantee that the UE will always be served over either of the flows with a sufficient channel quality, which affects not only on the successful packet reception probability but also the transmission power requirement. When the conditions are met in a cell, i.e. it is allowed to serve the UE, the cell's internal scheduler will weigh the priorities of each of its active UEs. The actual scheduling is discussed in the next section.

B. Scheduling and Power Control

After the schedulability of each UE is resolved, the cell should order its UEs based on their scheduling metrics. The scheduling and power control methods described here are applied to both baseline and Multiflow simulations in this study.

For best effort UEs, basic proportional fair scheduling is a commonly used method, which tries to provide some level of fairness, while at the same time promoting UEs whose relative channel quality is above those of other UEs [9]. The basic formula for proportional fair user selection is

$$n = \arg\max_{n \in N} \frac{r_n(l)}{\overline{r}_n(l)}, \tag{3}$$

where n denotes a user belonging to a group of active users N and $r_n(l)$ is the instantaneous achievable throughput for user n in TTI l based on the CQI report. $\overline{r}_n(l)$ represents the moving average data rate obtained by

$$\overline{r}_n(l+1) = (1-\alpha)\overline{r}_n(l) + \alpha r'_n(l). \tag{4}$$

Here, $r'_n(l)$ denotes the actual data rate from previous transmission in TTI l and α is the forgetting factor. This method is applied to the best-effort traffic flows in this study. According to the formulas above, if a UE is scheduled, its priority metric will decrease in the following TTI, whereas if an active UE was not selected by the scheduler, $r'_n(l)$ becomes zero and the priority is increased. This is to prevent the UE from being blocked for long periods of time.

With QoS-dependent voice data it is crucial to deliver the packets within a certain delay budget in order to maintain a good call quality. This is often done by applying a delay coefficient that modifies UE's scheduling priority based on how long the voice packets have stayed in the transmission buffer. In this paper a similar extended approach is used, with a basis on proportional fair. For voice users, (3) becomes

$$n = \arg\max_{n \in N} \frac{r_n(l)}{\overline{r}_n(l)} D_n, \tag{5}$$

where D_n is the delay factor:

$$D_n = max\{w \cdot c_n, 2^{\tau_n - (db - x)}\}. \tag{6}$$

c_n denotes the number of packets in UE's transmission buffer. This number is multiplied by a coefficient w, that in this study is set to 0.25. The latter part in the maximization function is the exponentially increasing delay term, where τ_n represents the Head-of-Line (HoL) delay in milliseconds, matched to delay budget db with an offset x. In the simulations, db is given the value of 80 milliseconds and the offset x is set to 20 milliseconds. As a result, the delay coefficient will reduce the scheduling priority of UEs whose HoL delay is small. Once the delay starts to approach the maximum delay budget, the priority will increase exponentially to ensure the packet can be delivered in time. The optional offset x is used to cope with the maximum hard limit of buffering time, which in this case is 80 milliseconds. The offset ought to guarantee that the packet will be transmitted before the hard limit is reached and the packet is discarded.

Another small but important modification for the voice traffic scheduling is required in the data rate filtering. The separation of r_n and r'_n in (3) and (4) should be revised for voice as the r_n represents the theoretical upper bound of the channel capability, while r'_n is the previous *real* data rate. As mentioned earlier, BE user's priority will be increased in the next TTI if it does not get scheduled (e.g. $r' = 0$), in order to prevent a long term starvation. This is actually dispensable for voice traffic, because a separate delay factor is utilized. Furthermore, data rate of the used Adaptive Multi-Rate (AMR) audio codec is relatively low and independent from the actual channel quality, which means r'_n does not provide useful information for measuring the relation between current channel quality and filtered, long term average of the channel. Due to these reasons, (4) for voice UEs should be replaced by

$$\overline{r}_n(l+1) = (1-\alpha)\overline{r}_n(l) + \alpha r_n(l), \tag{7}$$

which now allows ordering the voice traffic flows correctly according to their current channel quality relative to the average quality level.

Proportional fair-based scheduling is chosen to reduce the power requirement by scheduling UEs with relatively good channel conditions. For low velocity users, the CQI report is able to provide a channel quality estimation with a fairly high accuracy, since the de-correlation time of fast fading may often be clearly longer than the reporting delay. In other words, the scheduling algorithm in NodeB is able to benefit from fast variation of channel caused by multipath propagation. Increasing the user's velocity results in a more random fluctuation in adjacent CQI reports, due to fast fading becoming uncorrelated. However, slow fading and path loss create a slowly-changing trend in the channel envelope. By

nature, the moving average filtering given in (7) tends to avoid scheduling UEs during a negative slope in the channel quality, which actually is a very likely time for erroneous packet reception, as already discussed.

Selection of proportional fair scheduling for voice traffic is partially linked to power control implementation. When best effort traffic is transmitted, the served UE is allocated full transmission power of the cell so as to achieve a target BLER for the selected MCS. As discussed in [4], apart from bundling of packets in one transport block, usually the same MCS is used for voice, since the packet size remains the same. Conventional link adaptation is therefore of little use, and the BLER target can instead be reached by adaptive power control.

III. Simulation Model

A system simulator employing a hexagonal grid of a total of 21 cells was used for the evaluation of the voice enhancements. Voice users are deployed randomly within the simulation area, where they move in random directions during the simulation. When a user moves from the coverage of one cell to another, a hard handover is executed if the channel of the neighboring cell remains better during the whole time-to-trigger (TTT) duration than the channel of the primary serving cell plus the hysteresis value. The serving cell change (SCC) process includes a constant delay of 100 milliseconds that models the uplink signaling and RNC processing latencies, after which the handover takes place. This allows modeling the mobility procedures with a sufficient accuracy in order to assess the behavior of the algorithms in realistic scenarios where the channel quality of the primary serving cell may become worse than the channel of a neighboring cell, due to delays of the mobility procedures. Updating the secondary serving cell when Multiflow is enabled follows a similar RLC procedure as that for primary serving cell. Best effort UEs are also dropped in random positions in the network, but the mobility for them is disabled. The reason for including best effort users is to measure the remaining cell capacity that is left after scheduling the voice users.

A set of simulation parameters is provided in Table I. They are mostly based on the 3GPP simulation assumptions (e.g. [3]). The reporting range logically matching to 1A/1B measurement events, acts as the secondary serving cell activation threshold. When the UE enters this ”handover region”, it is possible to utilize the second Multiflow stream for transmission. Several simulations with the duration of 40 seconds were ran to obtain the results, with each simulation comprising a set of concurrent calls. Each voice call consists of talk and silence periods, according to the AMR 12.2 kbps voice codec. The durations of the periods are exponentially distributed around the mean value of 5 seconds. The main performance metrics gathered are cell transmission power allocated for voice users and residual cell throughput when voice users are scheduled. The performance numbers are obtained from TTIs when the scheduled voice user resides in the handover region, since the investigated methods are explicitly affecting only those TTIs.

Each simulation scenario was executed without and with Multiflow. In the ”Baseline” simulations, Multiflow is disabled altogether, while, in the ”Bicasting”, the second stream is activated for the users in the handover area. The Pedestrian-A 3 km/h (PA3) and Vehicular-A 30 km/h (VA30) channel

TABLE I. Simulation parameters.

Parameter	Value
Cell Layout	Hexagonal grid, 7 NodeBs, 3 sectors per NodeB with wrap-around
Inter-Site Distance	500 m
Path Loss	L=128.1 + 37.6log10(R), R in km
Log Normal Fading	
Standard Deviation	8dB
Inter-NodeB Correlation	0.5
Intra-NodeB Correlation	1.0
Correlation Distance	50m
Max BS Antenna Gain	14 dBi
2D Antenna Pattern	$A(\theta) = -min(12(\theta/\theta_{3dB})^2,\ Am)$, where $\theta_{3dB} = 70\ degrees,\ Am = 20dB$
Channel Model	PedA 3 km/h, VehA 30 km/h
UE Receiver Type	Type3i, 2 Rx ant. LMMSE equalizer
Max. Sector Transmit Power	43 dBm
Total Sector Overhead Power	20%
CPICH Transmit Power	10%
HS-SCCH Transmit Power	Controlled based on CQI
Max. number of HARQ Tx	4
BLER target	10% after 1st HARQ Tx
Avg. number of voice UEs/cell	4, 20, 40, 60
Traffic Model	AMR 12.2 kbps voice, 0.5 voice activity ratio
SID	Every 160ms during voice inactivity
Voice packet delay budget	80ms
Max. number of parallel HS-SCCH channels/cell	6
CQI	Ideal with 3 TTI delay
Event 1D Time-to-trigger	640 milliseconds
Event 1D Hysteresis	6 dB
Event 1A/1B Reporting range	6 dB

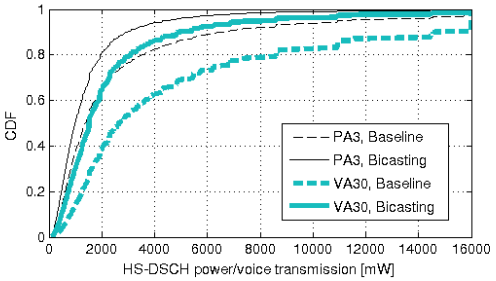

Fig. 2. HS-DSCH power allocated for voice transmission in HO region

models are utilized to see the performance gains with widely used simulation channel models. With both channel models, the power control algorithm is capable of keeping the voice packet drop rates very close to 0%, with only few exceptions. This is the case in both the baseline simulations without Multiflow and in Multiflow bicasting cases. It is therefore more interesting to take a closer look at the other results, namely transmission power saving and residual BE traffic throughput.

IV. Simulation Results and Analysis

Fig. 2 presents the cumulative distribution function (CDF) of the transmission power allocated for voice users that reside in handover area with on average four voice users per cell. The power allocation was observed to be approximately similar with other loads, so the figures for them are excluded. Apart

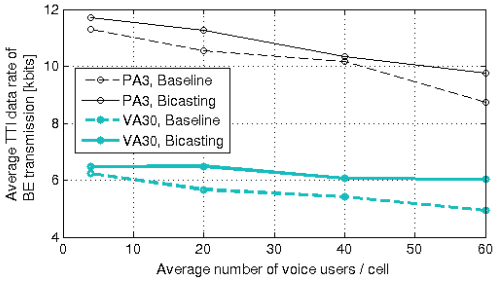

Fig. 3. Average TTI data rates for BE users

from the generally higher power requirement in the VA30 than in the PA3 simulation, a high similarity is observed between the results. Extracted from the figure, with bicasting, on average approximately 55% of baseline's transmission power in the PA3 case is required to serve the voice users in the handover region. One should notice that the major improvement is the reduced number of TTIs when very high transmission power is required.

On average, only 49% of the baseline power is required in the VA30 scenario after enabling Multiflow. Since the path loss and shadowing variation becomes faster than in PA3, the relative superiority of the average channel qualities of neighboring cells may change often, which allows good prospects for utilizing the second traffic channel. In the baseline VA30 simulations, around 10% of the samples reach the maximum High-Speed Downlink Shared Channel (HS-DSCH) transmission power of 16 watts. It is a result from bad channel quality where only the lowest MCS capable of transmitting one RLC layer PDU in single transport block is supported. To reach the 10% BLER target with such MCS the cell must allocate the maximum available power for one voice user, which naturally disables user multiplexing in one TTI. In most cases, this can be avoided by using bicasting. The small steps visible especially in VA30 curves also relate to the selection of MCS and are produced by the power control algorithm. The allocated power is based on the reported CQI, which is a discrete value. Thus there is only a finite number of possible powers to be designated for a user.

Data rates of the best effort users are gathered from the TTIs when the voice users are active in the handover zone. The average rates from the simulation scenarios are depicted in Fig. 3. The achieved BE data rate improvement is quite moderate. Depending on the scenario, the gain varies approximately from 2% to 12% with PA3 and from 4% to 22% with VA30. Although the power saving is significant, it cannot be translated linearly to higher throughput. Instead, the data rate gain depends on what is the effect of additional available cell power to the MCS selection. For example, being able to choose a more efficient MCS might often require at least around 1 dB (or approximately 26%) higher transmit power than the previous supported MCS. Nevertheless, when the voice load of the network approaches the saturation point, it is likely possible to benefit from the bicasting enhancements more frequently, resulting in an increased total cell throughput compared to conventional single-cell operation.

As mentioned earlier, packet drop rates are not significant in majority of the simulated scenarios. The only exception is the baseline VA30 simulation with a mean of 60 voice users per cell. There, the network starts to saturate, resulting in approximately 2% of the users being in outage condition if a 2% packet drop limit is set as an outage threshold. In the corresponding bicasting scenario, 0% of UEs are in outage, thus by applying the discussed methods, the voice capacity of the network can be extended. However, further investigation would be needed to determine the exact improvement.

V. Conclusions

This paper discussed enhanced voice-bicasting concept which allows the Multiflow-capable cell edge user to be served over either of the configured data streams. In the presented approach, the RNC duplicates each PDU related to voice traffic to both serving cells, and the cell decides whether it should discard the PDU or transmit it to the target UE. Utilization of SF-DC Aggregation for improving the real-time voice traffic delivery in downlink direction can be done without hardware updates and the software changes concentrate only on the HSPA access network. It was shown that delivering voice traffic in HSPA network may require a substantial amount of cell's resources if the user resides in the border of the serving cell, whereby conditional voice bicasting saves a significant amount of the transmission power in such cases which grants higher residual cell capacity and more efficient user multiplexing. Further optimizations on voice bicasting are possible for the channel selection conditions. The suitability of bicasting for other types of real-time traffic is also a sound target for research in the future, as well as the study on the impact of different CQI reporting delays on the accuracy of the discussed methods.

Acknowledgment

The author would like to thank Alexander Sayenko from Nokia Solutions and Networks for his guidance.

References

[1] Ericsson, "Ericsson Mobility Report," Technology report, Jun 2013.

[2] 4G Americas, "Delivering Voice Using HSPA," White Paper, Feb 2012.

[3] 3GPP TR 25.872, "High Speed Packet Access (HSDPA) Multipoint Transmission (Release 11)," Sep 2011.

[4] V. Hytönen, P. Gonchukov, A. Sayenko and A. Chandrashekar, "Downlink Bicasting with Multiflow for Voice Services in HSPA Networks," in *IEEE International Workshop on Selected Topics in Mobile and Wireless Computing (STWiMob)*, Lyon, France, Oct 2013, pp. 168–173.

[5] S. Mohan, R. Kapoor and B. Mohanty, "Enhanced HSDPA Mobility Performance: Quality and Robustness for Voice over HSPA Service," in *IEEE Vehicular Technology Conference (VTC 2010-Spring)*, Taipei, Taiwan, May 2010, pp. 1–5.

[6] F. Beritelli, A. Gallotta, S. Palazzo and C. Rametta, "Dual Stream Transmission to Improve Mobile VoIP Services over HSPA: a Practical Test Bed," in *Image and Signal Processing and Analysis (ISPA)*, Trieste, Italy, Sep 2013, pp. 773–777.

[7] A. Yaver, T. Höhne, J. Moilanen and V. Hytönen, "Flow Control for Multiflow in HSPA+," in *IEEE Vehicular Technology Conference (VTC 2013-Spring)*, Dresden, Germany, Jun 2013, pp. 1–5.

[8] 3GPP TS 25.212, "Multiplexing and channel coding (FDD)," Sep 2013.

[9] A. Jalali, R. Padovani and R. Pankaj, "Data throughput of CDMA-HDR a high efficiency-high data rate personal communication wireless system," in *IEEE Vehicular Technology Conference (VTC 2000-Spring)*, Tokyo, Japan, May 2000, pp. 1854–1858.

PV

HIGH-SPEED SINGLE-FREQUENCY NETWORK FOR HSDPA

by

Vesa Hytönen, Oleksandr Puchko, Thomas Höhne and Thomas Chapman 2011

Proceedings of the IEEE Swedish Communication Technologies Workshop
(Swe-CTW)

2011 IEEE Swedish Communication Technologies Workshop (Swe-CTW)

High-Speed Single-Frequency Network for HSDPA

Vesa Hytönen, Oleksandr Puchko
Department of Mathematical Information Technology,
University of Jyväskylä,
Finland
{vesa.a.hytonen, oleksandr.puchko}@jyu.fi

Thomas Höhne
CEF CTO Research,
Nokia Siemens Networks,
Espoo, Finland
thomas.hoehne@nsn.com

Thomas Chapman
Roke Manor Research Ltd.,
Hampshire, SO51 0ZN, United Kingdom
thomas.chapman@roke.co.uk

***Abstract*—This paper introduces a multi-cell transmission scheme for High-Speed Downlink Packet Access (HSDPA) networks, called High-Speed Single-Frequency Network (HS-SFN). While existing multi-point transmission features for WCDMA have concentrated on soft/softer handover (HO) mechanisms and are applicable only for Rel-99 based networks, HS-SFN brings an over-the-air combining approach to multi-cell transmissions for packet-oriented HSDPA. We introduce also a so-called "High-Speed Data-Discontinuous Transmission (HS-DDTx)" concept, an inter-cell interference mitigation scheme designed to improve the data throughput especially for low geometry users residing at cell borders. The presented results show how these low complexity concepts together offer a high gain for low and medium throughput users, without sacrificing the overall network performance. The proposed schemes also allow further upgradeability and there are ways to improve the efficiency by enhancements on both network side and user terminal equipment.**

I. Introduction

Continuously growing user data rate demands for wireless communications are the motivation behind many of the recent improvements to communications standards such as HSDPA. Peak data rates are often quoted as a measure of performance for an access technology, but lately operators have become also interested in providing improved user experience for cell edge users. The HS-SFN concept discussed in this paper is designed to offer increased data throughput for cell edge HSDPA users, boost network-wide fairness and thereby enhance the customer satisfaction. HS-SFN is designed as a low User Equipment (UE) implementation complexity concept. The aim of HS-SFN is to provide extended capacity for users who would otherwise suffer from low received signal level and high inter-cell interference. What makes HS-SFN especially interesting is its affiliation with HSDPA that currently is one of the most deployed techniques for wireless data communication.

As we will demonstrate, the composite concept of HS-SFN and HS-DDTx creates high throughput gains especially for cell edge users. The network's ability to accommodate a large number of UEs or otherwise extended load can be further improved by customized scheduling; clearly multi-cell scheduling offers advantages over single-cell schedulers. For instance, a combined scheduler more easily allows prioritizing a specific group of users by means of scheduling without sacrificing overall performance.

The rest of the document is organized as follows. Section II presents the background and motivation for the HS-SFN study, after which the HS-SFN and HS-DDTx concepts are explained in Section III, including a discussion of the most challenging implementation issues together with appropriate solutions. Thereafter we continue by presenting of the simulation results in Section IV. Section V concludes the paper.

II. Background and related techniques

The main contribution of this paper, HS-SFN, can be attributed to a wider group of Cooperative Multipoint (CoMP) schemes, in which several cells coordinate their transmissions with the general purpose of increasing network capacity. CoMP schemes have been studied in 3GPP for some time. The topic has been a study item (SI) in LTE since the beginning of 2008 and found its way to the specification [1]. The item's study targets were updated in 3GPP TSG RAN#50 meeting [2] and it is to be completed in the near future.

Recently, activities initiated in HSPA have been motivated by a desire to evolve also HSPA and to adopt similar techniques as in LTE. The need to improve cell edge performance discussed above is the primary goal of the work. An official 3GPP SI on Multipoint transmission techniques was opened recently, see [3], following some initial discussions on the proposed concepts however started during the second half of 2010. HS-SFN was first introduced in [4] and its possible performance – when disregarding scheduler behavior – analyzed in [5]. Therein the 3GPP work, two main types of technique have been proposed for further investigation, so called "Multiflow" (see [4], [6] and [7]) and HS-SFN, the topic of this paper.

While a new multi-point transmission SI has been opened, also existing techniques and previous studies in HSPA qualify as multi-cell enabled capacity enhancements. Namely, DL and UL soft and softer handover (for Rel-99) and also DL fast cell switching, which was studied in HSDPA Release 5, but not implemented.

Due to the novelty of the HSPA multi-cell studies, related literature is sparse. A good overview on CoMP principles in LTE, however, may be found in [8], along with performance demonstrated in field trials. The work highlights one of the major differences between the multipoint schemes in HSPA and LTE; the X2 interface in E-UTRAN enables coordination between different nodeBs. Direct inter-site coordination is not available in HSPA, but future deployment of Remote Radio Head (RRH) systems may open a similar approach.

978-1-4577-1878-6/11/$26.00 ©2011 IEEE

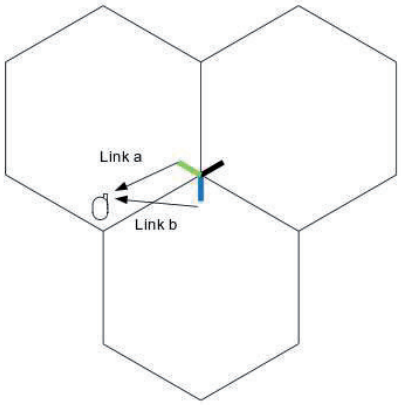

Fig. 1. Intra-site HS-SFN operation.

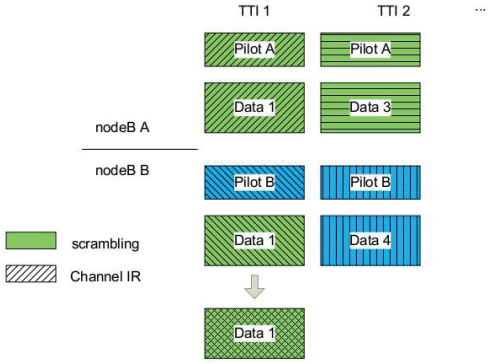

Fig. 2. HS-SFN data signal formation.

Single Frequency Networks (SFN) are also known from DVB-T and other broadcast enabled systems. This is studied e.g. in [9], [10].

III. HS-SFN and HS-DDTx concepts

In HS-SFN, same downlink (DL) data is transmitted on HS-PDSCH channel from two cells controlled by the same nodeB, as illustrated in Fig. 1. Both cells transmit data by using the same carrier frequency and the scrambling code of the UE's serving cell. Transmissions are sub-chip-aligned, so that the signals are combining over-the-air at the UE receiver, see Fig. 2.

In addition to an improvement in received signal strength, also the strongest interferer is removed. The enhanced C/I may thus be approximated as

$$C/I = \frac{0.7P_{0,tot} + 0.7P_{1,tot}}{\sum_{i=1}^{N} P_{i,tot} - 0.7P_{1,tot}}, \quad (1)$$

where i refers to the ith interfering cell and N to the total number of interfering cells. Here we assume a 30 % control channel (pilots and signaling) overhead, thus 70 % of the total transmission power is left for data on HS-PDSCH channel from serving cell ($P_{0,tot}$) and second strongest cell ($P_{1,tot}$).

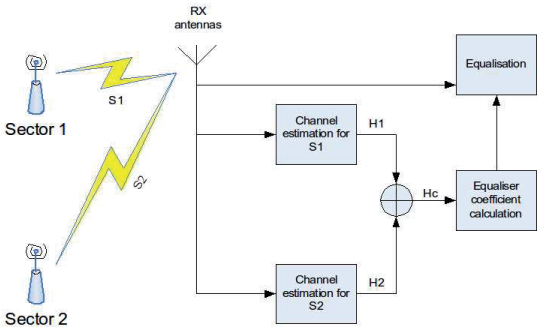

Fig. 3. Receiver architecture.

Beyond increased signal strength and reduced interference also the additional spatial diversity introduced by the additional transmitter will enable gains. Further, a site combined scheduler discussed in more detail later will access a larger pool of UEs and improve multi-user diversity.

The main requirement for the concept besides the sub-chip-level synchronization is the receiver's ability to deal with assisted transmission. During an HS-SFN assisted transmission, only the data part of the signal is transmitted using the same scrambling, whereas both cells use their own scrambling for control channels which still need to be received by UEs. UEs estimate the channel based on pilots transmitted in the control channel. As the pilots remain separated by scrambling also during an assisted data transmission, the UE needs to estimate the two channels separately, combine the estimates, and then perform equalization of the signal, as illustrated in Fig. 3.

Note that only a single equalizer is required at the receiver, leading to a relatively low complexity and consequently low power consumption at the UE. Section III-A presents more detailed description of a receiver equalizer adapted to the assisted transmissions.

The secondary contribution of this paper is the introduction of HS-DDTx. The performance of HS-DDTx relies on reduction of inter-cell interference. A cell in HS-DDTx mode strategically omits data transmission on HS-PDSCH during some TTIs, thus limiting the interference it produces to other cells and UEs in the network and improving overall network performance. Like HS-SFN, HS-DDTx works on a TTI-to-TTI basis, meaning that a cell that selected to perform HS-DDTx, DTXs HS-PDSCH during the whole TTI. An obvious disadvantage of HS-DDTx is naturally the lost possibility of serving intra-cell UEs during a HS-DDTx TTI. This should not be, however, as critical as first appears if the scheduler algorithm is able to accurately account for all the conceivable losses and gains across multiple cells. It also has a very minor impact in low load scenarios since most of the time cells have

no active UEs. As with HS-SFN, usage of control channels, such as the HS-SCCH and CPICH, are not changed during a data-discontinuous transmission.

In the simulations a nodeB may decide to perform either standalone transmission, HS-SFN or HS-DDTx, depending on which maximizes the aggregate proportional fair metric from each cell of the site. It has been noted in our experiments that a system with a support only for HS-DDTx has merely a marginal impact on performance, but since HS-DDTx does not create any additional complexity to the UE equipment, it is useful to combine with HS-SFN and choose the best transmission mode at each time instant.

A. Channel combining

In order to account for inter-cell interference, intra-cell multipath interference and equalization we may express the C/I according to [11], [12] more accurately as

$$C/I = \frac{P_{HS-PDSCH} \cdot \left|\mathbf{w}^T \mathbf{H}_c^T \delta\right|^2}{I_{own} + I_{col} + I_{thermal}}, \tag{2}$$

where $P_{HS-PDSCH}$ denotes the absolute transmission power on HS-PDSCH channel. Here $\mathbf{H}_c$ is the combined channel impulse response matrix given by

$$\mathbf{H}_c = \mathbf{H}_0 + \mathbf{H}_1 \sqrt{\frac{L_1 P_{1,data}}{L_0 P_{0,data}}} \tag{3}$$

and

$$\mathbf{H}_j = \begin{bmatrix} \mathbf{h}_j & 0 & 0 & \cdots & 0 \\ 0 & \mathbf{h}_j & 0 & \cdots & 0 \\ \vdots & 0 & \mathbf{h}_j & \ddots & \vdots \\ 0 & \vdots & 0 & \ddots & 0 \\ 0 & 0 & \cdots & 0 & \mathbf{h}_j \end{bmatrix}^T, \quad j = 0, 1, \tag{4}$$

where

$$\mathbf{h}_j = \begin{bmatrix} h_{j_1}(0) & h_{j_1}(1) & \cdots & h_{j_1}(\tau) \\ h_{j_2}(0) & h_{j_2}(1) & \cdots & h_{j_2}(\tau) \end{bmatrix} \tag{5}$$

is the channel impulse response matrix from either the serving or the assisting cell, assuming two receive antennas. The size of the matrix is determined by the number of Rx antennas and delay spread (τ). In (2), $\mathbf{w}$ denotes the equalizer weight vector and δ the delay of the equalizer. In equation (3), L_j is the path loss from *j*th cell to UE and $P_{j,data}$ the absolute transmit power for HS-PDSCH of the mentioned cell. In the above equations the subscripts 0 and 1 represent the serving ($j = 0$) and the assisting ($j = 1$) cell, respectively.

The total interference expressed by the denominator in (2) consists of three terms: own interference, or so-called Multiple Access Interference (MAI) (6), colored interference (7) and thermal noise (8):

$$I_{own} = P_{data} \mathbf{w}^T \mathbf{H}_c^T \hat{\delta} \mathbf{H}_c^* \mathbf{w}^* + P_{ctrl} \mathbf{w}^T \mathbf{H}_0^T \hat{\delta} \mathbf{H}_0^* \mathbf{w}^*, \tag{6}$$

$$I_{col} = \sum_{j=1}^{Num_{cells}} \frac{L_j P_j}{L_0 P_0} \mathbf{w}^T \mathbf{H}_j^T \mathbf{H}_j^* \mathbf{w}^*, \tag{7}$$

$$I_{thermal} = \frac{1}{L_0 P_0} \mathbf{C}_{thermal}, \tag{8}$$

where, in addition to previous definitions, P_{data} and P_{ctrl} are the relative powers for HS-PDSCH channel and control and pilot channels, respectively, and $\mathbf{C}_{thermal}$ denotes the thermal noise correlation matrix. $\hat{\delta}$ represents a $F \times F$ size identity matrix, F being the length of the linear filter.

In (6), we split the interference from the own cell into data and control channel inter-path interferences due to the data channel impulse response combining. In (7), if $j = 1$ (i.e. the strongest neighboring interferer) we should account for only 30 % of P_j for a combined transmission, since we do not have interference from the HS-PDSCH.

The calculations presented are used in our simulator to model the signal at the receiver end and the outcome of the receiver equalizer, based on which different SINR values for HS-SFN, HS-DDTx and standalone transmission may be derivated.

B. HS-SFN candidate selection

Utilizing multi-cell transmission possibility for UEs who observe big imbalance in the received signal powers from main cell and second strongest cell is not beneficial. Therefore the HS-SFN candidates should rather reside at cell borders. A straightforward approach to selection of the candidates is to use existing handover mechanisms and related measurements of link path loss by the UE. Those measurement reports can be e.g. triggered when certain path loss ratios are reached. For HS-SFN, it is possible to either reuse those existing reports or enable so far unused events. The specification defines only a limited number of usable events, thus making the latter option valid only if the network operator has not utilized all of them.

Further, due to the strict timing and frequency stability requirements and due to the need of a combined scheduler for the involved cells, HS-SFN eligible users must be located in the softer HO area, the border between two cells belonging to the same nodeB. This has implications on the total number of UEs available to the scheme and the achievable system gain.

C. Control channel considerations

As shown in Fig. 2, the pilot but also other control channels will remain on the native scrambling of cell B and will be subjected to higher interference by the use of scrambling A on data channel. As an example we may consider the HS-SCCH which carries coding and modulation information for the UE that will be scheduled in the following TTI. The power of the HS-SCCH can be adjusted to guarantee a certain error rate at the designated UE receiver. Thus, while the interference on the HS-SCCH is raised by assisted transmissions in cell B, the C/I at the UE can be maintained by increasing the HS-SCCH power share (and decreasing that of the assisting data transmission).

Depending on the UE, the achieved C/I for the control channel may be -9 dB down to -12 dB, as indicated in Chapter 9.4 in [13]. When mapping the geometry distribution of all UEs in the network to HS-SCCH power requirements, already 90 % of all UEs will be served with a share of 22 % of total transmit power on the HS-SCCH. With increased interference by HS-SFN assisted transmissions the 90 %tile is achieved with an HS-SCCH power share of 30 %. It should be noted that while the control channel power in cell B needs to be increased, it can be decreased in cell A. Furthermore, the above scenario is a worst case where an HS-SCCH needs to be transmitted to a user with poor C/I; for many users the power required for HS-SCCH, and the increase required for HS-SFN will be lower.

In the uplink, modifications to the CQI reporting are needed to enable the scheduler to quantify the benefits of HS-DDTx or HS-SFN scheduling. UL control channel modifications were not addressed in this study and in the simulations, the scheduler is assumed to have access to all required CQI information.

IV. System model

In this section we are evaluating the system performance of HS-SFN and HS-DDTx with a semi-static simulator. Hereafter in the text and results, "HS-SFN" refers to both multi-cell Tx schemes since HS-SFN is providing the main contribution to the results. However, impact of HS-DDTx is also present in the results although it is exiguous.

In the simulations, UEs are dropped randomly in the network, and generate traffic according to their traffic model. Slow fading is modeled by re-dropping UEs, and combining the statistics of several simulation runs. The SINR experienced at the UE is calculated according to the channel fast fading, interference from other nodeBs, and path loss according to (2). The SINR is then mapped to packet error probabilities using the actual value interface (AVI) approach. Simulation parameters are introduced in Table I.

TABLE I
Simulation parameters.

Parameter	Value
Cell Layout	Hexagonal grid, 19 nodeB, 3 sectors per nodeB with wrap-around
Inter-site distance	1000 m
Carrier Frequency	2000 MHz
Path Loss	L=128.1 + 37.6log10(R), R in kilometers
Log Normal Fading	
Standard Deviation	8dB
Inter-nodeB Correlation	0.5
Intra-nodeB Correlation	1.0
Correlation Distance	50m
Max BS Antenna Gain	14 dBi
Antenna pattern	
2D Pattern	$A(\theta) = -min(12(\theta/\theta_{3dB})^2,\ Am)$, where $\theta_{3dB} = 70\ degrees,\ Am = 20dB$
Channel Model	PedB 3 km/h
CPICH Ec/Io	-10 dB
Total Overhead power	30 %
UE Antenna Gain	0 dBi
UE noise figure	9 dB
UE Receiver Type	LMMSE
Tx/Rx diversity	1x2
Spreading factor	15
Maximum Sector Transmit Power	43 dBm
Handover reporting threshold	3dB
Number of HARQ processes	8
Traffic	
Traffic model	NGMN Traffic Source Model
Offered load level	0.25, 0.5, 1 and 2 Mbits/sec
File size	Fixed at 1 Mbit
Flow control on Iub	Ideal and instantaneous
HS-DPCCH Decoding	ACK decoded on UL; C2P used: 2 dB for Intra-NB, 4 dB for Inter-NB
CQI	Ideal with 3 TTI delay
Scheduling	Single intra-site scheduler, proportional fair algorithm

For simplicity, in the selection of HS-SFN enabled UEs only the two strongest links are evaluated. That is, if the second strongest cell resides in a different site than the main cell, we do not consider the UE an HS-SFN candidate. We apply a softer HO threshold of 3 dB in order to limiting the HS-SFN candidate locations to (intra-site) cell border regions. With the nodeB antenna model used in our simulator, the proportion of the UEs inside the HO region is 4-5 %. An alternative method for selecting HS-SFN UEs which allows all UEs that have links from the same site with $<$3 dB link imbalance would achieve a higher percentage of participation, and RRH scenarios a significantly higher percentage. Notice that the threshold value used for HS-SFN could be separated from the predefined handover reporting threshold, making HS-SFN flexible in the sense that it allows adjusting the amount of users under HS-SFN coverage without changing the legacy operations of the network. This might be useful in the case where one cell is heavily loaded while the neighboring cell might be nearly empty. There the neighbor cell would offer implicit load balancing by helping cell edge users in the heavily loaded cell to finish their data reception earlier, thus reducing load and the number of active users in the first cell.

Two scheduling approaches were evaluated: One without and one with prioritization of UEs within the softer HO area. The first approach follows well known proportional fair method (e.g. [14]), where the UE's probability of selection for transmission in the following frame decreases as it gets scheduled, and similarly increases while in a pending state. The second scheduling type favors HS-SFN candidates and users in softer HO region in both HS-SFN enabled and reference simulations. As a result, users in these groups are scheduled more often than other users which naturally improves their burst rates. We stress here that the later presented gains of HS-SFN over the reference case are unbiased in the sense that in both, HS-SFN and reference (disabled HS-SFN) case, the UEs under similar geometry conditions are prioritized.

The prioritization method inclines to give the upper bound achievable data rates for softer HO UEs, since they are now always scheduled if active in the network. In the worst case this may starve other UEs since they will not get scheduled during an existence of a softer HO UE. However, in the used

TABLE II
TTI ACTIVITY

Load level [Mbits/sec]	HS-SFN TTIs [%]	HS-DDTx TTIs [%]
0.25	62.3	0.3
0.5	57.0	0.3
1	48.6	0.7
2	34.9	2.6

traffic model terminals are removed from the network after completing the packet reception, so the starvation does not become a dominant issue. In any case the purpose of the second scheduling approach is to improve the situation for the softer HO UEs, without resorting to further air interface enhancements mentioned in section V, and also to demonstrate that even such a rigorous method may not have a big impact on other UEs in the network.

As mentioned before, we deploy common site-wide schedulers when HS-SFN is enabled. Regular independent scheduling for each cell is enabled in the reference simulations. The benefit from a combined scheduler arises from the fact that it is able to form a scheduling combination that will provide a highest possible total data rate for the whole site while also accounting for proportionally fair resource allocation.

A. Simulation Results

The decision for not separating HS-SFN and HS-DDTx results comes from the fact that HS-DDTx has a very minor impact on the final outcome of the simulations. This can be seen from Table II which shows the TTI statistics for softerHO area UEs who may utilize two cells for a single transmission. There, the average percentages of TTIs when HS-SFN or HS-DDTx transmission was selected are included for each load level. According to this table, it is not practical to separate the results, but rather include both schemes in the same result figures. The numbers presented are received by using the default scheduling algorithm in nodeBs.

The simulation results are broken down into two statistics: separate absolute burst rates (BR) for all UEs, softer HO UEs and soft HO UEs from inter-site borders of the cells, and burst rate gains where the reference case results are compared to those of HS-SFN simulations. We provide absolute burst rate cumulative distribution function (CDF) figures for 1 Mbit/s offered load level, but include all load levels in the gain figures.

In Fig. 4, we see the base scenario burst rates. HS-SFN affects only the softer HO users, due to which the curves for all UEs (including also softer HO and soft HO UEs) and soft HO UEs do not change much between the reference and HS-SFN simulations. If anything, we can see a slight improvement in these all UE CDF curves which may be partly explained by altered interference distribution, however the difference is marginal. Another noteworthy aspect of the results is the enhanced fairness of the system after HS-SFN deployment. This is a result of the increased burst rate of UEs that classify as low and medium throughput terminals. It should as well be noted that the HS-SFN/softer HO UEs have on average

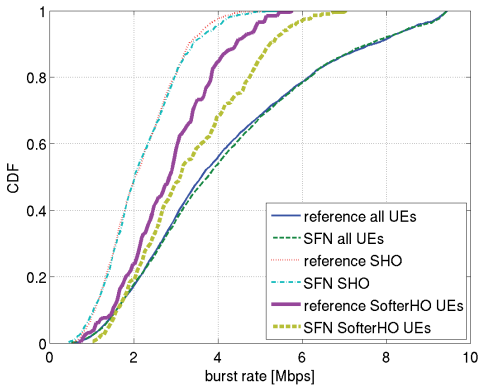

Fig. 4. Burst rate CDF, 1 Mbit/s offered load.

higher burst rates than soft HO UEs who suffer from high distance to transmitting antenna, resulting in strong fading of the signal, and also from high inter-site interference. HS-SFN can be applied between sites with a remote radio head implementation where several transmitting sites are controlled by a single nodeB unit. Study on RRH, however, is left outside from this analysis.

Fig. 5 presents the CDF curves for which the scheduler prioritization algorithm described previously is applied. In this case, HS-SFN candidates enjoy a higher data rate gain over softer HO UEs in the reference simulations from increased combined transmission opportunities, although the relative amount of schedules are at similar level in both as also the softer HO UEs in the reference case are prioritized. The gain is raised from 17 % to 35 % (see Fig. 6) by a single modification to the scheduling, but what should also be observed by comparison of Fig. 4 and Fig. 5 is that this change did not impact the burst rates of other UEs.

In Fig. 6, gains for UEs in the softer HO area at a range of offered load levels are presented. With proportional fair scheduling the gains drop towards higher loads, which is caused by a higher number of UEs in the system. This results in elevated total interference and fewer HS-SFN scheduling possibilities (which require simultaneous scheduling of a single UE from two cells). The higher loads also promote the reference case in the sense that although a softer HO UE was selected for transmission in one cell, at the same time the neighboring cell may still transmit to its own, either normal or softer HO, UE, since there is a smaller probability of having empty cells.

Conversely, the gains improve with prioritized scheduling as the load increases. This is caused by higher interference experienced by softer HO UEs in the reference simulations while it is being mitigated for HS-SFN candidates in the multi-point Tx case; recall that during a combined transmission the strongest interferer is removed in addition to signal enhancement. In the reference case this does not happen and with higher load

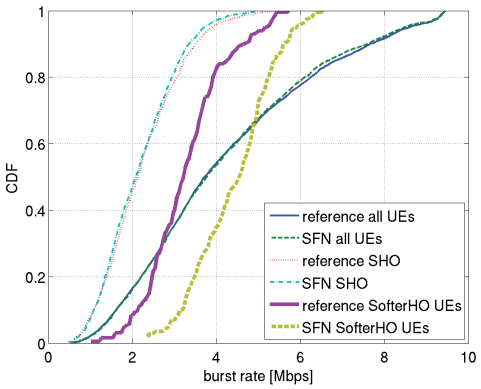

Fig. 5. Burst rate CDF, prioritization of UEs in softer HO area, 1 Mbit/s offered load.

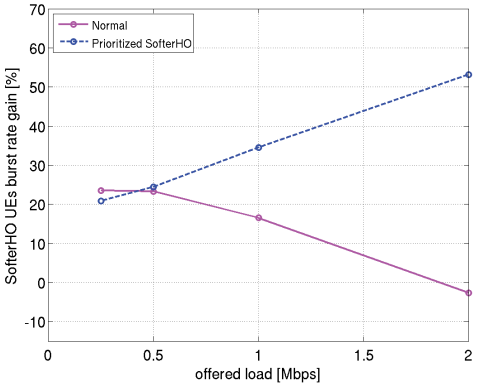

Fig. 6. Burst rate gain for UEs in softer HO area.

it is more likely that an interfering cell is not empty, thus inflicting maximum interference to scheduled softer HO UEs. Prioritization ensures that simultaneous HS-SFN scheduling occurs regularly for softer HO UEs whilst not impacting the overall throughput distribution.

V. Conclusion

In this paper, we have examined the main aspects of the HS-SFN and HS-DDTx concepts, discussed their benefits and drawbacks, and demonstrated the performance with a semi-static network simulator. HS-SFN is a recent candidate to 3GPP's HSDPA standard and enables significant throughput gains for cell-edge users without sacrificing system performance. The gains are obtained by increased spatial diversity, improved Rx power and improved inter-cell interference handling provided by HS-DDTx. Methods for amplifying HS-SFN performance further, such as the presented example scheduling modification, may significantly improve the burst rate gains for users in softer HO area. Due to the fact that HS-SFN can be enhanced by effective extensions to both network and mobile terminal side, it would provide a broad ground for research in several areas of interest to network service providers and terminal equipment manufacturers. The value of HS-SFN is also augmented by the widespread HSDPA platform for which it was designed.

Our future work will consist of studying further performance-enhancing techniques for HS-SFN, such as UE-feedback mechanisms allowing phase and power delay profile adjustments at the nodeB in order to improve the coherence of over-the-air signal combining. Also, scheduler upgrades may be important when targeting at more optimal resource management functionality for networks with multi-cell transmission capabilities. Moreover, our prospective nodeB architecture improvement study includes Remote Radio Heads which allow us to apply HS-SFN to terminals that in this paper were considered as low throughput soft HO area UEs, and thus unreachable for assisted transmission.

Acknowledgment

The authors would like to thank Alexander Sayenko and Petri Jolma from Nokia Siemens Networks for their valuable insights and counseling, and Henrik Martikainen and Vitaliy Tykhomyrov from Magister Solutions Ltd. for their contribution on the planning and modeling of HS-SFN functionality.

References

[1] 3GPP TR 36.814 v9.0.0, "User equipment (UE) radio transmission and reception (FDD)," Mar 2010.
[2] 3GPP TSG-RAN, RP-101425, Samsung, "Revised SID proposal: Coordinated multi-point operation for LTE," Dec 2010.
[3] 3GPP TSG-RAN, RP-101439, Nokia Siemens Networks, "Proposed study item on HSDPA multipoint transmission," Dec 2010.
[4] 3GPP TSG-RAN WG1, R1-104913, Nokia Siemens Networks, "Multi-cell transmission techniques for HSDPA," Aug 2010.
[5] 3GPP TSG-RAN, R1-106251, Ericsson, ST-Ericsson, "Multi-point transmission techniques for HSPA," Nov 2010.
[6] 3GPP TSG-RAN WG1, R1-103859, Qualcomm Incorporated, "On deploying DC-HSDPA UEs in single frequency networks," Jul 2010.
[7] 3GPP TSG-RAN WG1, R1-110123, Qualcomm Incorporated, "Candidate schemes for multi-point HSDPA," Jan 2011.
[8] R. Irmer, H. Droste, P. Marsch, M. Grieger, G. Fettweis, S. Brueck, H.-P. Mayer, L. Thiele and V. Jungnickel, "Coordinated multipoint: Concepts, performance, and field trial results," *Communications Magazine, IEEE*, vol. 49, pp. 102–111, Feb 2011.
[9] T. Kratochvil and V. Ricny, "Simulation and experimental testing of the DVB-T broadcasting in the SFN networks," in *Radioelektronika, 2008*, Prague, Czech Republic, Apr 2008.
[10] M. Tormos, C. Tanougast, A. Dandache, D. Masse and P. Kasser, "Evaluation performance analysis of DVB-T2 in a SFN network," in *Communications and Mobile Networks (ISVC), 2010*, Rabat, Morocco, Sep 2010.
[11] 3GPP TR 25.963 v9.0.0, "Feasibility study on interference cancellation for UTRA FDD user equipment (UE)," Dec 2009.
[12] T. Nihtilä, J. Kurjenniemi and E. Virtej, "System level analysis of interference aware LMMSE chip equalization in HSDPA network," in *IEEE Symposium on Computers and Communications, 2007. ISCC 2007*, Aveiro, Portugal, Jul 2007, pp. 133–138.
[13] 3GPP TR 25.101 v10.0.1, "User equipment (UE) radio transmission and reception (FDD)," Jan 2011.
[14] A. Jalali, R. Padovani and R. Pankaj, "Data throughput of CDMA-HDR a high efficiency-high data rate personal communication wireless system," in *Vehicular Technology Conference Proceedings, 2000*, Tokyo, Japan, May 2000, pp. 1854–1858.

PVI

ENHANCED LMMSE EQUALIZER FOR HIGH-SPEED SINGLE FREQUENCY NETWORK IN HSDPA

by

Oleksandr Puchko, Mikhail Zolotukhin, Vesa Hytönen, Thomas Höhne and Thomas Chapman 2011

Proceedings of the IEEE Swedish Communication Technologies Workshop (Swe-CTW)

Enhanced LMMSE Equalizer for High-Speed Single Frequency Network in HSDPA

Oleksandr Puchko, Mikhail Zolotukhin, Vesa Hytönen
Telecommunication laboratory, MIT department
University of Jyväskylä,
Finland
{oleksandr.puchko, mikhail.m.zolotukhin, vesa.a.hytonen}@jyu.fi

Thomas Höhne
CEF CTO Research
Nokia Siemens Networks,
Espoo, Finland
thomas.hoehne@nsn.com

Thomas Chapman
Roke Manor Research Ltd
Hampshire, SO51 0ZN, United Kingdom
thomas.chapman@roke.co.uk

***Abstract*—Currently, considerable interest has been shown in the research and standardization communities in multicell transmission schemes for HSPA, with a number of possible schemes under discussion that include Multiflow, Fast Cell Switching (FCS) and High-Speed Single Frequency Network (HS-SFN). In particular, HS-SFN is a promising technique that not only combines received energy from participating cells, but also reduces intercell interference with low UE complexity. In principle, HS-SFN can be implemented with a small modification to an LMMSE receiver at the UE. This paper introduces a more advanced LMMSE equalizer for High-Speed Single Frequency Network in HSDPA that achieves further performance gains.**

I. Introduction

In digital communications, an equalizer is a device that attempts to recover a signal transmitted through an intersymbol interference channel. A structure of an equalizer can vary from a simple linear filter to a complex algorithm. There are two basic approaches of equalization in wideband code division multiple access (WCDMA) systems: symbol-level and chip-level. A symbol-level equalizer depends on the user index and symbol index, and therefore varies from symbol to symbol. In the symbol-level equalizer spreading codes and the base station codes are incorporated into the equalizer itself. On the other hand, a chip-level equalizer does not depend on the spreading codes or the base station dependent code.

In this article, we concentrate on the chip-level LMMSE equalizer, i.e. based on the linear minimum mean square error estimator. LMMSE estimator describes the approach which minimizes the error between the transmitted signal and equalized received signal assuming that the system can be modeled as a linear transfer function. A lot of scientific and research papers were written about LMMSE equalizer and it is already researched quite deeply. This article will present a new algorithm for LMMSE equalizer which provides better performance for HS-SFN but will not have an impact on normal transmission.

The rest of the article is organized as follows. Section II presents the previous research of LMMSE equalizers after which the HS-SFN concept is explained in Section III. Section IV describes proposed LMMSE equalizer. After that Matlab verification and semi-static simulator results are presented in section V and VI respectively. Section VII concludes the paper.

II. Related Work

A significant amount of research effort has been devoted to the development of minimum mean square error equalization algorithms for code division multiple access (CDMA) networks.

A chip-rate MMSE equalizer which does not depend on the spreading codes, or the long code, employed at the base station is studied and the equalizer delay which minimizes the mean square error is found in [1]. In [2] the performance of chip-spaced MMSE is compared with the traditional RAKE receiver, and zero-forcing (ZF) equalizers for a random 4-path multipath channel with delay spread of 10 micro seconds, and an empirically derived random multipath channel generated by the commercial software package SMRCIM.

The study [3] considers sample added algorithm for interference mitigation-based LMMSE receiver in WCDMA high speed downlink packet access (HSDPA) system and shows that the algorithm proposed can improve the BER and BLER performance at a wide range of the number of the added samples. LMMSE chip equalizers in WCDMA systems are also examined in [4] and [5]. In [4] LMMSE receivers are studied from practical point of view by assuming that the number of receivers is gradually increased in the network, and the performance gain of interference aware LMMSE chip level equalizers with and without receiver diversity is evaluated in study [5].

In [6] an LMMSE equalizer, which takes out-of-cell interference into account, is examined for multiple-input-multiple-out (MIMO) HSDPA systems. Link level simulation results show that this out-of-cell interference aware equalizer together with LMMSE channel estimation improve performance throughput gains drastically.

LMMSE equalizers for the downlink of transmit antenna array (TxAA) HSDPA are presented in [7] and [8]. In TxAA users are distinguished by different spreading sequences and their data chip streams are weighted by individual precoding coefficients. An LMMSE equalizer taking the interference of

978-1-4577-1878-6/11/$26.00 ©2011 IEEE

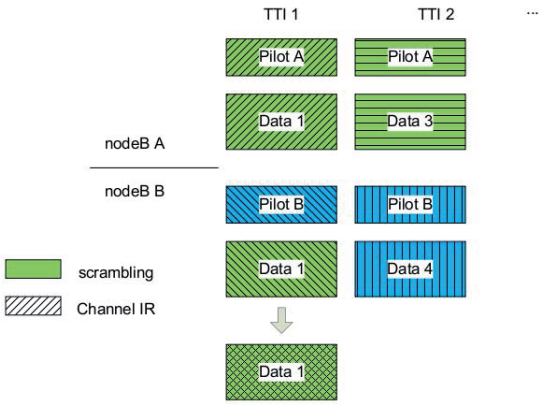

Fig. 1. HS-SFN data signal formation.

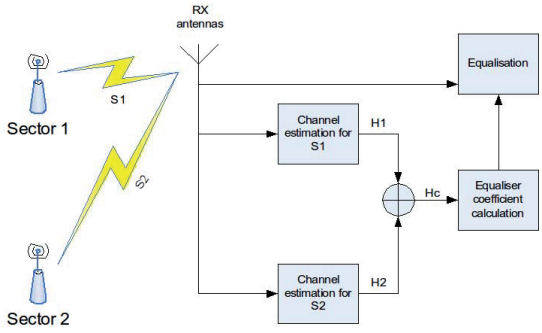

Fig. 2. Receiver architecture.

the other users into account is constructed in [7]. In [8] authors derive an enhanced space-time MMSE equalizer that uses the information about the beamforming vectors and restores the orthogonality perfectly with small increasing complexity compared to the conventional approach.

The study [9] offers the efficient hybrid equalizer scheme to improve the performance of the CDMA receiver in the multi-cell/multi gap filler SFN channel environments. The equalizer proposed overcomes a convergence speed problem in the SFN channel, what has been shown by evaluating equalizers performances in a simple short delay channel and SFN channel.

III. HS-SFN CONCEPT

The main idea of HS-SFN is to combine signals over the air from two cells by means of transmitting exactly the same data in downlink (DL) using the same carrier frequency and scrambling code. As a minimum data channel HS-PDSCH should be chip-aligned in each participating cell, as show in Fig. 1 [10].

The main requirement for the concept besides the TTI-level synchronization is the receiver's ability to deal with assisted transmission. During an HS-SFN assisted transmission, only the data part of the signal uses the same scrambling, whereas both cells use their own scrambling for control channels, which still need to be received by other UEs. On the other hand, UEs estimate the channel based on pilots transmitted in the control channel. As the pilots remain separated by scrambling also for an assisted transmission, the UE needs to estimate the two channels separately, combine the estimates, and then perform equalization of the signal, see Fig. 2 [10].

Note that only a single equalizer is required, leading to relative low complexity and consequently low power consumption at the UE.

IV. PROPOSAL AND ASSUMPTIONS

The served user receives a combined HS-PDSCH from both his serving cell and a second, so called "assisting" cell. While the signal component received from these NodeBs on PDSCHs is the same, the control channel component differs.

The spread and scrambled chip sequences transmitted from the j-th NodeB at time instant m is defined as

$$\begin{aligned} &d_{j,m} \\ &= [d_j(m+F-D-1), \ldots, d_j(m), \ldots, d_j(m-D-L)]^T, \\ &c_{j,m} \\ &= [c_j(m+F-D-1), \ldots, c_j(m), \ldots, c_j(m-D-L)]^T, \end{aligned}$$

for data and control channels, respectively. Here $j = 0$ for the serving NodeB and $j = 1$ for the "assisting" one, F is the equalizer length, L is the number of multipath components and D is the delay parameter satisfying the following inequality:

$$0 \leq D \leq F.$$

Let us assume that the power of the transmitted signal is equal to P_{data} and P_{ctrl} for data and control channels respectively. It is also pointed out that chip sequences transmitted through different channels are uncorrelated. Furthermore, d_{j,m_1} and d_{j,m_2} as well as c_{j,m_1} and c_{j,m_2} are uncorrelated for any $m_1 \neq m_2$.

Assuming that there are N_{Rx} rx-antennas at UE, $N_{Rx} \times L+1$ channel impulse response matrix for j-th NodeB is defined as

$$h_j = \begin{bmatrix} h_{j,1}(0) & h_{j,1}(1) & \ldots & h_{j,1}(L) \\ h_{j,2}(0) & h_{j,2}(1) & \ldots & h_{j,2}(L) \\ \vdots & \vdots & \ddots & \vdots \\ h_{j,N_{Rx}}(0) & h_{j,N_{Rx}}(1) & \ldots & h_{j,N_{Rx}}(L) \end{bmatrix},$$

where $h_{j,k}(l)$ is the channel impulse of k-th rx-antenna from j-th NodeB at l chip. Channel coefficient matrix H_j for j-th NodeB is the $(F + L - 1) \times (F \cdot N_{Rx})$ matrix which is

determined as follows:

$$H_j = \begin{bmatrix} h_{j,1} & \mathbb{O}_{1\times L+1} & \mathbb{O}_{1\times L+1} & \dots & \mathbb{O}_{1\times L+1} \\ h_{j,2} & h_{j,1} & \mathbb{O}_{1\times L+1} & \dots & \mathbb{O}_{1\times L+1} \\ h_{j,3} & h_{j,2} & h_{j,1} & \dots & \mathbb{O}_{1\times L+1} \\ \vdots & \vdots & \vdots & \ddots & \vdots \\ \mathbb{O}_{1\times L+1} & \mathbb{O}_{1\times L+1} & \mathbb{O}_{1\times L+1} & \dots & h_{j,N_{Rx}} \end{bmatrix}^T,$$

where $h_{j,k}$ is the k-th line of the matrix h^j.

Let us denote the data chip sequence transmitted by serving and "assisting" NodeBs as $d_m = d_{0,m} = d_{1,m}$ Thus, the received chip sequence r_m at time instant m can be constructed as

$$r_m = \sqrt{L_0}H_0^T(d_m + c_{0,m}) + \sqrt{L_1}H_1^T(d_m + c_{1,m}) + n_m,$$

where L_j is path gain for channel from the j-th NodeB to the UE and n_m is an white additive noise vector with zero mean value and real-valued covariation matrix equal to C_n. Let us assume that noise vector n_m is not correlated with signal sequences.

Introduce the following auxiliary matrix H_C as

$$H_C^T = H_0^T + \sqrt{\frac{L_1}{L_0}}H_1^T. \quad (1)$$

Using (1) the received chip sequence can be found as follows:

$$r_m = \sqrt{L_0}H_C^T d_m + \sqrt{L_0}H_0^T c_{0,m} + \sqrt{L_1}H_1^T c_{1,m} + n_m. \quad (2)$$

A. LMMSE Equalizer

The transmitted chip sequence of a user is reconstructed at the receiver using an LMMSE equalizer. To calculate the equalizer coefficient vector w of length $N_{Rx} \cdot F$ the following quadratic cost function should be minimized:

$$F(w) = E\left\{\left|w^T r_m - s(m-\tau)\right|\right\}, \quad (3)$$

which is the distance between the received chip sequence r_m equalized and the $(m-\tau)$-th transmitted chip $s(m-\tau)$ for a given value of delay $\tau \in \{-F+D+1, -F+D+2, \dots, D+L\}$.

In the simple LMMSE equalizer the signals transmitted through control channels are not taken into consideration:

$$s(m-\tau) = d(m-\tau),$$
$$r_m = \sqrt{L_0}H_C^T d_m + n_m.$$

The value of w which minimizes the cost function $F(w)$ can be found by deriving (3) with respect to w^T [11]:

$$\frac{\partial F}{\partial w^T} = 0. \quad (4)$$

Taking assumptions listed in the previous section into account, the equation (4) can be rewritten as

$$\left(L_0 H_C^T R_{dd} H_C^* + R_{nn}\right)w^* - \left(P_{data}\sqrt{L_0}H_C^T\delta_\tau\right) = 0,$$

where R_{dd} is the $(F+L-1)\times(F+L-1)$ autocorrelation matrix of signals transmitted through data channel, R_{nn} is the white noise autocorrelation matrix, and δ_τ is zero vector with the unit on the position τ. The matrices R_{dd} and R_{nn} can be found as follows:

$$R_{dd} = \begin{bmatrix} P_{data} & 0 & \dots & 0 \\ 0 & P_{data} & \dots & 0 \\ \vdots & \vdots & \ddots & \vdots \\ 0 & 0 & \dots & P_{data} \end{bmatrix},$$
$$R_{nn} = C_n.$$

Therefore, the simple LMMSE equalizer coefficient is equal to

$$w_s = P_{data}\sqrt{L_0}\left(P_{data}L_0 H_C^H H_C + C_n\right)^{-1} H_C^H \delta_\tau. \quad (5)$$

B. Enhanced LMMSE Equalizer

To improve the equalizer performance the control channels are also taken into account when constructing the quadratic cost function. In this case, the transmitted $(m-\tau)$-th chip in (3) is expressed as

$$s(m-\tau) = d(m-\tau) + c(m-\tau),$$

and received chip sequence is defined as (2).

The equation for calculating the enhanced equalizer coefficient can be rewritten:

$$\frac{\partial F}{\partial w^T} = \left(L_0 H_C^T R_{dd} H_C^* + L_0 H_0^T R_{cc} H_0^* + L_1 H_1^T R_{cc} H_1^* + \right.$$
$$\left. + R_{nn}\right)w^* - \left(P_{data}\sqrt{L_0}H_C^T\delta_\tau + P_{ctrl}\sqrt{L_0}H_0^T\delta_\tau\right) = 0,$$

where R_{cc} is $(F+L-1)\times(F+L-1)$ the autocorrelation matrix of signal transmitted through control channel, which can be found as follows:

$$R_{cc} = \begin{bmatrix} P_{ctrl} & 0 & \dots & 0 \\ 0 & P_{ctrl} & \dots & 0 \\ \vdots & \vdots & \ddots & \vdots \\ 0 & 0 & \dots & P_{ctrl} \end{bmatrix}.$$

Therefore, the enhanced LMMSE equalizer coefficient is equal to

$$w_e = \left(P_{data}L_0 H_C^H H_C + P_{ctrl}L_0 H_0^H H_0 + P_{ctrl}L_1 H_1^H H_1 + \right.$$
$$\left. + C_n\right)^{-1}\left(P_{data}\sqrt{L_0}H_C^H\delta_\tau + P_{ctrl}\sqrt{L_0}H_0^H\delta_\tau\right). \quad (6)$$

C. Performance Evaluation

To assess the performance of the proposed enhanced equalizer, the signal-to-interference ratio (C/I) is calculated for a given UE. We find the signal power for delay value equal to τ and use channel coefficient matrix H_C or H_0 for data and control channel respectively. The interference is modelled as the interpath interference of the combined data, plus the filtered interpath of the own control channels, plus colored noise from other cells, plus thermal noise. Thus, C/I for

evaluating the equalizer performance can be found as follows:

$$C/I = \frac{C}{I_{interpath} + I_{intercell} + I_{thermal}},$$

where

$$C = \begin{cases} P_{data} \left| w^T H_C^T \delta_\tau \right|^2, & \text{for data channel,} \\ P_{ctrl} \left| w^T H_0^T \delta_\tau \right|^2, & \text{for control channel,} \end{cases}$$

$$I_{interpath} = P_{data} w^T H_C^T \hat{\delta}_\tau H_C^* w^* + P_{ctrl} w^T H_0^T \hat{\delta}_\tau H_0^* w^*,$$

$$I_{intercell} = P_{ctrl} \frac{L_1}{L_0} w^T H_1^T H_1^* w^* + \sum_{j=2}^{N} \frac{L_j}{L_0} w^T H_j^T H_j^* w^*,$$

$$I_{thermal} = \frac{1}{L_0} w^T C_{thermal} w^*. \tag{7}$$

Here δ_τ is $(L+F-1) \times (L+F-1))$ identity matrix with zero in the main diagonal on the position τ, N is the number of NodeBs which are interfering the UE, H_j and L_j are channel coefficient matrices and path gains for these NodeBs respectively, and $C_{thermal}$ is thermal noise correlation matrix.

V. Matlab Verification

To demonstrate the superior performance of the proposed enhanced equalizer a pseudo-simulator has been created in Matlab. This simulator takes as inputs path gains for serving, "assisting" and interfering NodeBs, the power levels of signals transmitted through data and control channels and the thermal noise correlation matrix, then calculates the equalizer coefficients and returns the signal-to-interference ratios.

We consider different values of serving NodeB path gain to "assisting" NodeB path gain ratio L_1/L_0 expressed in dB. This ratio is assumed to vary from L_{min} to L_{max} dB with step equal to Δ_L dB. For each value of this ratio M simulations are run. In every simulation the impulse response matrices for serving, "assisting" and interferring NodeBs are set randomly. After constructing channel coefficient matrices and noise correlation matrix, the LMMSE equalizers coefficients are calculated as (5) and (6).

Finally, the signal-to-interference ratio C/I for data and control channel is found as (7) and the value of C/I average of M simulations is returned for each path gain ratio.

TABLE I
Matlab verification parameters.

Parameter	Value
Equalizer length	10
Number of receiver antennas	2
Number of multipath components	2
Power of the signal transmitted through data channel	0.7
Power of the signal transmitted through control channel	0.3
Number of interfering NodeBs	56
Minimal value of ratio L_1/L_0	-30 dB
Maximal value of ratio L_1/L_0	0 dB
Step of changing ratio L_1/L_0	1 dB
Number of simulations	1000

Fig. 3 and Fig. 4 show that the C/I gain when using the enhanced LMMSE equalizer increases with decreasing the difference in path gains of serving and "assisting" NodeBs, i.e. increasing the ratio L_1/L_0. When this ratio is large, the interference level of the control signal from the "assisting" NodeB is high. This interference is taken into account when calculating the enhanced LMMSE equalizer coefficients but not taken into account for the case of simple LMMSE equalizer. As a result, the gain of using enhanced equalizer is up to 4.6 dB for data channel and up to 6.0 dB for control channel, in this example.

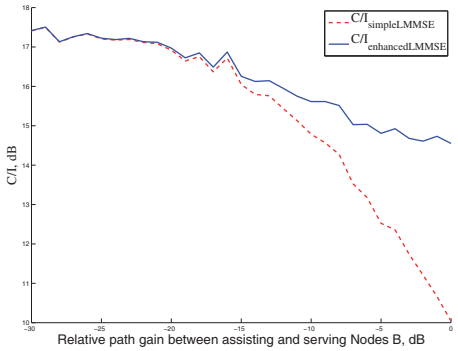

Fig. 3. C/I for HS-DPSCH.

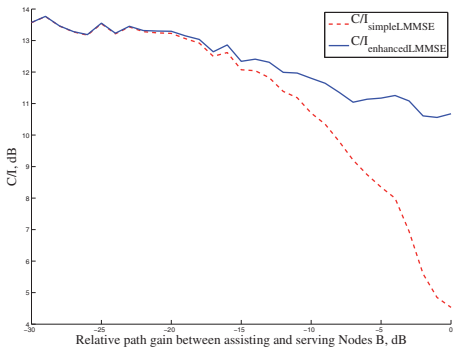

Fig. 4. C/I for signalling and contol channels.

VI. System model

This section presents performance of LMMSE equalizers in HS-SFN scheme with a semi-static simulator. Simulations were fulfilled with a macro cell scenario that includes 19 NodeBs and 57 hexagonal cells. Propagation model, slow fading, scheduling part and other parameters were simulated according to 3GPP simulation specification [12] and they are presented in Table II.

UEs are dropped randomly into the network for a definite number of times, depending on the amount of UEs per cell in

TABLE II
SIMULATION PARAMETERS.

Parameter	Value
Cell Layout	Hexagonal grid, 19 NodeB, 3 sectors per NodeB with wrap-around
Inter-site distance	1000 m
Carrier Frequency	2000 MHz
Path Loss	L=128.1 + 37.6log10(R), R in kilometers
Log Normal Fading	
Standard Deviation	8dB
Inter-NodeB Correlation	0.5
Intra-NodeB Correlation	1.0
Correlation Distance	50m
Max BS Antenna Gain	14 dBi
Antenna pattern	
2D Pattern	$A(\theta) = -min(12(\theta/\theta_{3dB})^2,\ Am)$, where $\theta_{3dB} = 70\ degrees,\ Am = 20dB$
Channel Model	PedA3
CPICH Ec/Io	-10 dB
Total Overhead power	30%
UE Antenna Gain	0 dBi
UE noise figure	9 dB
UE Receiver Type	LMMSE with RxD
Spreading factor	15
Maximum Sector Transmit Power	43 dBm
Handover reporting range	3dB
Number of HARQ processes	8
Maximum active set size	2
Traffic	
Traffic model	Bursty Traffic Source Model
Number of UE per cell	1, 2, 4 and 8
File size	Fixed at 1 Mbit
Inter-arrival time	Exponential, mean = 5 seconds
Flow control on Iub	Ideal and instantaneous
HS-DPCCH Decoding	ACK decoded on UL (unless mentioned otherwise); C2P used: 2 dB for Intra-NB, 4 dB for Inter-NB
CQI	Ideal with 3 TTI delay
Scheduling	Common intra-NodeB scheduler, proportional fair algorithm

order to gather proper statistics and not to spend much time. Number of runs is 120, 60, 30, 15 respectively to 1, 2, 4 and 8 UEs per cell. Simulation time is 40 seconds with additional 6 seconds for warming up time for the system.

A. Simulation Results

These results present intra-site HS-SFN, which means that HS-SFN transmission is possible only between two cells in the same site. HS-SFN candidate is the user that is located in softer handover area, i.e. path loss ratio of the two strongest cells is less than softer handover margin and in this article it is set to 3dB. HS-SFN candidate can receive normal transmission (from one cell) or HS-SFN transmission (transmission from two cells) depending on the transmission scheme selection made by the site scheduler. Even though these two transmissions are sub-chip synchronised, they may be uncorrelated thus combining of these signals can be either constructive or destructive.

Fig. 5 and Fig. 6 show burst rate CDFs for 1 UE per cell with normal and enhanced LMMSE equalizers, respectively. It can be seen from these figures that there is no negative impact on all other users even with increasing performance for softer HO users. HS-SFN usage can increase performance not only for low throughput users but also for all other users in softer handover area with enhanced LMMSE equalizer.

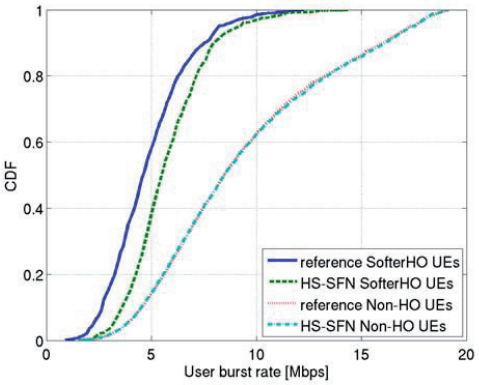

Fig. 5. Burst rate CDF for 1 UE per cell, Type 3.

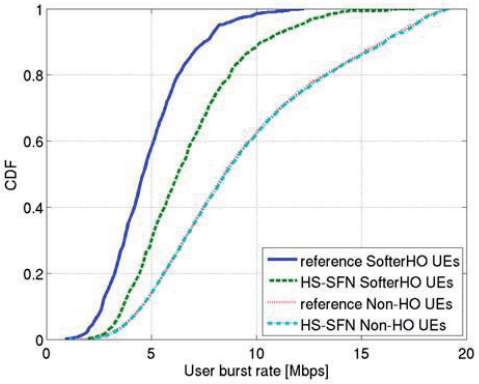

Fig. 6. Burst rate CDF for 1 UE per cell, enhanced Type 3.

Fig. 7 shows the average burst rate for UEs in the softer handover area. It presents three simulation scenarios: reference case or scenario without possibility of HS-SFN transmissions and HS-SFN enabled scenarios with the original and enhanced LMMSE equalizer.

Fig. 8 shows burst rate gains of HS-SFN transmission for normal and enhanced LMMSE equalizer. It can be seen from this figure that enhanced LMMSE equalizer can provide 15% of additional gain to normal LMMSE equalizer.

VII. CONCLUSION

In this paper an enhanced LMMSE equalizer for HS-SFN multipoint transmission scheme was derived. Simulation results from Matlab and a semi-static simulator show improved gains for HS-SFN when using the enhanced LMMSE equalizer. In future work the performance of these equalizers should be evaluated by using channels with more paths and longer delay spread. Also the design of interference-aware

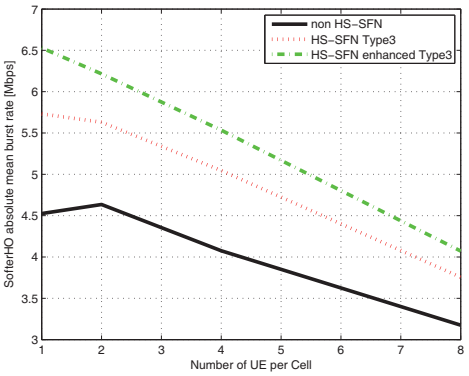

Fig. 7. Average burst rate.

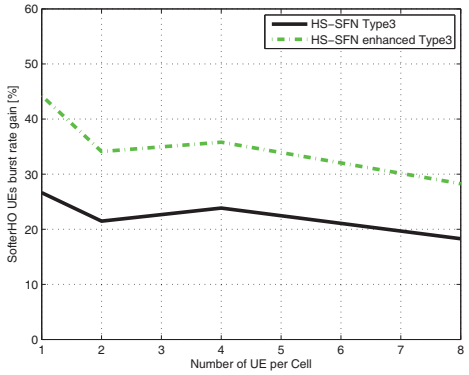

Fig. 8. Burst rate gain for SofterHO UEs.

equalizers suitable for HS-SFN is of considerable interest. Furthermore, HS-SFN performance can be improved by using uplink feedback that helps reaching better coherence between signals from different cells.

REFERENCES

[1] T. Krauss, M. Zoltowski, G. Leus, "Simple MMSE equalizers for CDMA downlink to restore chip sequence: comparison to zero-forcing and RAKE," in *Proc. of 2000 IEEE International Conference on Acoustics, Speech, and Signal Processing*, Jun. 2000, p. 2865.

[2] T. Krauss, M. Zoltowski, "Oversampling diversity versus dual antenna diversity for chip-level equalization on CDMA downlink," in *Proc. of 2000 Sensor Array and Multichannel Signal Processing Workshop*, Aug. 2000, p. 47.

[3] W. Chea, H. Zhao, W. Wang, "Improved sample added LMMSE receiver based on interference mitigation for HSDPA downlink," *The Journal of China Universities of Posts and Telecommunications.*, vol. 15, 2008.

[4] T. Nihtilä, J. Kurjenniemi, M. Lampinen, T. Ristaniemi, "Performance of receive diversity and LMMSE chip equalization in WCDMA HSDPA network," in *IEEE 16th International Symposium on Personal, Indoor and Mobile Radio Communications, Vol. 2*, Sep. 2005, p. 1245.

[5] T. Nihtilä, J. Kurjenniemi, E. Virtej, "System Level Analysis of Interference Aware LMMSE Chip Equalization in HSDPA Network," in *12th IEEE Symposium on Computers and Communications*, Jul. 2007, p. 133.

[6] R. Tresch, C. Mehlfuhrer, M. Guillaud, "LMMSE channel estimation for MIMO W-CDMA with out-of-cell interference mitigation," in *Signals, Systems and Computers*, Pacific Grove, CA, Oct. 2008, pp. 331–335.

[7] C. Mehlfuhrer, M. Wrulich, M. Rupp, "Intra-cell interference aware equalization for TxAA HSDPA," in *ISWPC. 3rd International Symposium.*, Santorini, Greece, May 2008, pp. 406–409.

[8] M. R. M. Wrulich, C. Mehlfuhrer, "Interference aware MMSE equalization for MIMO TxAA," in *ISCCSP. 3rd International Symposium.*, St Julians, Malta, 2008, p. 1585.

[9] Y. Hyunseok, P. Sungjin, H. S. Oh, K. Kyung-ho, "Hybrid chip-rate equalization of downlink CDMA in SFN channel," in *IWSSC. IEEE International Workshop.*, Toulouse, France, Oct. 2008, p. 285.

[10] 3GPP TSG-RAN, RP-110477, Nokia Siemens Networks, "HS-SFN performance evaluation," Jan 2011.

[11] D. H. Brandwood, "A complex gradient operator and its application in adaptive array theory," in *Communications, Radar and Signal Processing, IEE Proceedings F*, Nov. 2008, p. 11.

[12] 3GPP TR 25.8xx v0.1.3, "HSDPA Multipoint Transmission," Mar 2011.

PVII

PHASE ADJUSTMENT IN HS-SFN FOR HSDPA

by

Oleksandr Puchko, Mikhail Zolotukhin, Vesa Hytönen, Thomas Höhne and Thomas Chapman 2012

Proceedings of the 5th IFIP International Conference on New Technologies, Mobility and Security (NTMS)

Phase adjustment in HS-SFN for HSDPA

Oleksandr Puchko, Mikhail Zolotukhin, Vesa Hytönen
Department of Mathematical Information Technology, P.O.Box 35 (Agora), FI-40014 University of Jyväskylä, Finland
{oleksandr.puchko, mikhail.m.zolotukhin, vesa.a.hytonen}@jyu.fi

Thomas Höhne
CEF CTO Research
Nokia Siemens Networks, Espoo, Finland
thomas.hoehne@nsn.com

Thomas Chapman
Roke Manor Research Ltd
Hampshire, SO51 0ZN, United Kingdom
thomas.chapman@roke.co.uk

***Abstract*—High Speed Single Frequency Network (HS-SFN) is one of the possible multi-cell transmission schemes for High-Speed Downlink Packet Access (HSDPA). This technique helps user equipments (UEs) in the softer handover area by combining signals from two neighboring cells and also by reducing intercell interference. However, combining of two signals does not always have positive impact due to uncorrelated fast fading. This problem can be solved if the transmitted signals from the cells are adjusted such that the signals would arrive in phase. In this article the impact on HS-SFN is shown when phase adjustments are applied.**

I. Introduction

Multi-cell transmission schemes for HSDPA introduced in [1] are currently actively studied by several industrial companies. Their main target is to increase the wireless networking experience near the cell borders by applying data transmissions from multiple cells to a single UE, thus improving the throughput for low data rate users.

HS-SFN is an intra-site multi-cell transmission scheme where the same signal is transmitted from two cells simultaneously to one UE. Its target is to increase the received signal level by utilizing over-the-air signal combining while at the same time reducing interference from the nearest neighbour [2]. One of the advantages of HS-SFN is a fairly simple UE receiver architecture, where only a single equalizer is required. The overlapping signals from two cells might be additive, resulting in an increased Signal-to-Noise Ratio (SINR), but they might also destruct each other due to different phase. A method called phase adjustment is designed to prevent this by adjusting the phase of the transmission in one of the cells, based on feedback received from the UE.

The rest of the document is organized as follows. Section I-A presents the background and motivation for using Phase adjustment for HS-SFN, after which signal model is explained in Section II, including the presentation of the most challenging parts for the implementation and their solutions. Matlab verification and simulation results will be presented in Section III and Section IV correspondingly. Section V concludes the paper.

A. Background and related techniques

There are several multipoint transmission schemes which were described in [1]. Multiflow and HS-SFN are two most promises techniques. Both these techniques help UEs in the softer handover area by transmissions from two neighboring cells. However in Multiflow techniques each cell transmit different data flow on different scrambling codes. In HS-SFN, same downlink (DL) data is transmitted on HS-PDSCH channel from two cells in same site by using the same carrier frequency and scrambling code in both cells. Transmissions are TTI-aligned, so that the signals are combining over the air at the UE receiver, see Fig. 1. [3]

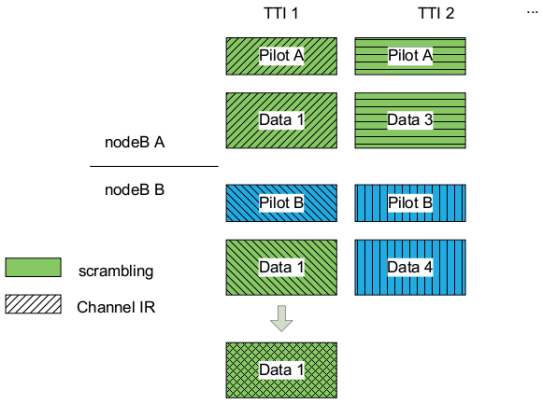

Fig. 1. HS-SFN data signal formation.

In addition to the gained signal strength, also the strongest interferer is removed. The thus enhanced C/I may be expressed as

$$C/I = \frac{0.7P_0 + 0.7P_1}{\sum_{i=0}^{N} P_i - P_0 - 0.7P_1} \quad (1)$$

where i is the i-th interfering cell and N the total number of interfering cells. P_0 and P_1 represent the power from serving (main) cell and assisting cell accordingly. Here we assume a 30 % control channel (pilots and signaling) overhead, thus 70 % is left for data on HS-PDSCH channel[3].

According to [3], HS-SFN can bring up to 25% of burst rate gain for low load for users in the softer handover area,

978-1-4673-0229-6/12/$31.00 ©2012 IEEE

but since the number of these users is not so big (around 4-5% from all UEs) gain for all UEs is not visible. One of the possible techniques that can increase performance of HS-SFN usage is enhanced equalizer. The main concept of this technique is to take into account combined data, control and pilot channels from two cells while calculating the weight of LMMSE equalizer.[4] Another possible technique, so called phase adjustment, can increase HS-SFN performance by adjusting the signal phase from one of the cells at the transmission stage, based on feedback relayed by the UE. A same technique called transmit antenna precoding is already used for downlink MIMO transmission [5].

II. Signal model

Let us consider the situation when two neighbouring cells transmit a signal to an UE. In this case one cell is serving the UE and another cell is assisting. Hereafter the control and pilot channels are not taken into account and only data channels are essential when combining a signal.

A specific number of orthogonal spreading sequences for transmitting a signal through data channel are assigned to every user. For serving and assisting cells the spread and scrambled chip sequence transmitted through data channel at time instant m is defined as

$$s_m = [s(m+F-D-1), \ldots, s(m), \ldots, s(m-D-L)]^T, \tag{2}$$

where F is the equalizer length, L is the number of multipath components and D is the delay parameter satisfying the inequality $0 \leq D \leq F$.

Let us assume that an UE has N_{Rx} Rx antennas. In this case, channel coefficient matrix H_j for j-th cell is the $(F+L-1)\times(F\cdot N_{Rx})$ matrix which is determined as follows:

$$H_j = \begin{bmatrix} h_{j,1} & \mathbb{O}_{1\times L+1} & \mathbb{O}_{1\times L+1} & \ldots & \mathbb{O}_{1\times L+1} \\ h_{j,2} & h_{j,1} & \mathbb{O}_{1\times L+1} & \ldots & \mathbb{O}_{1\times L+1} \\ h_{j,3} & h_{j,2} & h_{j,1} & \ldots & \mathbb{O}_{1\times L+1} \\ \vdots & \vdots & \vdots & \ddots & \vdots \\ \mathbb{O}_{1\times L+1} & \mathbb{O}_{1\times L+1} & \mathbb{O}_{1\times L+1} & \ldots & h_{j,N_{Rx}} \end{bmatrix}^T, \tag{3}$$

where $h_{j,k}$ is the k-th line of the channel impulse response matrix h_j for j-th cell. Matrix h_j is of size $N_{Rx}\times L+1$ and can be defined as

$$h_j = \begin{bmatrix} h_{j,1}(0) & h_{j,1}(1) & \ldots & h_{j,1}(L) \\ h_{j,2}(0) & h_{j,2}(1) & \ldots & h_{j,2}(L) \\ \vdots & \vdots & \ddots & \vdots \\ h_{j,N_{Rx}}(0) & h_{j,N_{Rx}}(1) & \ldots & h_{j,N_{Rx}}(L) \end{bmatrix}, \tag{4}$$

where $h_{j,k}(l)$ is the channel impulse response of k-th Rx antenna from j-th cell at l-th chip. For the serving cell index j equals zero and it equals one for the assisting cell.

The received chip sequence r_m at time instant m can be constructed as

$$r_m = \sqrt{L_0} H_C^T s_m + \eta_m, \tag{5}$$

where L_j denotes path gain for channel from the j-th cell to the UE, η_m is zero mean, Gaussian distributed, additive white noise with covariance matrix C_η, and normalized combined matrix H_C is defined as follows:

$$H_c = H_0 + \sqrt{\frac{L_1}{L_0}} H_1. \tag{6}$$

A. LMMSE Equalizer

The chip sequence transmitted from cell is reconstructed at the UE receiver using an LMMSE equalizer. The equalizer coefficient is estimated by minimizing the following quadratic cost function

$$F(w) = E\left\{\left|w^T r_m - s(m-\tau)\right|\right\}. \tag{7}$$

The function $F(w)$ represents the distance between the transmitted chip $s(m-\tau)$ for a given delay $\tau \in \{-F+D+1, -F+D+2, \ldots, D+L\}$ and the received chip sequence r_m equalized.

The minimal value of $F(w)$ is reached when w satisfies the following inequality:

$$\frac{\partial F}{\partial w^T} = 0. \tag{8}$$

Let us assume that the power of the signal transmitted through HS-PDSCH is equal to P_{data} for each cell, and chip sequences transmitted through different channels are not correlated with each other or with noise vector η_m. In this case, the equation (8) can be transformed to

$$\left(L_0 H_c^T R_{ss} H_c^* + R_{\eta\eta}\right) w^* - P_{data}\sqrt{L_0} H_c^T \delta_\tau = 0, \tag{9}$$

where R_{ss} denotes the autocorrelation matrix of signal transmitted, $R_{\eta\eta}$ is the noise vector autocorrelation matrix, and δ_τ is a zero vector with the unit on the position τ. Taking into account the assumptions mentioned above, matrix R_{ss} is $(F+L-1)\times(F+L-1)$ identity matrix multiplied by P_{data} and $R_{\eta\eta}$ is equal to C_η.

Thus, the LMMSE equalizer coefficient is calculated as follows

$$w = \sqrt{L_0} P_{data}\left(L_0 P_{data} H_c^H H_c + C_\eta\right)^{-1} H_c^H \delta_\tau. \tag{10}$$

B. Phase adjustment

To improve HS-SFN performance the transmitted signals from serving and assisting cells can be adjusted in such way that the signals arrive in phase. It is difficult to achieve exact in-phase arrival since precise feedback and frequency specific phase adjustment are required, but it can definitely improve performance of HS-SFN system.

Like in single cell MIMO transmission a set of transmitting antenna weights are defined. In the case considered, this set consists of two weights: the signal transmitted through HS-PDSCH from the serving cell is multiplied by the first weight, and the HS-PDSCH from the assisting cell by the second weight. The transmitting antenna weights are not applied to the pilot and control channels.

The first weight always remains fixed and equal to one:

$$\alpha_0 = 1. \tag{11}$$

The second weight provides a phase adjustment and is set to one of the following values according to the UE feedback:

$$\alpha_1 = \left\{ \frac{1+j}{\sqrt{2}}, \frac{1-j}{\sqrt{2}}, \frac{-1-j}{\sqrt{2}}, \frac{-1+j}{\sqrt{2}} \right\}, \tag{12}$$

where j is an imaginary unit. As one can notice weights applied to the assisting cell's HS-PDSCH differ by ninety degrees. Thus, there are four possible sets of transmitting antenna weights and one of these sets is chosen based on the UE feedback information.

C. Computation of feedback information in a terminal

After applying the weights the received signal in a terminal transforms to following equation:

$$r_m = \sqrt{L_0} H_{pa}^T s_m + \eta_m, \tag{13}$$

where

$$H_{pa} = \alpha_0 H_0 + \alpha_1 \sqrt{\frac{L_1}{L_0}} H_1. \tag{14}$$

The equalizer coefficient for the phase adjustment case can be estimated as

$$w_{pa} = \sqrt{L_0} P_{data} \left(L_0 P_{data} H_{pa}^H H_{pa} + C_\eta \right)^{-1} H_{pa}^H \delta_\tau. \tag{15}$$

Signal-to-interference plus Noise Ratio (SINR) C/I is calculated to decide which transmitting antenna weight should be applied. The estimation of the signal power for delay value equal to τ:

$$C = P_{data} \left| w_{pa}^T H_{pa}^T \delta_\tau \right|^2. \tag{16}$$

Let us assume that transmitted power for control channel is equal to P_{ctrl}. The interference is modelled as the interpath interference of the combined data $I_{interpath,comb}$, plus the filtered interpath interference of the own control channels $I_{interpath,ctrl}$, plus colored noise from other cells $I_{intercell}$, plus thermal noise $I_{thermal}$:

$$I = I_{interpath,comb} + I_{interpath,ctrl} + I_{intercell} + I_{thermal},$$

where

$$\begin{aligned}
I_{interpath,comb} &= P_{data} w_{pa}^T H_{pa}^T \hat{\delta}_\tau H_{pa}^* w_{pa}^*, \\
I_{interpath,ctrl} &= P_{ctrl} w_{pa}^T H_0^T \hat{\delta}_\tau H_0^* w_{pa}^*, \\
I_{intercell} &= P_{ctrl} \frac{L_1}{L_0} w_{pa}^T H_1^T H_1^* w_{pa}^* + \sum_{j=2}^{N} \frac{L_j}{L_0} w_{pa}^T H_j^T H_j^* w_{pa}^*, \\
I_{thermal} &= \frac{1}{L_0} w_{pa}^T C_{thermal} w_{pa}^*,
\end{aligned} \tag{17}$$

where δ_τ is $(L+F-1)\times(L+F-1))$ identity matrix with zero in the main diagonal on the position τ, N denotes the number of cells that interfere the UE and $C_{thermal}$ is the thermal noise correlation matrix.

After calculating the SINR for all the four transmitting antenna weights the maximal SINR value can be used to decide the future weight, while the SINR value corresponding to the currently applied weight can be used for evaluating the SINR of the HS-PDSCH transmission.

III. Matlab verification

The improvement in the HS-SFN performance caused by phase adjustment mechanism can be evaluated in Matlab. A set of scripts and functions have been created which uses path gains, power of signal transmitted through HS-PDSCH and control channel, etc. for deriving the signal-to-interference ratio. The calculation of SINR for different values of relative path gain between serving and assisting cell is expressed in decibels. For each value of this ratio M simulations are run, and the impulse response matrices for serving, assisting and interfering cells are set randomly in each simulation. An average value of SINR from M simulations is calculated for each relative path gain.

Basic parameters of Matlab verification are presented in Table I.

TABLE I
Matlab verification parameters.

Parameter	**Value**
Equalizer length, F	10
Number of receiver antennas, N_{Rx}	2
Number of multipath components, L	6
Power of the signal transmitted through HS-PDSCH, P_{data}	0.7
Power of the signal transmitted through control channels, P_{ctrl}	0.3
Number of interfering cells, N	56
Number of simulations, M	1000

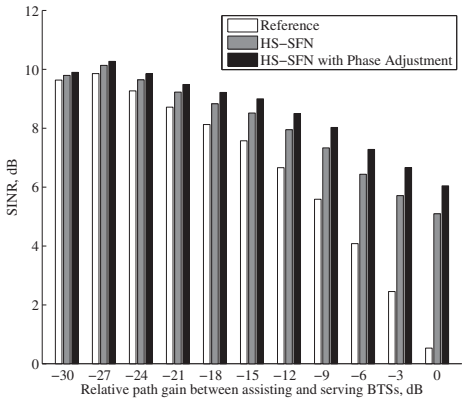

Fig. 2. SINR for reference and HS-SFN with and without Phase adjustment cases.

The comparison of signal-to-interference ratios for transmitting in standalone case, i.e. without possibility of HS-SFN transmission (reference case), HS-SFN and HS-SFN with phase adjustment cases is shown in Fig. 2. It can be seen from the Fig. 2 that the gain of using HS-SFN is increasing with

decreasing the difference between path gains of serving and assisting cells. This happens because in HS-SFN transmission we avoid interference from the second best interferer. Further difference between HS-SFN and HS-SFN with Phase adjustment is also increasing with decresing the difference between path gains. This happens due to the summarizing two signals in proper phase.

IV. System model

This section presents the performance results of HS-SFN with and without phase adjustment, gathered with a semi-static simulator. Simulations were fulfilled with a macro cell scenario that includes 19 NodeBs and 57 hexagonal cells. Propagation model, slow fading, scheduling part and other parameters were simulated according to 3GPP simulation specification [6] and they are presented in Table II.

UEs are dropped randomly into the network for a definite number of times, depending on the predefined amount of UEs per cell in order to gather proper statistics. Simulation time is 40 seconds with additional 6 seconds for warming up the system. Number of runs is 120, 60, 30, 15 respectively to 1, 2, 4 and 8 UEs per cell. For each run a new shadowing map for slow fading is created. Although UEs are stationary during the simulation time, fast fading is enabled to create channel variations. Selection of HS-SFN capable UEs is based only on two strongest links. That is, if the second strongest cell belongs to a different site than the main cell, UE will not be considered as an HS-SFN candidate. Softer HO threshold is 3 dB which limits the HS-SFN candidate locations in the border of two cells. In conjunction with the NodeB antenna model used in our simulator, UE proportion inside the HO region is 4-5 % of all UEs, and the exact share varies between different simulation runs.

TABLE II
Simulation parameters.

Parameter	Value
Cell Layout	Hexagonal grid, 19 NodeB, 3 sectors per NodeB with wrap-around
Inter-site distance	1000 m
Carrier Frequency	2000 MHz
Path Loss	L=128.1 + 37.6log10(R), R in kilometers
Log Normal Fading	
Standard Deviation	8dB
Inter-NodeB Correlation	0.5
Intra-NodeB Correlation	1.0
Correlation Distance	50m
Max BS Antenna Gain	14 dBi
Antenna pattern	
2D Pattern	$A(\theta) = -min(12(\theta/\theta_{3dB})^2,\ Am)$, where $\theta_{3dB} = 70\ degrees,\ Am = 20dB$
Channel Model	PedA3, PedB
CPICH Ec/Io	-10 dB
Total Overhead power	30%
UE Antenna Gain	0 dBi
UE noise figure	9 dB
UE Receiver Type	Type3 (LMMSE)
Spreading factor	15
Maximum Sector Transmit Power	43 dBm
Handover reporting range	3 dB
Number of HARQ processes	8
Maximum active set size	2
Traffic	
Traffic model	Bursty Traffic Source Model
Inter-arrival time	Exponential, Mean = 5 seconds
File size	Fixed at 1 Mbit
Flow control on Iub	Ideal and instantaneous
HS-DPCCH Decoding	ACK decoded on UL (unless mentioned otherwise); C2P used: 2 dB for Intra-NB, 4 dB for Inter-NB
CQI	Ideal with 3 TTI delay
Scheduling	Common intra-NodeB scheduler, proportional fair algorithm

A. Simulation Results

This section presents the simulation results that were gathered with a semi-static simulator.

Fig. 3 shows user burst rates for 1, 2, 4, 8 and 16 UEs per cell. Green lines represent results with ITU Pedestrian A channel and black lines show results with ITU Pedestrian B channel. Dash, solid and circled solid lines show results for reference, HS-SFN and HS-SFN with Phase adjustment, respectively. This figure indicates that even though the overall burst rates with Pedestrian B channel are less than those of Pedestrian A, the performance of HS-SFN and HS-SFN with Phase adjustment when compared to the reference results stays almost the same.

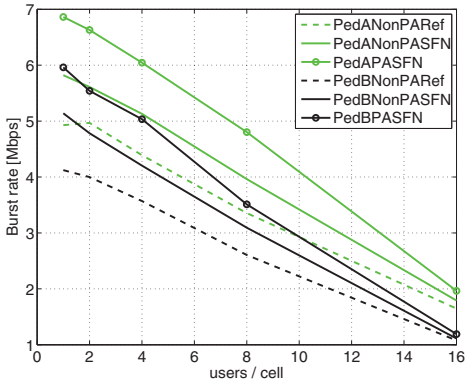

Fig. 3. Burst rate for HS-SFN UEs.

Fig. 4 and Fig. 5 show cumulative distribution function (CDF) of user burst rates (throughputs) for one UE per cell case with ITU Pedestrian A and ITU Pedestrian B channels, respectively. Each figure consists of reference, HS-SFN and HS-SFN with Phase adjustment case that show performance of HS-SFN UEs. As mentioned, HS-SFN UEs are the UEs in the softer HO area that have the second strongest interfering cell from the same NodeB as the primary cell. Reference case refers to simulations without possibility of HS-SFN transmission. HS-SFN and HS-SFN with Phase adjustment show results from simulations where HS-SFN transmission is allowed and Phase adjustment is turned off or on according to the simulation scenario. From these figures can be seen that Phase adjustment can almost double the HS-SFN performance in terms of user burst rate.

Fig. 6 and Fig. 7 show mean burst rate gain for all

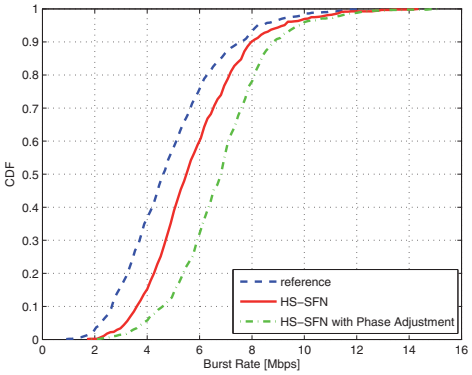

Fig. 4. Burst rate CDF for 1 UE per cell with PedA channel .

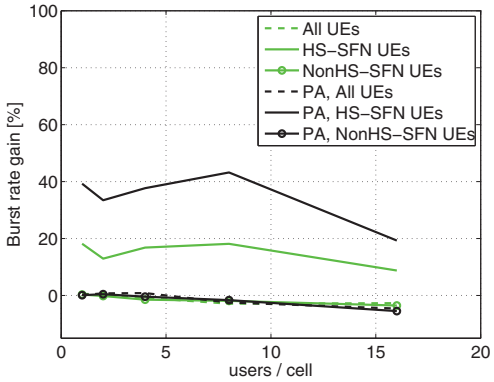

Fig. 6. Burst rate gain of HS-SFN with and without Phase Adjustments compared to non-HS-SFN operation with PedA channel.

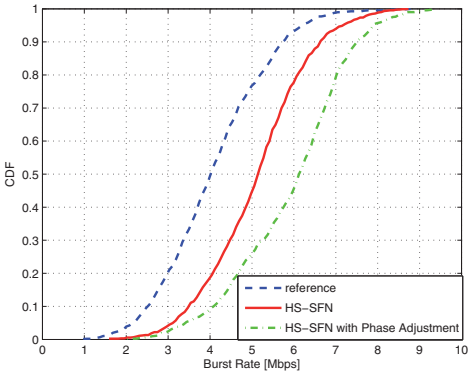

Fig. 5. Burst rate CDF for 1 UE per cell with PedB channel.

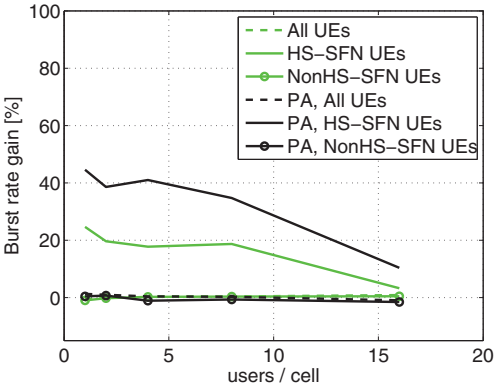

Fig. 7. Burst rate gain of HS-SFN with and without Phase Adjustments compared to non-HS-SFN operation with PedB channel.

UEs, HS-SFN UEs and nonHS-SFN UEs with and without Phase adjustment for Pedestrian A and Pedestian B channels, respectively. From the figures it can be seen that a good gain can be achieved for HS-SFN UEs with a very small overall negative gain for all UEs in the network. The burst rate gains are decreasing with higher load that may be explained by the fact that for low load neighbouring cells often do not have own users to schedule and a short-term load balancing effect is observed there. Further, by the same token the additional interference created by their assisting transmission to other cells is not having a big effect. For high load the load balancing effect disappears.

V. Conclusion

In this paper HS-SFN with Phase Adjustment has been presented. This technique is providing around 40% gain to burst rates for HS-SFN UEs in lightly loaded cells with small impact on overall performance. The gain is however degraded with high loads. Further work could include studying modified scheduling algorithms that try to keep the overall user experience constant while utilizing HS-SFN when it provides a high improvement to the signal.

References

[1] 3GPP TSG-RAN WG1, R1-104913, Nokia Siemens Networks, "Multi-cell transmission techniques for HSDPA," Aug 2010.
[2] 3GPP TSG-RAN WG1, R1-111489, Nokia Siemens Networks, "Text proposal on the performance of HS-SFN," May 2011.
[3] V. Hytonen, O. Puchko, T. Hohne, T. Chapman, "High-speed single-frequency network for hsdpa," in *Communication Technologies Workshop (Swe-CTW), 2011 IEEE Swedish*, Nov. 2011, pp. 1–6.
[4] O. Puchko, M. Zolotukhin, V. Hytonen, T. Hohne, T. Chapman, "Enhanced lmmse equalizer for high-speed single frequency network in hsdpa," in *Communication Technologies Workshop (Swe-CTW), 2011 IEEE Swedish*, Nov. 2011, pp. 92–97.
[5] 3GPP TR 25.214 v8.9.0, "Physical layer procedures (FDD)," Mar 2010.
[6] 3GPP TR 25.8xx v0.1.3, "Hsdpa multipoint transmission," Mar 2011.

PVIII

SCHEDULING MULTIPOINT-TO-POINT TRANSMISSIONS OVER HSDPA BASED SINGLE FREQUENCY NETWORK

by

Fabian Montealegre Alfaro, Vesa Hytönen, Oleksandr Puchko and Timo Hämäläinen 2013

Proceedings of the 3rd IEEE International Conference on Information Science and Technology (ICIST)

Third International Conference on Information Science and Technology
March 23-25, 2013; Yangzhou, Jiangsu, China

Scheduling Multipoint-to-Point Transmissions over HSDPA Based Single Frequency Network

Fabian Montealegre Alfaro, Vesa Hytönen, Oleksandr Puchko and Timo Hämäläinen

***Abstract*—Quick growth in the amount of wireless subscribers coupled with the necessity to provide desired level of user experience for broadband, stimulates mobile operators to improve the efficiency of their limited air resources by using different technologies. This paper discusses the study on Single Frequency Network (SFN) based multipoint-to-point transmission scheme as a possible way to improve the usage of air resources of the High-Speed Downlink Packet Access (HSDPA) network. The results presented show that cooperative transmission from several cells can improve user throughput when the number of UEs sharing the same resources within an SFN is fairly low. Due to this reason a suitable size for the created SFN cluster is strongly dictated by the load level of the network.**

I. Introduction

MULTIPOINT transmission concepts have been more and more in the limelight during the past years first with Long Term Evolution (LTE) and nowadays within HSDPA especially with the concept called Multiflow [1]. This method improves the user specific data rate by enabling two separate data streams to be transmitted from two different cells. In Multiflow, however, the transmissions are not orthogonal and thus may have an interfering impact on each other. Therefore the concept is best suitable for terminals with sophisticated receiver architecture that are capable of active interference cancellation.

A closer relation to the multipoint-to-point (M2P) SFN concept is the Multimedia Broadcast/Multicast Services (MBMS) introduced by the 3rd Generation Partnership Project (3GPP) in Release 6, where broadcast content is transmitted via common physical channels accessible to all users in a cell [2]. A promising candidate for enhancing the spectral efficiency of MBMS is the Multicast/Broadcast Single Frequency Network (MBSFN) scheme, which operates on the WCDMA physical layer. In WCDMA, MBSFN operation requires a complete 5 MHz carrier band to be allocated for MBMS [3]. All base stations in a service area form a MBSFN cluster and transmit coordinated signals in a synchronised fashion, i.e., the same information using one scrambling code common to all cells. This is the main confluence to the topic of this paper, where the common air interface is used for delivering user specific data instead of multicast or broadcast information.

Another multipoint transmission scheme with a strong convergence to the M2P SFN is High-Speed Single Frequency Network (HS-SFN) introduced in [4] and [5]. This technique allows transmitting the same user data using shared scrambling code, spreading factor and frequency from two cells in order to combine the signals over the air to gain more throughput and better networking experience for the users. During an HS-SFN transmission, only the High-Speed Physical Downlink Shared Channel (HS-PDSCH) is transmitted over SFN using the same scrambling code, whereas the control channels, such as High-Speed Shared Control Channel (HS-SCCH), are delivered by using the original scrambling codes of the serving cells. As the Common Pilot Channel (CPICH) also remains separated by scrambling codes, the UE is able to estimate both channels separately and perform equalisation of the signals based on those estimates [4]. The utilization of different scrambling codes for control and data channels produces high interference as the orthogonality of the signals is lost.

For this paper the behaviour and performance of multipoint-to-point transmissions over Single Frequency Network were studied. In the discussed concept the cells are transmitting both control and data channels over SFN in a coordinated and synchronized way. Thereby the issue of non-orthogonality is avoided. Further, not only two cells will be capable of sharing the same network parameters, but the SFN cluster may consist of several cells, though, it is required that the cells are controlled by the same Radio Network Controller (RNC). A MATLAB® simulator was used to evaluate the performance of SFN by a comparison to normal HSDPA operation with single-cell transmissions.

The rest of the article is organised as follows. In Section II the SFN concept is described in more detail. Section III discusses the modelling of the system. The simulation results are presented and analysed in Section IV. Finally, Section V summaries the main findings of the study.

II. Description of the SFN Concept

In conventional HSDPA operation, users are served only by one cell. The transmissions of each cell are separated by applying unique scrambling codes. By this separation the UEs are able to distinguish the signals originating from its serving cell. The concept of SFN assumes that downlink data (HS-PDSCH), control (HS-SCCH) and other common channels are being transmitted from two or more cells by using the same scrambling code such that signals can combine over the air as multi-path components. As a result, the UE sees a group of cells in SFN as a single bigger cell with several multi-paths components, as depicted in Fig. 1 and Fig. 2. It is significant to make clear that the scrambling code not necessarily need

F. M. Alfaro, V. Hytönen, Oleksandr Puchko and Timo Hämäläinen are affiliated with the Department of Mathematical Information Technology, Faculty of Information Technology, University of Jyväskylä, Finland (email: fmontealegre@gmail.com, {vesa.a.hytonen, oleksandr.puchko, timo.t.hamalainen}@jyu.fi, Tel: +358408053263).

978-1-4673-2764-0/13/$31.00 ©2013 IEEE

to be changed in Fig. 2 from Transmit Time Interval (TTI) to another. Instead, the transmission parameters of the cell should rather stay unchanged for a longer period of time in order to avoid issues with user mobility caused by sudden disappearance and emergence of the cells. In the system model used for this study the formed SFN areas are static, thus the mobility issues are not faced.

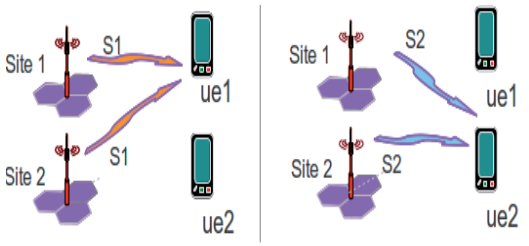

Fig. 1. Concept of SFN over HSDPA

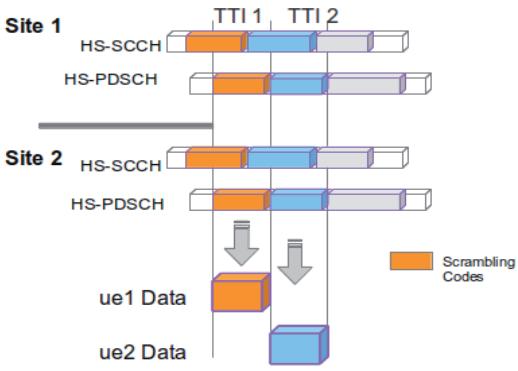

Fig. 2. Scrambling code utilisation in SFN

III. System Model

For simulating the performance of M2P SFN a MATLAB® model was created for this particular purpose. The modelled HSDPA network consists of 61-site hexagonal layout (4 rings + centre site). Every site is divided into 3 sectors by three-sectored-antennas at the centre of the site. The size of the SFN area is varying between 1, 7 and 19 sites. The exact simulation scenarios are depicted in Section IV. Some elementary assumptions were made for the simulations:

1) Transmissions from SFN cells are sub-chip-aligned, such that the signals combine over-the-air as multi-path components at the UE receiver.
2) It is assumed that the CPICH and control channel power remains the same between the SFN and non SFN sites. Correspondingly, HS-PDSCH power in each cell stays constant.
3) Channel Quality Indicator (CQI) feedback is not modelled. Shannon capacity was used to calculate achievable rates on each link.
4) The UEs in the simulation remained static during the simulation period. Several simulation drops were executed to produce channel variation.
5) No fast fading was assumed, i.e. channels stay constant during a simulation run in your simulations.

The simulation parameters used are listed in Table I.

TABLE I
Summary of Simulation Parameters

Parameter	Value
Cell Layout	Hexagonal grid, 63 NodeB, 3 sectors per NodeB.
Inter-site distance	1000 m
Carrier Frequency	2000 MHz
Bandwidth	5 MHz.
Path Loss	L = 128.1 + 37.6log10(R), R in kilometres
Log Normal Fading	Standard Deviation: 8 dB Inter-NodeB correlation 0.5
Maximum Antenna Gain	14 dBi
Maximum Sector Transmit Power	43 dBm
Thermal Noise density	-174 dBm/Hz
Penetration Loss	10 dB
CPICH E_c/I_o	-10 dB
Number of UEs/cell	1, 2, 4, 8
SFN cluster size	1, 7 and 19 sites
Traffic	SFN area: Bursty traffic source model File Size: Mean 1 Mbyte. Inter-arrival time: Exponential, Mean 5 seconds. Non SFN area: Full buffer traffic model
UE noise figure	9 dB
UE Antenna Gain	0 dB
UE Distribution	UEs uniformly distributed within the system
Front to Back Ratio	$A_m = 20dB$
Antenna beamwidth	$\Theta_{3dB} = 70^o$
Antenna Gain	$A(\Theta) = -min\left(12\left((\frac{\Theta}{\Theta_{3dB}})^2\right), A_m\right)$ $A_m = 20dB$ & $\Theta_{3dB} = 70^o$
HS-DSCH	Up to 15 SF 16 codes per carrier for HS-PDSCH Total available power of HS-PDSCH is 70% of NodeB Tx power.
Scheduling	Proportional Fair ($\alpha = 0.9$)

A. Channel Model

A wave propagation model in which the signal strength is exponentially attenuated with the distance is assumed. The received signal strength from transmitting node i to receiving node j is modelled as

$$P_{i,j} = PL_{i,j} * F_{i,j} * G_{i,j}, \quad (1)$$

where $PL_{i,j}$ is the Path Loss on receiver j from transmitter i calculated according with [6] as

$$PL_{i,j} = 128.1 + 37.6 * log_{10}(d_{i,j}), \quad (2)$$

where $d_{i,j}$ is the distance in kilometres. The Fading factor $F_{i,j}$ represents shadow fading modelled as log-normal random variable with zero mean and σ=8 dB, with Inter-NodeB correlation of 0.5.

Antenna gain $G_{i,j}$ depends on the difference of the location of the receiver j with regard to the boresight angle of the transmitter i. It is calculated using a Gaussian sector antenna with attenuation limited to front to back ratio:

$$A(\Theta) = -min\left(12\left(\frac{\Theta}{\Theta_{3dB}}\right)^2, A_m\right), \tag{3}$$

where $\Theta_{3dB} = 70^o$, A_m=20 dB. Offsets of -120, 0 and 120 degrees are applied to create 3 sectors in each site.

SFN affects the total signal-to-interference and noise ratio (SINR) at receiver j, and is modelled as an adaptation from [7] in decibels as

$$SINR_j = 10 * log_{10}\left(\frac{SF \cdot Tx_{Data\_power} \cdot \sum\limits_{i \in \mathbb{U}_j} P_{i,j}}{\sum\limits_{i \in \mathbb{I}_j} P_{i,j} - \sum\limits_{i \in \mathbb{U}_j} P_{i,j} + N_P}\right) \tag{4}$$

where the Spreading Factor (SF) used for HS-PDSCH is 16. Also a 30 % control channel (pilots and signalling) overhead is assumed, thus 70 % of the total transmission power is left for data on HS-PDSCH ($Tx_{Data\_power} = 0.7$). $P_{i,j}$ is the received signal power at receiver j originating from transmitter i, $\mathbb{U}_j \subseteq \mathbb{TX}_{\mathbb{SFN}}$ is the set of transmitters in the SFN assigned to receiver j (the useful signals); $\mathbb{I}_j \subseteq \mathbb{TX}$ denotes the total set of transmitting cells and N_P is the noise and external interference power.

The noise level N_P, in dBm, is assumed to be constant and is obtained from the parameters in Table I. The noise power is calculated as the difference from the receiver noise power and the Equivalent Isotropic Radiated Power (EIRP) [8]:

$$N_P(dB) = Rx\_Noise_P - EIRP \tag{5}$$

where both of them are obtained as follows; the receiver noise power is obtained from:

$$Rx\_Noise_P(dB) = TND + UE_{nf} + PG; \tag{6}$$

here, Thermal Noise Density (TND) for a 2000 MHz frequency is -174 dBm/Hz, UE_{nf} stands for UE noise figure and PG is the *Processing Gain*. The Equivalent Isotropic Radiated Power (EIRP) is calculated as:

$$EIRP(dB) = Max\_Tx_P + Max\_Ant_G \tag{7}$$

the sum of the maximum sector transmission power (Max_Tx_P) and the maximum antenna gain (Max_Ant_G).

B. Traffic Model And Scheduling

For the users in the SFN area, we use a bursty traffic model with file size fixed on 1 Mbit. The packet arrival rate is based on exponential distribution, with a 5 seconds mean. For the non-SFN area fully load traffic is used so as to produce worst case scenario regarding inter-cell interference. In a beginning of a simulation run a number of UEs based on defined load level are first selected and randomly dropped into the network. Once the UE has received its packet it switches to inactive state and waits for a new packet to arrive. During the inactivity period the UE will not be scheduled, thus only the active users with data in their dedicated transmission buffers can be allocated resources in a TTI. The amount of data received per TTI depends on the SINR of the UE. This is explained in more detail in the next section.

A common scheduler controls each cell in the SFN cluster in a coordinated fashion. A proportional fair scheduler algorithm was implemented in the simulator which schedules the channel for the station that maximises the priority function. The algorithm used in this simulator selects receiver j in per-TTI basis according to the following equation:

$$j = argmax_{1 \le j \le n} \frac{r_j(l)}{\overline{R}_{av\_j}(l)}, \tag{8}$$

where n is the number of active users, r_j is the instantaneous throughput for user j and l denotes the number of TTI. $\overline{R}_{av\_j}(l)$ is the moving average throughput obtained by

$$\overline{R}_{av\_j}(l+1) = \begin{cases} (1-\alpha)\overline{R}_{av\_j}(l) + \alpha\, r_j(l) & \text{if scheduled} \\ (1-\alpha)\overline{R}_{av\_j}(l) & \text{otherwise.} \end{cases} \tag{9}$$

Here, $0 \le \alpha \le 1$ is the weighting factor that determines whether to favour either fairness or maximum spectral efficiency in user selection. The basic purpose of the scheduling method is to exploit user diversity by selecting the user with the best condition to transmit while also considering the fairness [9]. The selected value of $\alpha = 0.9$ targets at rather fair resource allocation regardless of the channel characteristics, which is suitable for demonstrating the impact of the SFN concept on a large pool of users.

C. Throughput Calculation

In this simulator, the Shannon capacity formula for the theoretical channel spectral capacity is calculated as a function of SINR. The throughput is measured with the adaptation of Shannon capacity formula presented in [10] as

$$C(bits/s) = BW * \eta * log_2\left(1 + \frac{SINR}{SINR_{eff}}\right). \tag{10}$$

BW adjusts the system bandwidth (BW) efficiency, which in HSDPA is assumed as the chip rate of 3.84 Mcps. The correction factor η, is optimised in [10] for a value of 0.75. The $SINR_{eff}$ adjusts the SINR implementation efficiency. In HSDPA, it will take the value of the HS-PDSCH spreading factor 16. Finally the SINR is calculated as in Equation 4. In order to cope with the HSDPA physical layer capacity limitation, the user throughput calculation based on the Shannon formula was extended such that the highest achievable throughput was truncated to match the data rate for 64-QAM modulation derived from the following formula:

$$DataRate = \frac{CR * ECR * BpS * N_{codes}}{SF}, \tag{11}$$

where CR stands for Chip Rate, which in WCDMA is fixed to 3.84 Mcps, the effective code rate (ECR) is set at 0.97 according to [11]. Bits per Symbol (BpS) depends on the modulation, and for 64-QAM modulation the number of bits is 6. Number of spreading codes (N_{codes}) depends on the UE category and for the simulations 15 codes will be used. Spreading Factor (SF) for WCDMA is fixed at 16, thereby the maximum possible throughput will be truncated to

$$TP_{max} = \frac{3.84 * 10^6 * 0.97 * 6 * 15}{16} = 20.952\ Mbps. \quad (12)$$

IV. Simulation Scenarios and Results

A. SINR Measurement

Four main scenarios were selected where either 0, 1, 7 or 19 sites in the centre of the simulation area form a SFN cluster, while the entire simulation area consist of 61 sites. The first case represents a conventional HSDPA operation. A general idea how the SINR could be improved with the introduction of SFN in a HSDPA network is depicted in Fig. 3. Notice that these figures present only the theoretical improvement of the channel quality and are not taking into consideration user throughput which is strongly dependent on the scheduling mechanism as well as the size of the SFN. In the last three scenarios the cells forming the SFN cluster share a common scrambling code, therefore avoid posing interference to each other, whereas the cells in the outer rings of sites user their own scrambling codes. Due to this reason the highest improvement of SINR is achieved in the centre of the whole SFN area.

For the four different scenarios a Cumulative Distributions Function (CDF) of SINR graph is depicted in Fig. 4, for all users in the network, revealing that with a sound approach of creating the SFN the signal quality could be improved significantly.

B. User Throughput

For the measurement of the per-user performance the simulations were ran with the enabled traffic model and scheduling explained in Section III-B. During the simulation the instantaneous SINR (and data rate) will remain invariable for the users, since their positions do not change. Different cell load levels were simulated to demonstrate the impact of resource sharing among increasing amount of users within the SFN area. In Fig. 5 and Fig. 6, throughput of users in the network are displayed. In the scenarios with enabled SFN, throughputs are gathered from the UEs served by the SFN. Due to the 64-QAM modulation capacity limit the throughputs are truncated to approximately 21 Mbps as explained earlier.

In very low load scenario with one UE in the cell the throughputs of the UEs can be improved quite significantly when compared to the normal HSDPA operation. Even with a large SFN area, where a higher amount of UEs compete in resource allocation, the signal enhancement is predominant to fewer scheduling opportunities. Besides the explicit improvement of the data rates, the activity time of the UEs is

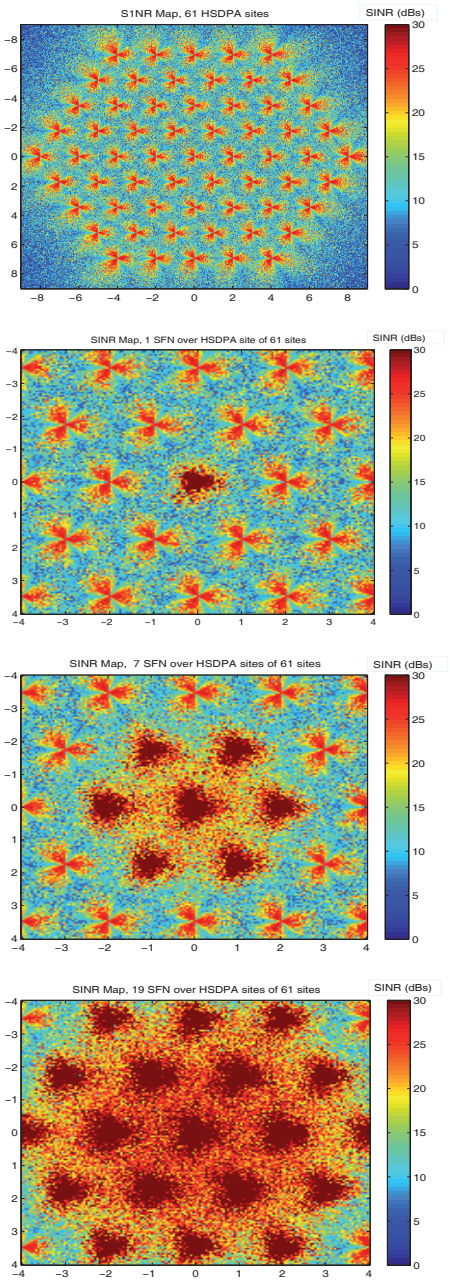

Fig. 3. SINR to Location Mapping, a) Conventional HSDPA, b) 1 SFN site, c) 7 SFN sites, d) 19 SFN sites.

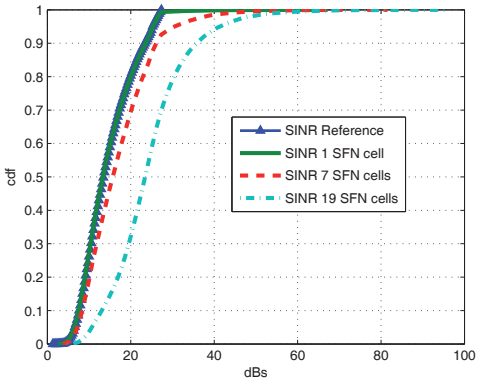

Fig. 4. CDF for location based SINR mapping

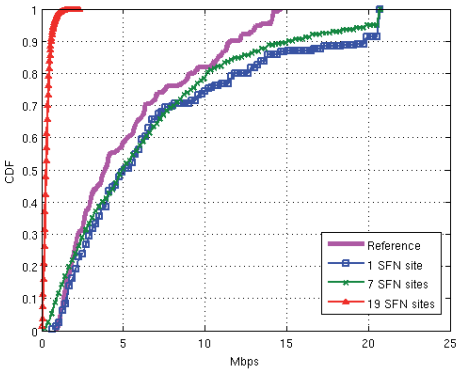

Fig. 6. UE throughput CDF, 2 UEs/cell

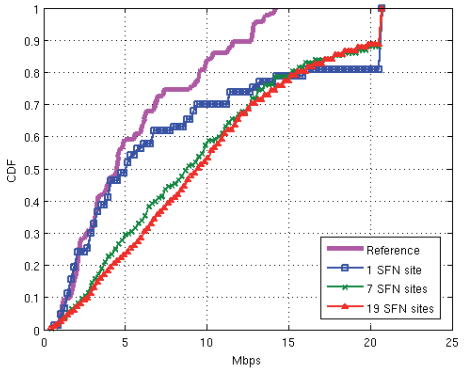

Fig. 5. UE throughput CDF, 1 UE/cell

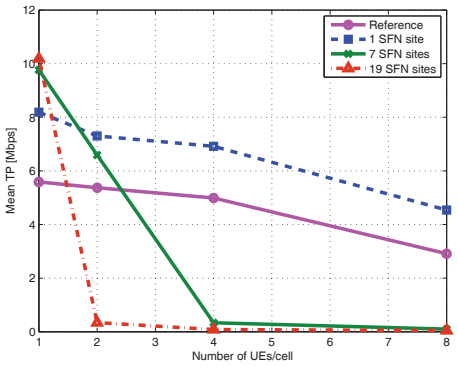

Fig. 7. Mean UE throughput

reduced, which in part leaves more resources to be used for the remaining active users.

The resource allocation becomes a limiting factor when the number of UEs in the SFN cluster is increased, which is clearly visible already with 2 UEs/cell curves in Fig. 6. This is a result from the fact that all cells in the SFN will serve the same UE in one TTI. If the SFN size was set too large, as example 19 sites shown in the figure, the users need to wait very long before they are scheduled again, thus rapidly reducing data rates. This is certainly expected as the used scheduling parameters should provide high fairness of the system.

Higher load levels were also simulated, from which the average user throughput levels are gathered to Fig. 7. An obvious observation is that too large an SFN area will lead to declined performance if the load of the area rises. The efficiency of SFN is determined by controlling the balance between improved channel quality and frequency of scheduling opportunities. Given that a proper algorithm for choosing the cells in an SFN is found that takes into account the prevailing traffic conditions, data rates of users could be enhanced noticeably.

V. Conclusions

In this paper, the performance and applicability of using the Single Frequency Network concept for multipoint-to-point data transmission in HSDPA system were discussed. Based on the simulation results, user specific SINR and thereby throughput can be increased by the utilization of the concept. However, the performance is susceptible to traffic load changes and improper formation of an SFN may result in fast deterioration of data rates.

Dynamic switching of SFN was not discussed, which would be required in the real network in order to cope with varying traffic conditions and user mobility. Nevertheless, in a very static part of the network, for example in rural or even suburban areas, using an immutable formation of SFN could be an option. Considering a general utilization of the concept the emergence of multi-carrier networks could also provide a good

basis for the M2P SFN technique.

REFERENCES

[1] V. Hytönen, O. Puchko, T. Höhne and T. Chapman, "Introduction of Multiflow for HSDPA", *IEEE New Technologies, Mobility and Security (NTMS)*, pp.1-5, May 2012.

[2] 3GPP TS 25.346, "Introduction of the Multimedia Broadcast/Multicast Service (MBMS) in the Radio Access Network (RAN)", March 2011. [Online]. Available: http://www.3gpp.org/ftp/Specs/html-info/25346.htm.

[3] C. a. Jotten, C. Sgraja, and H. Schoneich, "Performance Evaluation of Multicast/Broadcast Single Frequency Network Operation for WCDMA, *IEEE International Symposium on Spread Spectrum Techniques and Applications*, pp. 79-84, August 2008.

[4] V. Hytönen, O. Puchko, T. Höhne, and T. Chapman, "High-speed single-frequency network for HSDPA", *IEEE Swedish Communication Technologies Workshop (Swe-CTW)*, pp. 1-6, October 2011.

[5] R1-104913, "Multicell transmission techniques for HSDPA", Nokia Siemens Networks, 3GPP RAN1# 62, August 2010.

[6] R1-110563, "Simulation Framework for System Evaluation of Multi-Point HSDPA", 3GPP, 3GPP RAN1# 63, January 2011.

[7] M. Eriksson and A. Mahmud, "Dynamic Single Frequency Networks in Wireless Multihop Networks - Energy Aware Routing Algorithms with Performance Analysis", *IEEE International Conference on Computer and Information Technology*, pp. 400-406, June 2010.

[8] H. Holma and A. Toskala, "WCDMA for UMTS HSPA EVOLUTION AND LTE". Fourth Edition. England : John Wiley & Sons Ltd, 2007.

[9] Mingyu Kang, Young Jin Sang, Hae Gwang Hwang, Hyung Yeol Lee and Kwang Soon Kim, "Performance Analysis of Proportional Fair Scheduling with Partial Feedback Information for Multiuser Multicarrier Systems", *IEEE Vehicular Technology Conference (VTC2009-Spring)*, pp. 1-5, April 2009

[10] P. Mogensen , Wei Na, I. Z. Kovacs, F. Frederiksen, A. Pokhariyal, K. I. Pedersen, T. Holding, K. Hugl and M. Kuusela, "LTE capacity compared to the Shannon bound", *IEEE Vehicular Technology Conference (VTC2007-Spring)*, no. 1, pp. 1234-1238, April 2007

[11] 3GPP TS 25.306, "UE Radio Access capabilities", December 2010. [Online]. Available: http://www.3gpp.org/ftp/Specs/html-info/25306.htm.